Three Approaches Towards one aim: Nanostructured Photovoltaic Devices

Dissertation zur Erlangung des Grades
"Doktor der Naturwissenschaften"

im Fachbereich Chemie, Pharmazie und Geowissenschaften
der Johannes Gutenberg-Universität Mainz
vorgelegt von

Dominik Koll
geboren in [redacted]

Mainz, 2011

Dekan: [redacted]

Erster Berichterstatter: [redacted]

Zweiter Berichterstatter: [redacted]

Datum der mündlichen Prüfung: [redacted]

Datum der Einreichung: [redacted]

Erklärung

Die vorliegende Dissertation wurde zwischen September 2008 und August 2011 unter Anleitung von Herrn [redacted] am Institut für Anorganische Chemie und Analytische Chemie der Johannes Gutenberg Universität Mainz angefertigt.

Ich versicher hiermit, dass ich die Dissertation selbstständing verfasst habe, so wie alle angewandten Quellen und Hilfsmittel angegeben habe,

Mainz, im August 2011

Acknowledgments

When working on a PhD thesis for three years a lot of people contribute to the the work in one way or another. There are people who you work with in the laboratory on a daily basis, with others you will discuss your results over and over again, there are people who will help you with the administrative issues that just need to be dealt with and of course there are people who provide you with the opportunity to do measurements or who will do some measurements for you. Finally, some have just listen to your complaints when nothing is working properly anymore. I want to thank all of this people personally here in this section. If I forgot anybody, don't be offended and you are allowed to forget my birthday in return.

I sincerely thank [redacted] for allowing me to work on such interesting topics and for the fruitful discussions about science and related topics, such as Walter von Manger. Also thank you for giving me the opportunity to travel the world to be on conferences or for an extended research stay in Seoul, which certainly provided me with interesting scientific results as well as personal experiences. I was also very pleased with my teaching responsibility, which allowed me to literally blow off steam every once in a while.

A sincere Kam-Sa Hamni-Da goes to [redacted] and [redacted] from [redacted] provided me with the opportunity to work in his lab for a three months research stay. Since then we have met several times and he continuously supported my work on dye-sensitized solar cells. [redacted] deserves a very special thank you for the hours he spent measuring my solar cells and also for the explanations and help about the working principles of DSSCs and the device fabrication.

In this context I would also like to thank the graduate school IRTG and [redacted] [redacted] for giving me the opportunuity to do research in the far east and for other interesting and entertaining trips around Germany.

I would also like to thank [redacted], [redacted] and [redacted] [redacted] for the discussions about my work during the meetings held in the context of the extension of my stipend. Additionally, our group just started a collaboration with the group of [redacted] and I am sure it will be fruitful.

Thanks to [redacted] and [redacted] for being on my thesis committee.

A lot of people from the [redacted] group deserve a thank you as well:
To [redacted] for the fruitful cooperation in the lab throughout my entire thesis. Also thanks for proof-reading large parts of my thesis and for showing that is is actually possible to make computers do what you want and teaching me the value of nice images. Thanks to both [redacted] and [redacted] for the great time together in Korea and in Mainz.
To [redacted] for proof-reading a "short" chapter of my thesis, help in the lab and for the great time together in Mainz.
Thanks to [redacted] and [redacted] for the help with the anodization of bloody vanadium. It was probably better that we did not give up...
I would like to thank [redacted] for the help with the preparation of photoanodes, even if it meant to work in a dark sauna.
Thanks to [redacted], who is not only trusted by women, but also a great help in the lab.
I would like to thank [redacted] for the help with the structure solution of the sodium titanante nanowires and also for other clues concerning X-ray diffraction or daily work in the lab.
And of course, thanks to the whole [redacted] group!

A big thank you goes to [redacted] and [redacted] for the structure solution of the sodium titanate nanowires and the big help with the "Snapshots"-Chapter. Thank you for spending hours in front of the microscope looking at nanowires. Additionally I would like to thank [redacted] for the help on the structure solution of sodium titanates and [redacted] for the support of, and the discussions on this project.

Many people provided me with the opportunity to use their instruments or did measurements for me, I would like thank these people, too:
Thanks to [redacted] for technical support at the SEM and the HRTEM measurements of the chalcogenide nanowires.
Thanks to the center of electron microscopy in Mainz, in person of [redacted] and [redacted] for allowing me to use both TEM and SEM.
Thanks to Prof. [redacted] for the opportunity to use both SEM and XPS and to [redacted] for patiently explaining the operation of these instruments to me.
Also thanks to [redacted] for the AFM measurements.

I would like to thank [redacted] and [redacted] for allowing me to borrow half of the inventory of the AC1-Praktikum, so I could do my experiments.
Thanks to the work shop for the continuous supply with setup for the electrochemical experiments and for other help. In some weeks they were mainly working for me.
[redacted] deserves a thank you for countless X-ray diffraction experiments she performed for me.

I would like to thank the graduate school of excellence, "MAterials Science in MaiNZ" for the financial support and for the opportunity to go to various conferences, summer schools and for the great seminar in 2010.

I would also like to thank my parents [redacted] and [redacted], who supported me morally and financially during my studies and "just" morally during my PhD thesis. Also my siblings, [redacted] and [redacted] deserve a thank you, they always felt obliged to give things to their little brother because he was only a poor student and on the other hand I kept forgetting their birthdays. Thanks for your patience with me.

Finally, the biggest thank you of all goes to my wife [redacted] for always being there for me, which was probably not always the easiest task. Thank you!

Abstract

Abstract in english:

While this PhD-thesis consists of four chapters considering seemingly different aspects of the chemistry of nanomaterials, there is a least common denominator: Nanostrutured photovoltaics. The first part of the thesis deals with an investigation of the growth mechanism of sodium titanate nanowires. "Snapshots" of the reaction progress using a microwave-assisted hydrothermal synthesis were made and it was found that the growth of nanowires not only involves morphologically different nanostructures, such as nanotubes, but is also accompanied by changes in the crystal chemistry of the species involved. In the second chapter the sodium titanate nanowires are converted into hydrogen titanate- and TiO_2 nanowires. All three species are subsequently incorporated into the photoanode of dye-sensitized solar cells, in form of a composite electrode consisting of nanowires and nanoparticles. The chemical properties of the materials influence the photoanode and thus the performance of a device prepared from them. In the next part of the thesis, titanium and vanadium metal foils are electrochemically oxidized to form ordered arrays of nanotubes or nanopores. In the case of titanium these arrays could be obtained rather easily by slight modifications of a method reported in literature. The synthesis of an ordered array of vanadium oxide nanopores by a careful adjustment of the experimental parameteres

was achieved for the first time. Finally, chalcogenide nanowires were precipitated inside the pores of a polycarbonate track-etched membrane. While the method itself is well established, indium sulfide nanowires were synthesized *via* this technique for the first time, additionally the first steps towards the synthesis of ternary $CuInS_2$ nanowires were performed. On first sight, the last chapters seem to be independent, but in fact they represent an evolution of concept underlying the preparation of photovoltaic devices based on composite electrodes. Anisotropic nanostructures are used in order to improve the electron conduction in photovoltaic devices based on nanomaterials, however, while the wires in photoanodes were randomly oriented, TiO_2 or V_2O_5 nanopore arrays are well ordered. Finally, $CuInS_2$ nanowires can used as the sensitizer or photoactive material in the TiO_2 or V_2O_5 nanopore array.

Auszug in deutscher Sprache:

Im Rahmen dieser Doktorarbeit wurden vier scheinbar verschiedene Projekte bearbeitet, die aber eine gemeinsame Basis haben: Nanostrukturierte Photovoltaik. Im ersten Teil wurde das Wachstum von Natriumtitanat Nanodrähten mittels "Schnappschüssen" im Verlauf einer Mikrowellen basierten, hydrothermalen Synthese untersucht. Nicht nur die Morphologie der Nanostrukturen änderte sich im Verlauf der Reaktion, sondern auch deren chemische Zusammensetzung. Im nächsten Abschnitt wurden aus den Natriumtitanat Nanodrähten zunächst Wasserstofftitanat- und schließlich TiO_2 Nanodrähte hergestellt. Alle drei Verbindungen wurden anschließend als Material zur Herstellung von Komposit-Elektroden benutzt, die jeweils aus Nanopartikeln und Nanodrähten bestanden. Die chemischen Unterschiede zwischen den Nanodrähten hatten Einfluss auf die Morphologie der entsprechenden Photo-Anoden und damit auf die Effizienz der daraus hergestellten Farbstoff-Solarzellen. Im weiteren Verlauf der Doktorarbeit wurden Titan- und Vanadiumfolien elektrochemisch oxidiert um geordnete Filme, bestehend aus Nano-Röhren oder -Poren, herzustellen. Im Fall von Titan wurde dazu eine publizierte Methode leicht modifiziert um die gewünschten Ergebnisse zu erhalten. Desweiteren gelang zum ersten mal die Darstellung von geordneten Vanadiumoxid Nanoporen, mittels systematischer Variation der Reaktionsbedingungen. Im letzten Teil der Arbeit wurden sulfidische Nanodrähte durch Ausfällen derselben in einer Poly-Carbonat Membran synthetisiert. Während diese Methode schon für andere Systeme erprobt wurde, gelang erstmals die Herstellung von Indiumsulfid Nanodrähten mittels einer Fällungsreaktion. Ebenso wurden erste Erfolge bei der Fällung des ternären Halbleiters $CuInS_2$ erzielt. Die letzten beiden Abschnitte stellen eine Weiterentwicklung des der Herstellung von Komposit-Elektroden zugrunde liegenden Konzeptes dar. Auch hier werden anisotrope Nanopartikel genutzt um die Elektronenleitung in nanostrukturierten Solarzellen zu verbessern. Während die Nanodrähte in den Kompositelektroden aber ungeordnet vorliegen, sind die Nano-Röhren oder -Poren im Falle der elektrochemischen Herstellung geordnet. $CuInS_2$ Nanodrähte können als photoaktives Material in eben diesen Nanoporen verwendet werden.

List of Publications

1. "Interaction of Alkaline Metal Cations with Oxidic Surfaces: Effect on the Morphology of SnO_2 Nanoparticles" Alexander Birkel, Niklas Loges, Enrico Mugnaioli, Robert Branscheid, **Dominik Koll**, Stefan Frank, Martin Panthöfer and Wolfgang Tremel, *Langmuir*, **2010**, *26* (5), 3590-3595, DOI: 10.1021/la902994r.
2. "Comparison of Hybrid Blends for Solar Cell Application" Maria C. Lechmann, **Dominik Koll**, Daniel Kessler, Patrick Theato, Wolfgang Tremel and Jochen S. Gutmann, *Energies*, **2010**, *3*, 301-312; DOI:10.3390/en3030301.
3. "Electrodeposition of ZnO nanorods on opaline replica as hierarchically structured systems" Lorenz Steidl, Stefan Frank, Stefan A. L. Weber, Martin Panthöfer, Alexander Birkel, **Dominik Koll**, Rüdiger Berger, Wolfgang Tremel and Rudolf Zentel, *Journal of materials chemistry*, **2011**, *21*, 1079-1085, DOI: 10.1039/c0jm02759f.
4. "Photochemical "Self-healing" pyrrole based treatment of CdS/CdTe photovoltaics" **Dominik Koll**, Ahmad H. Taha, Dean M. Giolando, *Solar Energy materials and solar cells*, **2011**, *95*, 1716-1719, DOI:10.1016/j.solmat.2011.01.038.

5. "The interplay of crystallization kinetics and morphology during the formation of SnO_2 nanorods: snapshots of the crystallization from fast microwave reactions" Alexander Birkel, Frank Reuter, **Dominik Koll**, Stefan Frank, Robert Branscheid, Martin Panthöfer, Eva Rentschler and Wolfgang Tremel, *Crystal Engineering Communications*, **2011**, *13*, 2487-2493, DOI: 10.1039/c0ce00573h.

6. "Structure Analysis of Titanate Nanorods by Automated Electron Diffraction Tomography" Iryna Andrusenko, Enrico Mugnaioli, Tatiana E. Gorelik, **Dominik Koll**, Martin Panthöfer, Wolfgang Tremel and Ute Kolb, *Acta crystallograhpica B*, **2011**, *B67*, 218-225, DOI: 10.1107/S0108768111014534.

7. "Properties of Spark Plasma Sintered Nanostructured $Zn_{1+x}Sb$" Christina S. Birkel, Tania Claudio, Martin Panthöfer, Alexander Birkel, **Dominik Koll**, Gregor Kieslich, Jürgen Schmidt, Raphael Hermann and Wolfgang Tremel, *Phys. Status Solidi A*, **2011**, *8*, 1913-1919, DOI: 10.1002/pssa.201026665.

8. "Highly Efficient and Stable Dye-Sensitized Solar Cells Based on SnO_2 Nanocrystals Prepared by Microwave-Assisted Synthesis" Alexander Birkel*, Yong-Gun Lee*, **Dominik Koll***, Xavier Van Meerbeek, Stefan Frank, Mi Jin Choi, Yong Soo Kang, Kookheon Char and Wolfgang Tremel (*All three authors contributed equally), *Journal of Energy and Environmental Science*, **accepted**.

9. "The Role of an Unknown Phase of Sodium Titanate Nanotubes as an Intermediate in the Formation of $NaTi_3O_6(OH) \cdot 2\,H_2O$ Nanowires", **Dominik Koll**, Iryna Andrusenko, Enrico Mugnaioli, Martin Panthöfer, Ute Kolb and Wolfgang Tremel, **in preparation**.

10. "Dye-Sensitized Solar Cells with Nanoparticle/Nanowire Composite Electrodes: Influence of Different Nanowires on the Preparation of the Photoanode and the Device Performance" **Dominik Koll***, Yong-Gun Lee*, Alexander Birkel*, Xavier Van Meerbeek, Stefan Frank, Patrick Leidich, Yong Soo Kang, Kookheon Char and Wolfgang Tremel, (*All three authors contributed equally), **in preparation**.
11. "Synthesis of Highly Ordered Vanadium Oxide Nanopores *via* Electrochemical Anodization" **Dominik Koll**, Daniel Jacobs, Hannes Kerschbaumer, Alexander Birkel, Stefan Frank, Steffen Pfeiffer and Wolfgang Tremel, **in preparation**.

Contents

5 Chalcogenides via Precipitation 183

List of Figures

List of Tables

CHAPTER 1

Three Approaches Towards one aim: Nanostructured Photovoltaic Devices

The design and improvement of photovoltaic (PV) devices based on nanomaterials has received enormous attention over the last two decades after the introduction of dye sensitized solar cells (DSSCs) based on TiO_2 nanoparticles by Graetzel and co-workers.[3] The schematic setup of a DSSC or Graetzel Cell is shown in Figure 1.1. The components of a DSSC and their respective functions are:

- **The front electrode** consists of glass coated with a transparent conductive oxide; generally fluorine doped tin oxide (FTO) or indium doped tin oxde (ITO) are used.

- **The dye** The dye is commonly a ruthenium complex, which binds to the surface of the nanoparticular anode *via* carboxylic acid groups, which effectively bind to the surface of oxides, such as TiO_2. The sensitizer, which is present in the ground state, is excited by an incoming photon. An electron of a dye molecule in the electronically excited state is now injected into the conduction band of the semiconductor, meaning the Ru-complex undergoes oxidation.

- **The anode** commonly consists of TiO_2 nanoparticles, which transport the injected electron to the front electrode and thus acts like a semiconductor in a conventional solar cell. Other oxides, such SnO_2 and ZnO can also be used as semiconducting material.

- **The electrolyte** consists of a mixture of I^-/I^{3-} dissolved in acetonitrile. I^{3-} is reduced to I^- at the back electrode, which is subsequently utilized to reduce the dye while undergoing an oxidation to I^{3-}.
- **The back electrode** consists of the same transparent conducting oxide as the front electrode, but it is additionally coated with a thin layer of platinum.
- **The platinum layer** is needed to increase the conductivity of the back electrode and to catalyze the reduction of I^{3-} to I^-.

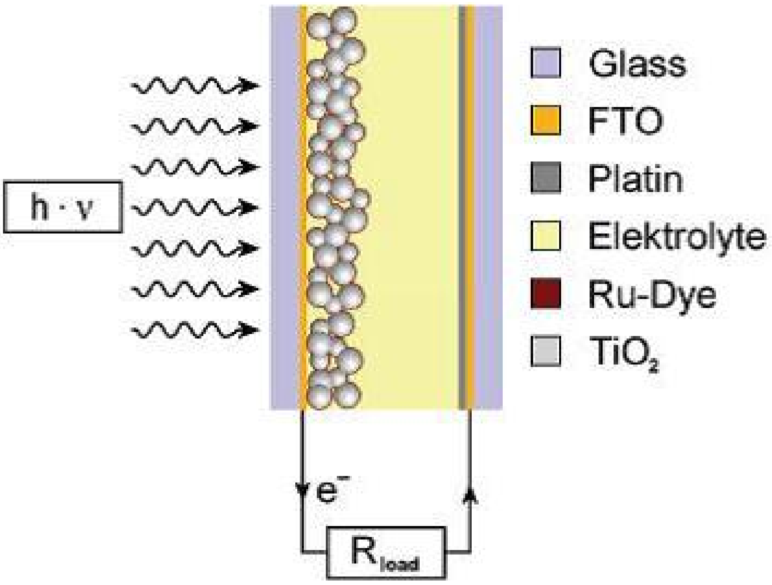

Figure 1.1: Schematic setup of a DSSC.[1]

Despite the advantages of this kind of device, e.g. cheap and energy efficient fabrication, high semiconductor surface area for efficient photon absorption and the possibility to use flexible substrates,[4] there are drawbacks to be overcome. Among others, one of the major issues for devices based on nanoparticles devices is the electron loss due to particle-particle boundaries.[5][6] In most cases the semiconducting material in a DSSC consists of TiO_2 nanoparticles whose size is in the range from 15 to 30 nm. The use of small particles (with high surface area) is necessary to ensure that a sufficient amount of dye can be loaded onto the photoanode, which is a prerequisite for the generation of high photo currents. On the other hand this leads to the above mentioned electron losses. One possible solution to this problem is the use of composite electrodes consisting of a mixture of TiO_2 nanoparticles and nanowires (see Figure 1.2). The nanowires support electron conduction towards the front electrode by acting as electron pathways without particle-particle-, ideally even without grain-grain boundaries.

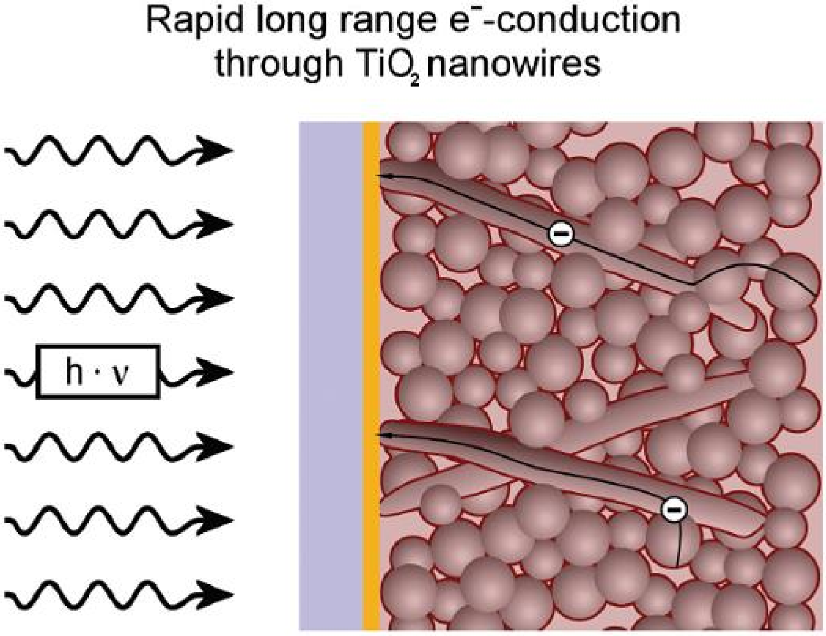

Figure 1.2: Schematical drawing of a composite electrode consisting of nanowires and nanoparticles.[1]

The common thickness for the semiconducting layer in DSSCs is around 10μm.[7] In an ideal case, the nanowire reaches from the top of the photoanode to the bottom leading to an unhindered electron diffusion throughout the entire film, i.e. the length of the nanowires should be in the same size regime as the electrode thickness. To achieve optimum results the nanowires need to be evenly distributed within the photoanode. The concept behind the use of a composite electrode is the utilization of the enhanced electron diffusion in anisotropic nanostructures.[8] This concept can be widened to systems other than a mixture of particles and wires, for example ordered arrays of nanotubes can be utilized.[9] However, more sophisticated synthetic methods are necessary to obtain such advanced nanostructures, some of which will be described in this thesis. Additionally the "classical" approach to use TiO_2 nanoparticles in DSSCs will be widened to other materials. The search for novel and materials possibly leading to more efficient solar cells is one of the main challenges for the design of nanostructured photovoltaic devices.

In the first part of this work the effect of the incorporation of sodium titanate, hydrogen titanate and TiO_2 nanowires into the photoanode of a DSSC will be elucidated. After the synthesis of the nanomaterials, the ideal ratio of nanoparticles to nanowires was determined using TiO_2 nanowires, followed by a study of the chemically different nanowires. The results reveal that 5 wt% is the ideal nanowire content. Furthermore, it it was shown that both the use of hydrogen titanate and TiO_2 nanowires led to an improvement of the device performance, while the incorporation of sodium titanate nanowires led to decreased performance. However, significantly higher open circuit voltages were measured for this material. The differences in device performance could be attributed to the short circuit current almost exclusively. The focus of the work presented herein was the synthesis of the nanomaterials and the influence of chemically different species on the preparation of a photoanode. One special aspect was the use of sodium titanate nanowires in DSSCs, which was not carried out before, to the authors best knowledge. Before their utilization in DSSCs, the groth mechnanism of sodium titanate nanowires was elucidated. It was found that the nanowires grow in multiple steps, not only accompanied by morphological changes, but also by variations in the composition of the nanostructures involved. After the dissolution of the precursor nanotubes are formed, which have a crystal structure that was unknown so far. The nanotubes unfold under a "NaOH-uptake" to form nanowires.

It was mentioned above that the nanowires are supposed to be aligned towards the electrode ideally, which is hardly possible if the wires are synthesized as a powder. On the other hand, if the wires are grown directly onto FTO, it is difficult to incorporate a sufficiently large number of nanoparticles into the electrode, which results in a low surface area.[10] Wires grown by a template based method often require rather complicated reaction sequences to remove the template and/or they lack crystallinity,[11] which hinders electron conduction. A promising approach to circumvent this problem is the design of nanostructured photovoltaic devices, based on dense, ordered arrays of oxidic nanotubes, which can be obtained by electrochemical anodization (or anodic oxidation) of valve metals, such as titanium or vanadium, under suitable conditions. Herein the growth of ordered arrays of titanium- and vanadium oxide nanotube or nanopore arrays on the respective metal foils is described. In the case of titanium this is a well established experimetal method;[12][13] the TiO_2nanotube arrays prepared as part of this thesis were synthesized based on the method of Lee *et al.*[2] First the as-purchased titanium foils were polished electrochemically, subsequently followed by the anodization that yielded the desired ordered arrays of oxidic nanotubes. To the authors best knowledge, vanadium oxide nanopore or nanotube arrays have not been prepared by eletrochemical anodization so far. A method to electrochemically polish the as-purchased vanadium foils was evaluated, subsequently followed by the development of a procedure which allowed the synthesis of ordered arrays of nanopores on vanadium foil. This was achieved by a systematic variation of experimental parameters. It was found that the solvent used for the anodization had the largest influence on the outcome of the reaction. Nanotube or nanopore arrays can be utilized for nanostructured photovoltaic (PV) devices in different ways, for example by directly sensitizing the nanotubes with a dye [14] or by depositing quantum dots, e.g. CdS or CdSe, on the nanotubes, which also leads to a sensitation of the nanotube array.[15] Additionally it is possible to significantly increase the surface area of the nanotube arrays by depositing semiconductor nanoparticles of the same kind on them.[14] In general, as-grown TiO_2 nanotubes arrays are intrinsically n-doped, therefore, a second processing option is the growth of p-type semiconductor, such as CdTe or $CuInS_2$, inside the nanotubes.[16]

One general issue in DSSCs is the need for sensitation of the semiconductor since the used oxides only absorb light in the UV-region of the suns' spectrum. However, most dyes suffer from degradation when used over extended periods of time.[17] Another issue is the necessity to recover the dye utilizing a liquid electrolyte, requiring an efficient method to seal the final device in order to achieve long term stability. Among other possible solutions,[18] it would be advantageous to directly utilize a solid state, p-type semiconductor, such as $CuInS_2$, which is long-term stable and renders the use of an electrolyte unnecessary. One synthetic option is the growth of $CuInS_2$ inside an array of oxidic nanotubes, as mentioned above. A versatile method to grow nanowires is the template assisted precipitation.[19] Hereby, the nanowires are precipitated inside the pores of a porous template, such as a polycarbonate track etch membrane or a TiO_2 nanotubular array. The first steps towards the growth of the ternary semiconductor $CuInS_2$ inside the pores of a polycarbonate membrane were performed by synthesizing the binary compounds CuS and In_2S_3 in form of nanowires. By adjusting the experimental conditions CuS nanotubes could also be obtained. It was found that a co-precipitation to form $CuInS_2$ was difficult, due to the different reaction rates of the synthesis of the binary compounds. First attempts towards the synthesis of a ternary compound were carried out combining the methods for the synthesis of CuS nanotubes and In_2S_3 nanorods.

CHAPTER 2

The Role of an Unknown Phase of Sodium Titanate Nanotubes as an Intermediate in the Formation of $NaTi_3O_6(OH) \cdot 2\,H_2O$ Nanowires

2.1 Introduction

When TiO_2 powders are treated hydrothermally in concentrated caustic solutions, a sodium titanate is formed during the synthesis. Sodium titanates have attracted considerable attention for more than ten years, due to their wide range of interesting applications for example in catalysis, i.e. for the direct use as photocatalyst,[20] as well as a carrier material for catalytically active nanoparticles.[21] Titanate nanowires can be used as an ion exchange material for the removal of heavy metal ions,[22] gas sensing,[23] lithium ion batteries [24] or dye-sensitized solar cells.[25] In some applications sodium titanate nanowires are first converted to hydrogen titanate- or TiO_2 nanowires, respectively. Owing to the rapid ion-exchange in the layered titanate structure,[26] the obtained sodium titanates can easily be converted to hydrogen titanate *via* an acidic treatment and subsequently to TiO_2 *via* calcination.

Kasuga *et al.* were the first to report the formation of "anatase" nanotubes *via* the hydrothermal treatment of TiO_2 powder in concentrated NaOH solutions in 1998.[27] Four years later Chen *et al.* identified the nanotubes to in fact be a layered titanate, rather than anatase type TiO_2.[28] Numerous publications deal with the synthesis as well as growth mechanism of sodium titanate nanowires, compare the review by Bavykin *et al.* [29] However, despite the great effort put into the investigation of this reaction system the mechanism is still not fully understood. In the widely accepted model, sodium titanate nanotubes are formed at temperatures below 180°C, while the formation of nanowires is favored above 180°C. Recent findings by Huang *et al.* show that nanotube formation is indeed possible at high temperatures, because it is an inevitable step in the formation of sodium titanate nanowires, which are the thermodynamically favored product.[30] The mechanism proposed includes the dissolution of the precursor (crystalline anatase type TiO_2 nanoparticles), followed by the formation of nanosheets, which roll up to form nanotubes. According to Huang *et al.* these nanotubes form an extended wire like structure *via* oriented attachment. The holes in the tubes are filled with amorphous sodium titanate from the dissolution of crystalline TiO_2. Despite the detail of this study, an important factor in the growth mechanism is only casually mentioned; crystallographic phases and the composition of the intermediates found during the reaction and the final product. The crystal structure of the sodium titanates was only recently resolved by means of automated diffraction tomography (Andrusenko *et al.* [31]) and the composition of the material was determined to be $NaTi_3O_6(OH) \cdot 2\,H_2O$, an so far unknown phase in the sodium titanium oxygen system.[31] Similar findings were made in other systems, e.g. the intermetallic nano-Zn_4Sb_3,[32] in which a crystallographic phase that differs from the bulk system was also found in the nano-size regime. These observations add an interesting aspect to the discussion of the growth mechanism. Not only the morphological evolution of nanoparticles must be considered, but also the crystal structure and composition of all the species involved.

In this study microwave-assisted hydrothermal reactions were used to investigate the growth mechanism of sodium titanate ($NaTi_3O_6(OH) \cdot 2\,H_2O$) nanowires. Compared to conventional hydrothermal reactions in stainless steel autoclaves, chemistry utilizing microwave radiation offers several advantages, such as rapid heating due to a direct response of the solvent to the microwave radiation, short cooling cycles due to the lowered heat capacity of the reaction vessel compared to a stainless steel autoclave. Due to the lowered cooling time, active quenching, for example via immersing the reaction vessel to an ice bath, is not necessary for microwave assisted reactions. Furthermore, stirring the reaction mixture can be continued during the cooling process leading to a homogeneous cooling process. Another advantage of the microwave-assisted reaction is the overall lower energy consumption and most importantly, a reduced reaction duration.[33] The conventional hydrothermal synthesis of sodium titanate nanowires normally takes at least 24 h,[29] compared to 2 h in a microwave oven. Owing to the aforementioned lower heat capacity, the microwave reaction vessel cools down radiatively in a short time, therefore it is possible to quench the reaction at every point during the synthesis. With this method "snapshots" of the reaction progress were made and intermediate products could be investigated. Since the exact composition of the final product was known, it was possible to compare the crystal structure of the intermediates with that of the final product. Thus, a very detailed investigation of the reaction mechanism, including both morphological aspects as well as crystal chemistry, was possible.

2.2 Experimental section

2.2.1 Materials and synthesis

Materials and synthesis: A MARS XPress microwave digestion system (CEM Corporation) was used for the microwave-assisted hydrothermal synthesis. The synthesis is based on the method published by Kasuga *et al.*,[27] smaller modifications were necessary in order conduct a synthesis suitable for the reaction system. Each "snapshot" of the reaction progress was made the same way. 500 mg of TiO_2-P25 nanoparticles (Degussa) were mixed with 50 ml of a 10 M NaOH solution (made from NaOH pellets, 98.5% p.A., Acros Organics and MilliQ Water) by magnetic stirring in a 100 ml Teflon liner for 15 minutes. The vessel was sealed and subjected to a microwave-assisted hydrothermal treatment. After 10 minutes of heating at a maximum power output of 800 W, an internal pressure of 20 bar was reached. This pressure was kept for various times between 0 and 120 minutes. The microwave system is equipped with a temperature sensor, however, a temperature control was not possible because the sensor made from sapphire would dissolve in the NaOH-solution. Afterwards the reaction mixture was allowed to cool down radiatively for 30 minutes. All reaction products were thus obtained after a heating time of 10 minutes, a reaction time of X minutes and a cooling period of 30 minutes. From now on the samples will be refered to as "X minute sample". The nanopowders were seperated from the supernatant solution *via* centrifugation at 9000 rpm for 10 minutes. Finally the reaction product was washed several times with methanol, until neutral reaction of the supernatant solution. The samples were dried in vacuum over night. The as-prepared samples were subjected to X-ray diffraction (XRD) and transmission electron microscopy (TEM) without additional treatment.

2.2.2 Materials Characterization

X-ray powder diffraction: X-ray powder diffraction data were collected using a Bruker-AXS D8-Discover diffractometer equipped with a HiStar detector in reflection geometry using graphite-monochromated CuKα radiation. Samples were glued on top of glass and (111) silicon substrates using a VP/VA copolymer (vinylpyrrolidone/vinylacetate).

TEM, HRTEM and EDX: The sodium titanate nanowires were characterized by *transmission electron microscopy* (TEM) and *high resolution rransmission electron microscopy* (HRTEM). For TEM and HRTEM investigations the samples were dispersed in ethanol using an ultrasonic bath. Afterwards they were sprayed on carbon-coated copper and gold grids. For high-resolution TEM investigations the material was embedded in epoxy resin and sliced by microtome. The cuts were then placed on a carbon coated copper grid; the resin was removed with chloroform.

TEM measurements were carried out with either a Philips 420 instrument with an acceleration voltage of 120 kV or a FEI TECNAI F30 S-TWIN transmission electron microscope working at 300 kV. TEM images and diffraction patterns were acquired with a CCD camera (14-bit GATAN 794MSC). *Scanning transmission electron microscopy* (STEM) images were acquired by a FISCHIONE high angular annular dark field (HAADF) detector. Elemental analysis was done by *energy dispersive X-ray* (EDX) spectroscopy and quantified within Emispec ESVision software. For a quantitative EDX analysis the sample was deposited on a Gold grid.

2.3 Results and Discussion

2.3.1 XRD

First the phase purity of the "120 minute sample" (i.e. final reaction product) was verified *via* X-ray diffraction. The diffraction pattern of the sample obtained after 120 minutes in course of this study was compared to the XRD pattern of $NaTi_3O_6(OH) \cdot 2\,H_2O$, see Figure 2.1. No differences in the diffraction patterns were found, indicating both sample possess the same crystallographic phase, i.e. the final product in this study is also $NaTi_3O_6(OH) \cdot 2\,H_2O$.

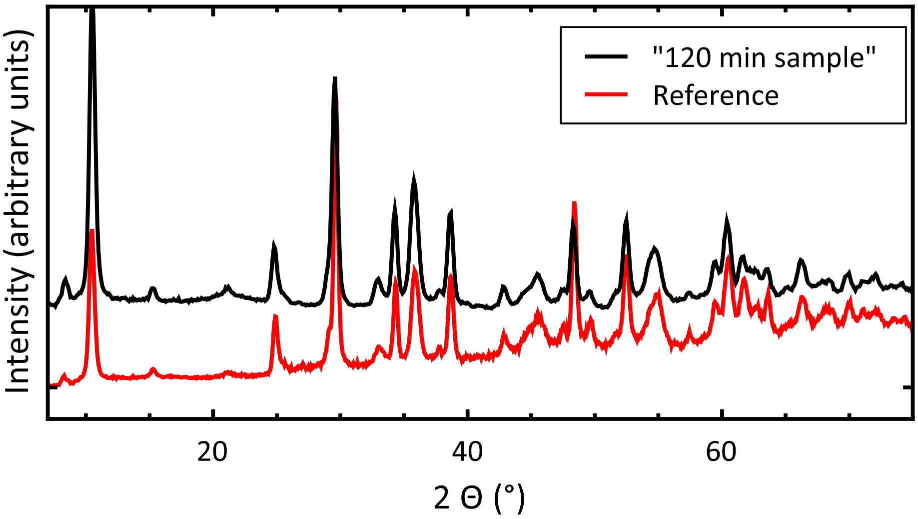

Figure 2.1: X-ray diffraction patterns of $NaTi_3O_6(OH) \cdot 2\,H_2O$(Blue) compared to the "120 minute sample" (Red).

In Figure 2.2 X-ray diffraction patterns of multiple samples obtained during this study are compared to the pattern of TiO_2-P25 nanoparticles, which consist of a phase mixture of anatase and rutile. The first observation is the complete disappearance of all reflections connected with TiO_2-P25 already after the 10 minute heating ramp ("0 minute sample"). New reflections appeared in the range between 2θ=10° and 50°, which could neither be assigned to anatase, rutile nor any other known phase of TiO_2. This result suggests that the precursor completely reacted with the NaOH solution to form a new compound, which could not be identified based on the

X-ray diffraction pattern. The positions of the reflections at 2Θ= 9.6°, 24.2°, 48° and 61.2° suggest a crystal structure with some similarities (e.g. interlayer distances) to the final product $NaTi_3O_6(OH) \cdot 2\,H_2O$. The reflections are broad, indicating the low crystallinity of the compound. It is reasonable to assume that the unidentified compound is also a sodium titanate with a composition that differs from the final product. This assumption is further backed up by EDX data (see section 2.3.3).

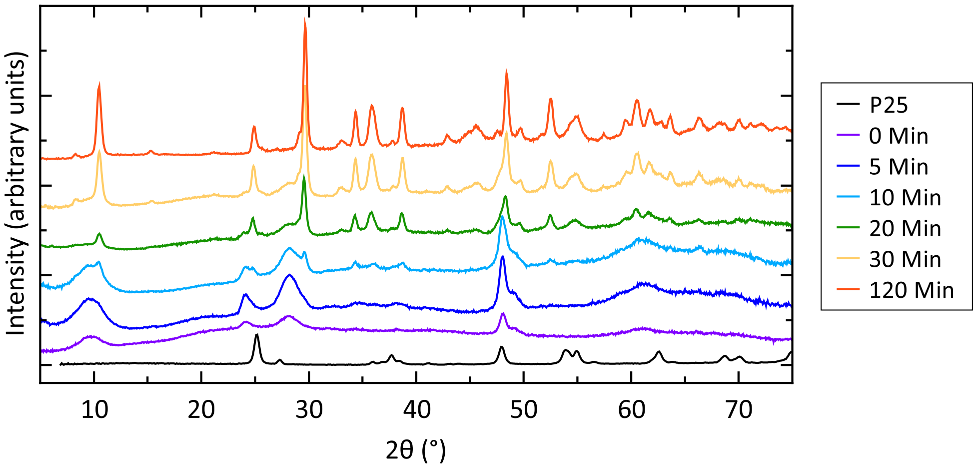

Figure 2.2: X-ray diffraction patterns of various samples synthesized in course of this study, compared to TiO_2-P25 nanoparticles, which were used as precursor. From bottom to top: TiO_2-P25 Precursor, "0, 5, 10, 20, 30 and 120 minute samples".

After a reaction time of 5 minutes, the measured intensity of the aforementioned reflections increased, indicating a higher crystallinity of the unidentified compound. However, the positions of the reflections did not change. A different X-ray diffraction pattern was measured for the "10 minute sample". While all reflections of the unidentified compound were still present, the first reflections of the final product $NaTi_3O_6(OH) \cdot 2\,H_2O$ appeared at 2θ= 10.5°, 24.9°, 29.6° and 3 reflections around 36°. The new signals were found at higher angles, compared to the unidentified intermediate. However, all reflections of this compound are still present in the diffraction pattern, so at this point of the reaction two different phases coexist in the sample. The presence of new reflections next to the old ones cannot be explained by an increase in crystallinity, which may also lead to smaller interlayer distances and thus higher diffraction angles. After the $NaTi_3O_6(OH) \cdot 2\,H_2O$ phase appeared while the reaction progressed, the reflections assigned to this compound became more prominent and the ones of the unidentified phase start to disappear. In the "20 minute sample" no reflections assigned to the unidentified phase were detected anymore. However, due to the higher crystallinity of $NaTi_3O_6(OH) \cdot 2\ H_2O$ and the obviously decreasing amount of the unidentified compound, it is possible that the reflections assigned to the latter are not detected anymore, which does not necessarily mean the compound completely disappeared. Reflections beyond a value of 2θ =40° can be attributed to the titanium-oxygen network. These reflections are most pronounced in the samples that were treated for 30 minutes or more. The increasing crystallinity of the $NaTi_3O_6(OH) \cdot 2\ H_2O$ can be seen from a shift of these reflections toward higher angles (e.g. 48.1° (in the "30 minute sample") → 48.4° (in the "120 minute sample")). These observations give a first indication that an unknown phase was formed in the early stages of the synthesis. For verification, HRTEM and EDX studies were conducted.

2.3.2 TEM and HRTEM

Precursor and "0-3 minute samples"

Using a microwave digestion system allows to quench the reaction at any given point during its progress. Due to the direct response of the solvent to the energy source, i.e. microwave radiation, the reaction mixture heats up rapidly. Compared to a conventional reaction in a furnace, the vessel itself does not have to warm up before the solvent is heated. The time required to cool down the mixture is also lowered, since the heat capacity of the microwave reaction vessel is much lower than the one of a stainless steel autoclave. Additionally, it is possible to stir the reaction mixture during the reaction; a feature that is not common for stainless steel autoclaves. The temperature cannot directly be determined during the reaction because the cover of the temperature sensor is made from sapphire; a material that dissolves in the concentrated sodium hydroxide solution used for the reaction. In the following chapter, transmission electron microscopy is used to elucidate the morphological evolution of the nanoparticles synthesized in this study.

The precursor TiO_2-P25 was characterized *via* TEM; as shown in Figure 2.3. TiO_2-P25 consists of irregularly shaped nanoparticles with the diameters ranging from as small as 10 nm up to 100 nm, while the majority of the particles are in the size range from 20-40 nm. The nanoparticles have the tendency to form agglomerates that cannot be separated easily.

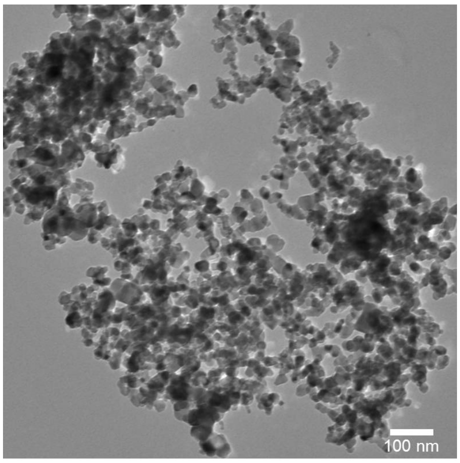

Figure 2.3: TEM image of TiO_2-P25nanoparticles.

In Figure 2.4 TEM images of the "0 minute sample" are shown. For the most part, the sample consists of agglomerates that can range up to a few micrometers in size. Besides the agglomerates few isolated nanotubes are found, see Figure 2.4 b. The fact that no trace of the precusor is present at this early stage of the reaction demonstrates one of the the advantages of the microwave-assisted reaction, i.e. the enhanced reaction velocity. From the magnified images of the agglomerates in Figure 2.4 b it can be seen that they exclusively consist of nanotubes. Like the final product $NaTi_3O_6(OH) \cdot 2\,H_2O$, the nanotubes have a strong tendency to form agglomerates (compare Figures 2.4 and 2.10 a), despite continuous stirring of the reaction mixture. Due to the strongly caustic pH value of the reaction solution, a negative charge on the surface of nanotubes is expected, which would lead to repulsion. However, the presence of sodium counter ions on the surface of the nanotubes may lead to the agglomeration.[34]

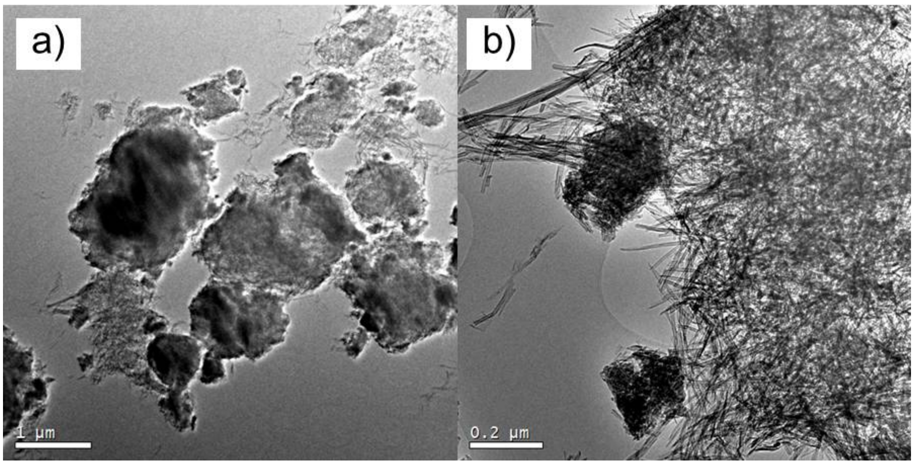

Figure 2.4: Overview TEM images of the "0 minute sample".

As mentioned before. even in this early stage of the reaction neither any trace of the precursor TiO_2-P25 nor amorphous, irregularly shaped sodium titanate nanoparticles or nanosheets was observed. In other publications dealing with the growth mechanism these types of particles are usually found. There are two possible explanations for this observation:

- The occurrence of amorphous nanoparticles or nanosheets is not a necessary, i.e. unavoidable, step in the formation of $NaTi_3O_6(OH) \cdot 2\,H_2O$ nanotubes. However, sheets of sodium titanate (formed from the amorphous particles by continued reaction with NaOH) are most likely a necessary prerequisite for the formation of nanotubes. Due to the high surface energy of the nanosheets, which is caused by dangling bonds, [30] they roll up to form nanotubes. If this widely accepted mechansim for the nanotubes formation is considered, this explanation seems unlikely.

- Since the "0 min sample" exclusively consists of nanotubes, it is possible that the reaction already proceeded beyond the point of the occurrence of amorphous sodium titanate particles and nanosheets. "Snapshots" of the reaction during the heating ramp will be carried out to verify this assumption.

Figure 2.5 a, showing nanotubes of the "0 minute sample" reveals that they are very polydisperse if one considers the length of the tubes.

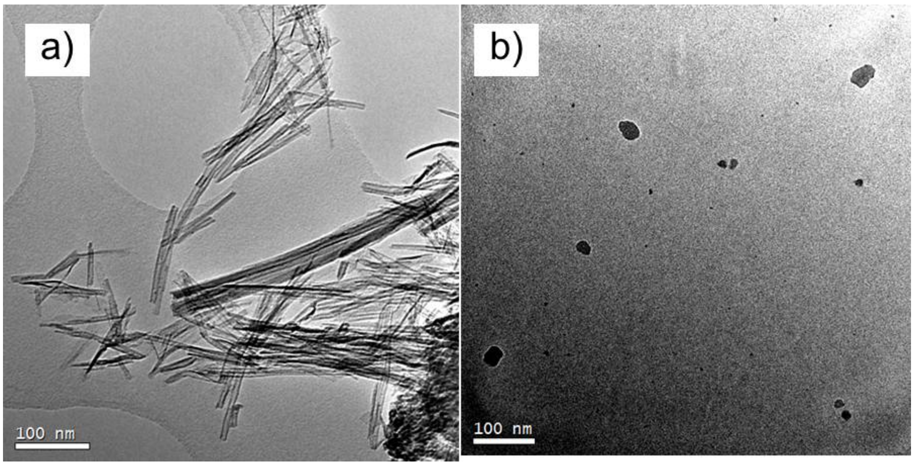

Figure 2.5: a) TEM image of isolated nanotubes in the "0 minute sample" b) TEM image of "NaO" particles.

The shortest tubes are around 30 nm long, while the length of the longest ones can reach up to several hundred nanometers. The diameter of all tubes on the other hand is around 10 nm, no matter how long they are. Additionally, no change in diameter is observed throughout the entire reaction. In Figure 2.5 b small particles are shown, which are present throughout the entire progress of the reaction. It is noteworthy that these particles are only observable when Gold TEM grids are used. The particles are roundish and the diameter ranges from a few nanometers up to 30 nm. EDX analysis (see section 2.3.3) revealed that these nanoparticles do not contain titanium, only sodium and oxygen are found. A quantification of the sodium to oxygen ratio was not possible due to the weak signal of the oxygen in EDX. Since the exact composition of these particles cannot be determined, they will be referred to as "NaO" particles from now on. However, it is likely that the "NaO" particles are in fact sodium carbonates, i.e. $NaHCO_3$ or Na_2CO_3. The reaction was not carried out in a controlled atmosphere, i.e. a contamination with CO_2 is bound to occur, before as well as during the reaction. The same observations were also made by other groups.[35]

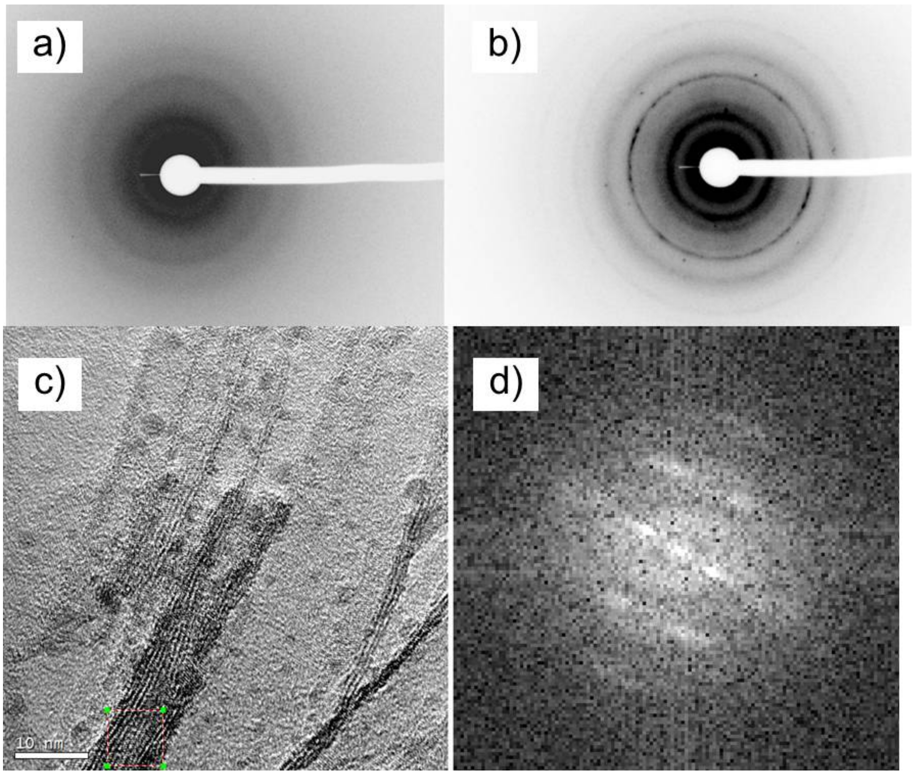

Figure 2.6: "0 min samples": a) SAED on agglomerates of nanotubes b) SAED on isolated nanotubes c) HRTEM image of nanotubes and d) the corresponding Fourier transform showing a d-spacing of 6.5 Åbetween the layers of the structure.

Selected area electron diffraction (SAED) was performed on agglomerates of nanotubes and on isolated nanotubes. The results presented in Figure 2.6 a and b show that the agglomerates as well as the single tubes have a similar d-spacing, suggesting that both consist of the same material, i.e. nanotubes of the same composition.

The tubes are nano-crystalline (compare Figure 2.6 c) and their d-spacing was found to be between 6.5 Å and 7 Å (see igure 2.6 d), which most likely represents the distance between the titanium-oxygen layers. The mismatch between the d-spacing of different nanotubes can be explained by their low crystallinity, which was already observed in XRD measurements. The measured d-distances cannot be matched to any known phase of sodium titanate or TiO_2, including the final product $NaTi_3O_6(OH) \cdot 2\,H_2O$.

Together with the EDX analysis (see section 2.3.3), which confirms the presence of sodium, titanium and oxygen in the nanotubes, and the results obtained from X-ray diffraction, in which the reflection could neither be assigned to any known compound, this suggests that an hitherto unknown phase of sodium titanate, which is only found in tubular nanoparticles, is formed at the beginning of the synthesis. An identification of this phase *via* automated diffraction tomography [31] is the subject of ongoing research. Snapshots of the reaction after 1 and 3 minutes do not show any significant difference to the "0 min sample". The length and diameter of the nanotubes did not change, just slightly more isolated nanotubes were found. The bigger part of the sample still constitutes of large agglomerates of nanotubes.

"5- 10 minute samples"

After a reaction time of 5 minutes the sample still mostly consists of agglomerated and isolated nanotubes (see Figure 2.7 a and b). Neither the agglomerates nor the nanotubes exhibit a significant change in size, compared to the earlier samples. It is noteworthy that the amount of isolated nanotubes was further increased in the "5 min sample". The same trend was already observed for the "1 and 3 minute sample", as compared to the "0 min sample".

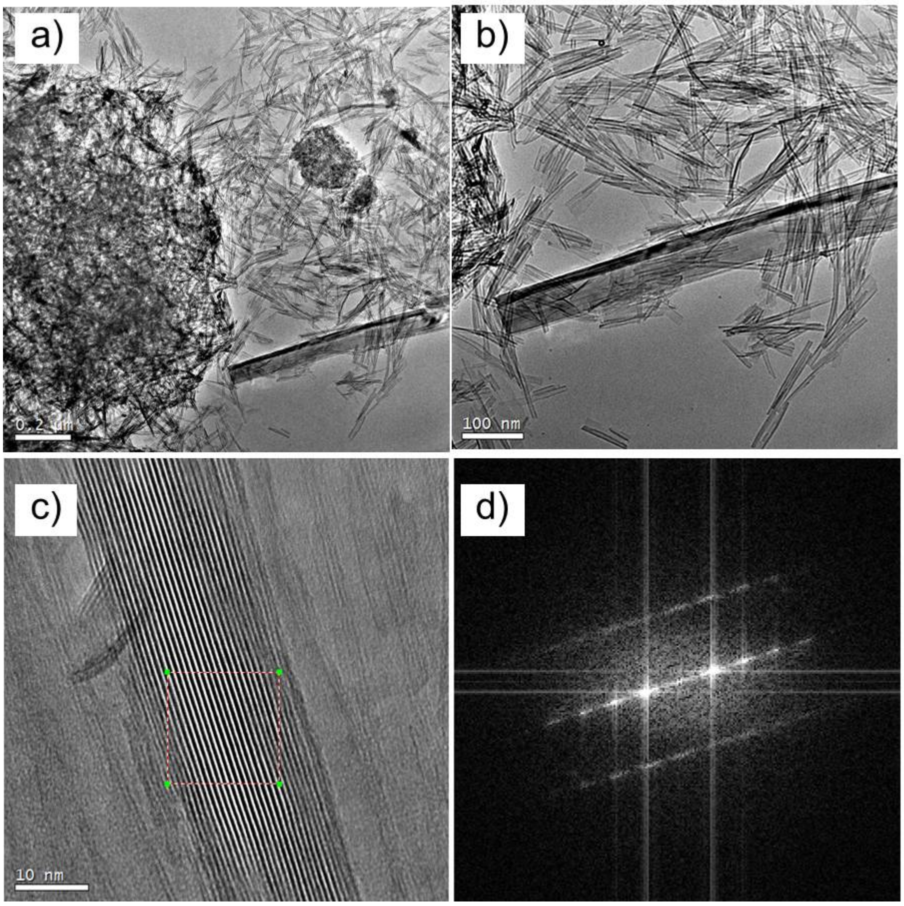

Figure 2.7: "5 min sample": a) and b) overview TEM images c) HRTEM TEM image of a nanosheet/nanowire d) Fourier transform corresponding to the HRTEM image in c).

After 5 minutes anisotropic structures other than tubes are observed for the first time. These objects are probably nanosheets since their contrast in TEM is rather low, indicating that they are rather thin. Figure 2.7 c shows the HRTEM image of such a nanosheet; the corresponding Fourier transform can be seen in Figure 2.7 d. The d-distances found correspond well with the d-spacing of the final product $NaTi_3O_6(OH) \cdot 2\,H_2O$; clearly indicating that the nanosheets are a thin version of the final product, i.e. $NaTi_3O_6(OH) \cdot 2\,H_2O$ nanowires. The d-spacing represents the distance between the titanium-oxygen layers. In this early stage of the reaction, the disorder in the material is very high, which is indicated by a streaking of the reflections in the Fourier transform of the HRTEM image in Figure 2.7 d. The amount of the nanosheets found is rather low, which explains why they cannot be detected in XRD. Additionally, they are only found in the immediate proximity of nanotubes, which can be seen as a first indication that the tubes are needed for the growth of the nanosheets or wires, respectively. The second indication is the appearance of the sheet-like structures only after a certain amount of nanotubes exists in an isolated form. Even at this early stage, the diameter of the nanosheets can already reach up to 80 nm. At the same time, the size and crystallinity of the nanotubes remains unchanged. SAED and HRTEM show the same d-spacing as observed before.

When the reaction is allowed to progress for 10 minutes the amount and size of the nanosheets increases drastically. In Figure 2.8 a and b multiple "nanosheets" of diameters up to 100 nm are shown. Additionally, the contrast of most nanosheets is significantly higher at this point of the reaction. From now on it is justified to refer to them as "nanowires", which in fact means a thicker nanosheet. The length of the wires reached several micrometers, yet multiple significantly shorter wires are found as well. The combination of all three observations shows that the sheets/wires grow in all directions at the same time (diameter and length), while they show a preferred growth direction leading to the anisotropic shape. Single nanotubes and agglomerates of tubes are still present in the sample, while their amount begins to decrease due to the formation of the nanowires. The size of the tubes, on the other hand, remains unchanged. HRTEM and Fourier transforms of HRTEM images still confirm the results discussed for the "0 min sample". At this point it can be stated that the tubes do not undergo any morphological or chemical changes after their formation, until they are transformed into nanowires; i.e. the tubes solely serve as a reservoir for the growth of the nanowires.

Figure 2.8 c and d show that nanotubes are located at the borders and tips of the forming nanowires. This observation points to an oriented attachment mechanism, where chemically similar surfaces approach each other to form chemical bonds.[30] The tubes are unfolded at the edges of the nanowires; the large amount of small tubes thus leads to the formation of bigger wires. In the "5 min sample" there were already indications for this behavior, the nanosheets only formed near non-agglomerated nanotubes. Completely isolated nanowires were not found.

It is noteworthy that the as-formed nanowires are not porous from the beginning (see Figure 2.8 d and e), as opposed to the results of Huang *et al.*,[30]. They found that the tubes form wire like structures *via* oriented attachment, but these structures were porous in nature. According to Huang *et al.* the pores were later filled with amorphous sodium titanate particles from the reaction mixture. Based on the findings presented here, this mechanism seems unlikely, since no amorphous sodium titanates are found in the reaction mixture before the first wires appear. It should be mentioned that the experimental conditions used here were different from the conditions used by Huang *et al.*, so it is possible that deviations arise from that factor. Especially the use of microwave irradiation instead of a conventional oven may lead to variations in the reaction progress.

The overall crystallinity of the nanowires increases with advanced reaction duration (see Figure 2.8 e and f), which is probably due to annealing effects. However, multiple defects could still be observed, such as stacking faults or bent layers, compare Figure 2.8 e.

The growth of larger particles at the expense of smaller ones is called Ostwald-ripening. Nanowires are formed from nanotubes because they are the thermodynamically more stable form [36], which is mostly due to the lowered surface energy of the bigger and non-porous structure. Phase changes, that are observed at the transformation from multiple tubes to a single wire in this study, are not normally observed in an Ostwald-ripening process. As previously discussed, the growth of the wires also shows characteristics of an oriented attachment mechanism. However, also the oriented attachment mechanism is not commonly associated with phase changes. So far, neither one of the aforementioned mechanism nor a combination of both can completely explain the growth of the nanowires, since a phase change occurs during the growth of the nanowires. Still characteristics of both well known growth mechanisms can be observed, which will be discussed in detail in section 2.3.4.

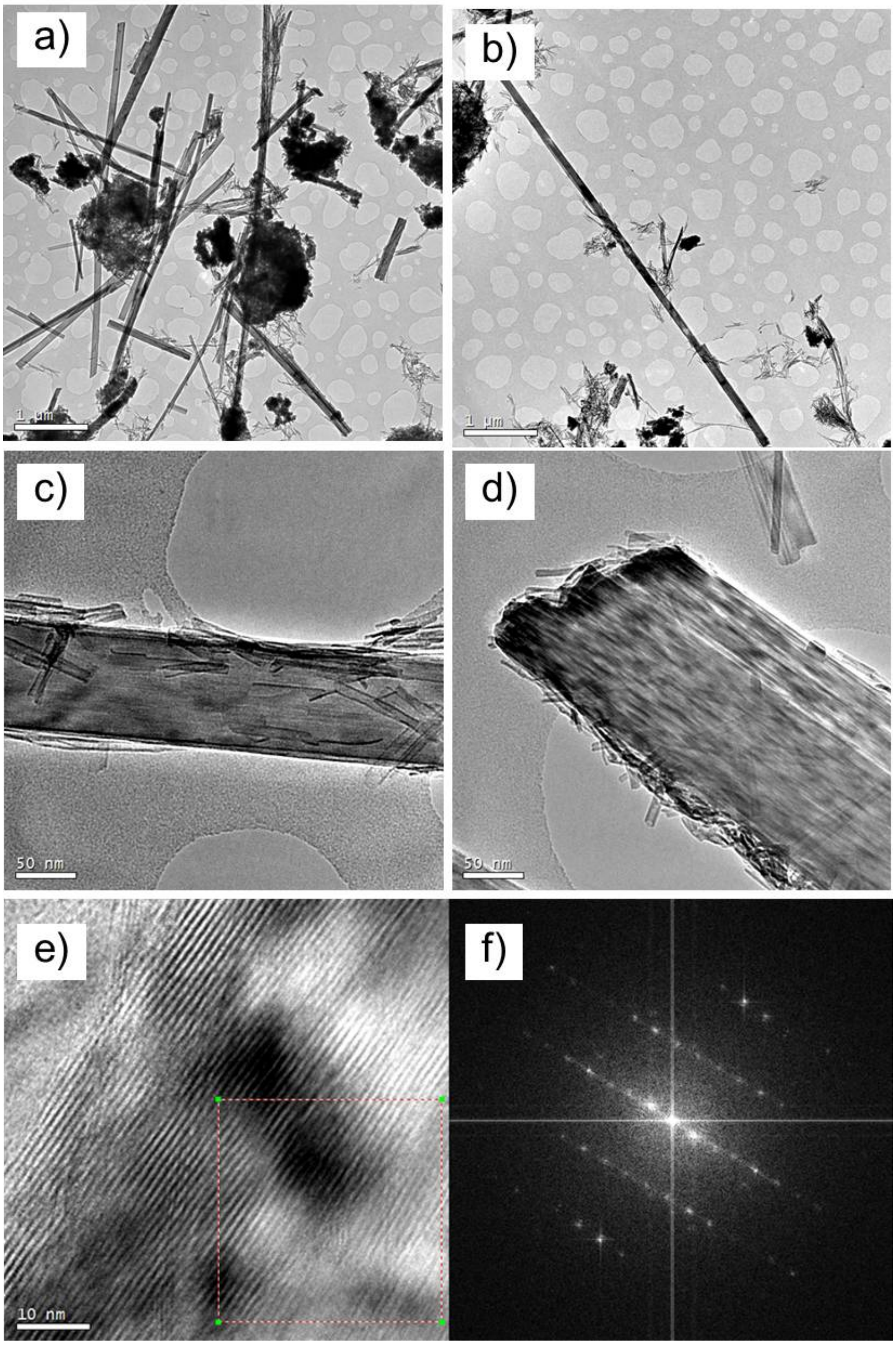

Figure 2.8: Various TEM and HRTEM images of the "10 min sample": a) and b) Overview TEM images c) and d) TEM images showing the presence of nanotubes at the borders and tips of the nanowires e) HRTEM image of a nanowire and f) the corresponding Fourier transform.

"20-120 minute samples"

By allowing the mixture of TiO_2-P25 and 10 M NaOH to react for 10 more minutes (yielding to an overall reaction time of 20 minutes), the amount and size of the wires was further increased (see Figure 2.9). Diameters of up to 200 nm are now found, which is shown in Figure 2.9 a and b. The wires are still polydisperse, while the longest ones reach lengths of up to several micrometers, significantly shorter wires, with length below 500 nm, are also found. The growth process of the nanowires is still far from completion, isolated nanotubes and agglomerates of tubes are still abundantly found (compare Figure 2.9 a and b).

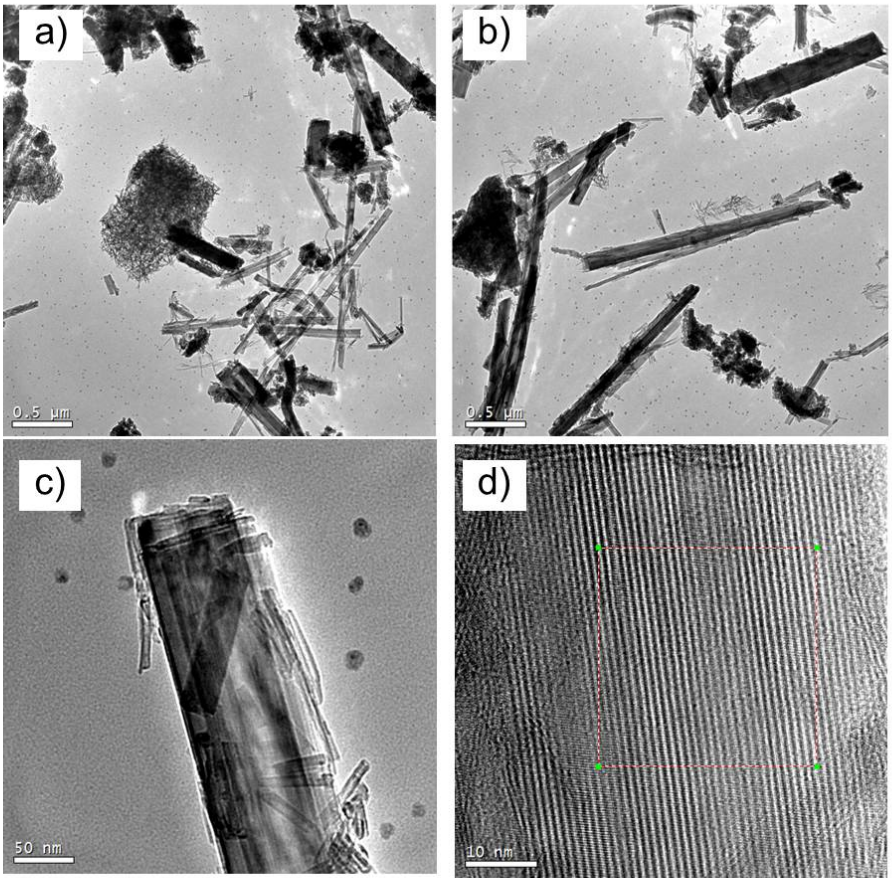

Figure 2.9: TEM and HRTEM images of the "20 min sample": a) and b) overview TEM images c) TEM image showing the presence of nanotubes at the borders and tips of the nanowires, recorded on a Gold-grid d) HRTEM image of a nanowire.

It is noticeable that fewer isolated nanotubes are observed at this stage of the reaction, which means that the nanotubes are consumed by the nanowires more rapidly than they can be replaced *via* diffusion. Hence, a more effective separation of the nanotubes would be desirable to ensure a shorter reaction time and a more homogeneous growth of the nanowires.

The image in Figure 2.9 c was recorded on a Gold TEM grid, which explains the observation of the aforementioned "NaO" particles, i.e. most likely sodium-bicarbonate and carbonate nanoparticles. Figure 2.9 c also shows the presence of nanotubes at the tip of the nanowire, an observation that was already made in the earlier samples. The disorder in the nanowires decreases further, which becomes evident from the HRTEM image in Figure 2.9 d. It should be mentioned that the nanowires are not single crystalline, even if the disorder has decreased. The defects mentioned above are still present, just to a lower extent.

For the "30, 60 and 90 minute samples" the reaction proceeds in the way described above. More wires of a larger size were found while the amount of isolated tubes decreased, until no more can be found after 60 minutes. However, the agglomerates are still present, even in the "90 min sample". These findings are in agreement with the observations discussed above.

Figure 2.10 a shows the sample after 120 minutes. The sample almost exclusively consists of nanowires. Their diameter can reach up to 400 nm for single nanowires and even more for agglomerated ones. The length can be as high as 10 micrometers in a few cases, while the majority of the wires is 500 nm to a few micrometers long.

Very few agglomerates consisting of nanotubes can be found after 2 h reaction duration (see Figure 2.10 b). While few are observed, their presence again shows the slow conversion of the nanotubes that are located in agglomerates. Only nanotubes separated from these accumulations contribute to a swift growth of the nanowires.

HRTEM images in Figure 2.10 c and d show an increasing order in the nanowires. The aforementioned defects (stacking faults and bent layers) are still present, but to a limited extent. The observation can be attributed to an annealing of nanowires in the solution upon prolonged exposure to heat. This finding is in agreement with the work of Andrusenko *et al.* [31] Additonally, an evaluation of the Fourier transform of the HRTEM data yields d-values that are consistent with crystal structure of $NaTi_3O_6(OH) \cdot 2\ H_2O$ and thus confirm the XRD results. Both the crystallinity and the amount of the nanotubes is too low, to allow a detection *via* XRD. It can be stated that the reaction is nearly complete after 2 h, a much shorter reaction time, compared to a conventional synthesis in a furnace using a stainless steel autoclave.

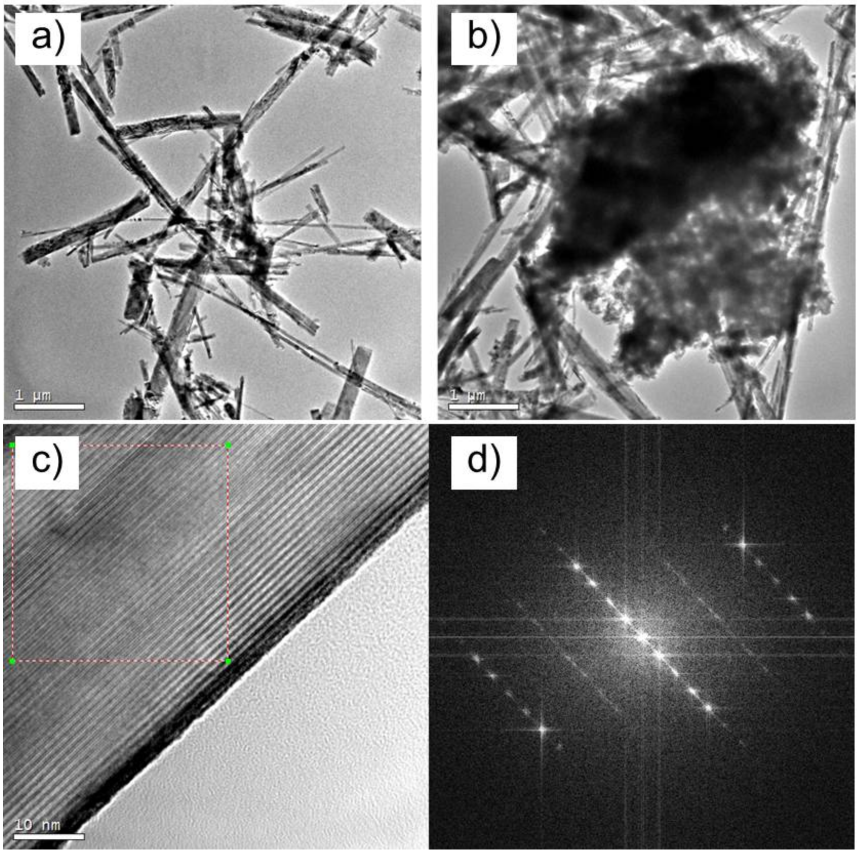

Figure 2.10: TEM and HRTEM images of the "120 min sample": a) and b) overview TEM images c) HRTEM image of a nanowire and d) the corresponding Fourier transform.

2.3.3 EDX

EDX was performed on all four nanostructures that are found during the course of the reaction.

- "NaO" particles, which are most likely sodium-bicarbonates or carbonates
- Agglomerates of nanotubes and isolated nanotubes
- Nanosheets/Nanowires

As mentioned earlier, the "NaO" particles are only visible, if a Gold TEM grid is used. These particles are found in each sample that was investigated in course of this study. They originate from a CO_2 uptake of the strongly basic solution from the ambient atmosphere. Since the mixture is continuously stirred during the entire reaction (including the heating ramp), it is reasonable to assume that the CO_2 is completely absorbed while the sample is being heated. The reaction vessel is sealed, meaning only CO_2 that was already inside the vessel before the reaction can be assimilated. The deprotonation of the carbonic acid that follows the CO_2 uptake is is a very quick process in the caustic NaOH solution, meaning that after a short time the "NaO" particles are formed completely. A participation of the carbonates in the reaction is neither anticipated nor observed, so they remain unmodified in the mixture the entire time. Due to the low solubility of sodium-bicarbonate or carbonate in methanol,[37] they could not be removed by the washing process. A quantification of the sodium to oxygen ratio was not possible due to the low contrast of oxygen in EDX.

A quantification of the sodium to titanium ratio is difficult on copper TEM grids, due to a line overlap of the Na K-series (from 1040.98-1071.1 eV) and the Cu L-series (929.7-949.8 eV). For the same reason the "NaO" particles were not visible on copper TEM grids. Hence Gold TEM grids were used in order to quantify the sodium to titanium ratio. It was stated earlier that the agglomerates consist of nanotubes with the same crystallographic phase as the isolated nanotubes. EDX was used to determine the sodium to titanium ratio of both species. Throughout the entire synthesis this ratio was constantly at a value of 1:4 for agglomerates and isolated nanotubes, demonstrating once again that the nanotubes and agglomerates do not undergo any changes in chemical composition during the course of the reaction. These results are also in good agreement with the HRTEM and SAED data discussed above and they further consolidate the assumption that the nanotubes indeed exhibit an hitherto unknown phase of sodium titanate.

The sodium to titanium ratio for the sodium titanate nanowires was found to be 1:2 for all nanowires investigated, irrespective of the reaction progress. From the formula of the final reaction product, i.e. $NaTi_3O_6(OH) \cdot 2\,H_2O$, one would expect a ratio of 1:3. The overestimation of the sodium content in the sample was also observed by Andrusenko *et al.* It can be partially explained by the presence of residual NaOH nanoparticles that were not completely removed by the washing process. More importantly, an excess of Na^+ ions may be bound to the surface of the nanowires, an observation already made by Nagase *et al.* [38] and also Meng *et al.*[39] Additional sodium cations may also be present in between layers of the structure, which would also be an explanation for the disorder found in late samples and the final product. Considering these arguments it is reasonable to assume that the sodium content is also overestimated in case of the nanotubes, but due to the missing crystal structure of the nanotubes the extent cannot be determined. However, no sodium titanate with a sodium to titanium ratio as low as 1:4 is not known, let alone one with an even lower sodium content. Such low sodium contens only occur in partially ion exchanged sodium titanates, which is an unlikely explanation in a strongly caustic reaction medium. However, XRD shows a very broad reflection around $2\theta = 10^\circ$ (compare Figure 2.2) for the samples containing only nanotubes, which is characteristic for sodium titanates.

The results presented here can only be interpreted in terms of a phase change upon the transition from nanotubes to nanowires, which accompanies the morphological change. The nanotubes do not simply unfold to form sheets and later wires, this process is accompanied by a "NaOH uptake". Apparently, NaOH in the solution undergoes a reaction with the already formed sodium titanate nanotubes, thereby forming a compound with a higher amount of sodium, i.e. $NaTi_3O_6(OH) \cdot 2\,H_2O$. No tubes are formed by $NaTi_3O_6(OH) \cdot 2\,H_2O$, it rather crystallizes in a sheet like morphology. *Via* an oriented attachment of nanotubes onto the sheets, wires are formed later during the reaction. The clear difference between the crystal structure and the chemical composition of the nanotubes and nanowires, which is observable for each of the aforementioned nanostructures until the end of the reaction, allows to conclude that the "NaOH uptake" is a necessary and thus unavoidable step in the formation of sodium titanate nanowires.

2.3.4 Discussion of the Growth Mechanism

The growth process of $NaTi_3O_6(OH) \cdot 2\,H_2O$ nanowires was elucidated with respect to both morphology and crystal structure of the final product and the intermediates. Four stages of growth were identified:

1. Conversion of the precursor: Complete conversion of the crystalline TiO_2-P25 precursor into sodium titanate nanotubes, which are present mostly in form of agglomerates. The tubes are formed by breaking of Ti-O bonds due to the NaOH; a sodium titanate of an unknown composition and crystal structure is formed. However, it can be stated that the sodium content of the nanotubes is lower than for any known sodium titanate.
2. Oriented attachment phase: The number of isolated nanotubes increases and the first sheets are formed; they posses a crystal structure and a composition that differs from the one of the nanotubes. The sheets are formed upon an oriented attachment of the sodium titanate nanotubes, followed by a chemical reaction with NaOH to form a phase that is sodium rich, compared to the tubes.
3. "Ostwald-ripening phase": Sheets grow to form wires, which become larger in course of the reaction, at the expense of smaller isolated nanotubes; their number decreased in this phase. The term Ostwald-ripening can only be applied for the already existing wires; even in this phase a formation of new wires occurs, a process that is not taking place in the definition during the Ostwald-ripening process. However, the term helps to describe the growth mechanism of the nanowires.
4. Slow growth and re-crystallization: No isolated nanotubes are present anymore, the growth process is limited due to the diffusion of single tubes from the agglomerates and thus slows down. The number of agglomerates of nanotubes decreases, yet they do not completely vanish even after a reaction time of 120 minutes. Annealing of the $NaTi_3O_6(OH) \cdot 2\,H_2O$ nanowires takes place in-situ during the reaction.

The growth process shows that it does not make sense to separate the morphological changes from the changes of the crystal structure (and thus composition) of the occurring species during the reaction. Each change in the morphology is directly linked to a change of the samples' composition. The precursor consists of TiO_2 as an anatase/rutile phase mixture in the form of nanoparticles with a diameter in the range of 20-40 nm. The highly concentrated NaOH-solution breaks bonds in TiO_2-P25 to form sodium titanate nanotubes. Due to the rather rapid transition, the exact nature of this process remains unknown. Sodium titanate sheets are possibly formed from the particles, which roll up to develop nanotubes. One remarkable feature of this nanotubes is the constant diameter of around 10 nm. This finding cannot be explained solely with the proposed roll-up of sheets. Knowing the crystal structure of the tubes may shed light on the mechanism of this transition.

The as formed nanotubes, as well as the $NaTi_3O_6(OH) \cdot 2\,H_2O$ nanowires and the TiO_2-P25 nanoparticles, have a strong tendency to form agglomerates. However, this tendency is especially pronounced in the case of nanotubes. It was found that in order to form nanosheets, and later nanowires, isolated tubes are a necessity. After the formation of the first nanosheets/nanowires, the tubes can be attached to the wires' edges *via* oriented attachment. The transition from nanotubes to nanowires is accompanied by a chemical reaction of the sodium titanate nanotubes with NaOH in solution, increasing the amount of sodium in the nanowires. The exact nature of the reaction cannot be determined until the crystal structure of sodium titanate nanotubes is resolved. Although the nanowires grow in all directions (thickness, diameter and length increase in course of the reaction), the growth along the Ti-O layers is strongly favored due to the higher binding energy of the Ti-O bond, as compared to the Na-O bond, which would favor a stacking of layers. Thus the preferred growth direction of the nanowires is oriented along the layers of the interconnected TiO_6 octahedra. This also explains the large number of nanotubes found at the tip of the nanowires. The first nanowires are possibly formed in a similar fashion. Non-agglomerated sodium titanate nanotubes are accumulated to each other *via* oriented attachment; preferably at the tips of tubes; and they unfold to form non-porous sheets *via* a chemical reaction with NaOH.

No changes in the crystal structure or chemical composition of the nanosheets/ nanowires was found after their first formation. The wires simply grow on expense of the isolated nanotubes and the wires' crystalinity is enhanced *via* an in-situ annealing process. The process can be seen as Ostwald-ripening; the wires do have the smaller surface energy due to their size, as compared to the nanotubes. However, an Ostwald-ripening process is commonly not accompanied by a phase change of the species involved. Possibly the wires are not only the thermodynamically favored phase due to their lower surface energy, but also due to an energetically favored crystal structure. This can again only be verified if the crystal structure of the sodium titanate is resolved. No evidence is found for the growth of smaller nanowires on cost of bigger ones, despite the observed differences in size. The driving force in this case could only be the reduction of the surface energy, since the composition of the wires cannot be changed. Apparently this driving force is too small, which can be ascribed to the relatively large size of the nanowires and/or missing energy gain from the change of the crystal structure. As mentioned earlier, the term Ostwald-ripening may not be applied to this stage in its' literal meaning, since no sign for a halt of the nanowire formation is found until the end of the synthesis. However, the term helps to illustrate the growth of wires after their formation.

The last -and slowest- phase of the nanowire growth starts after all isolated nanotubes have been consumed for the formation of nanowires. The consumption of nanowires is apparently kinetically favored compared to the seperation of nanotubes from the reservoir, i.e. the agglomerated nanotubes. No sheet formation is observed within the agglomerates themselves, which is most likely due to the random attachment of the nanotubes and a hindered percolation with the NaOH solution necessary to promote the conversion. An effective separation of the agglomerates during the synthesis may enhance the reaction velocity at this stage, on the other hand the oriented attachment of the nanotubes may be prevented in an earlier stage, if, for example, ultrasonication is used to separate the agglomerates during the synthesis.

The results obtained in this study differ from results found by other groups. Huang *et al.* determined the formation of sodium titanate nanotubes as a necessary prerequisite for the growth of sodium titanate nanowires.[30] In earlier studies the formation of either sodium titanate nanotubes or nanowires was believed to be temperature-dependent.[40] At temperatures below 180°C nanotubes were obtained, while nanowires were formed at higher temperatures. The findings of Huang *et al.*, namely the dependence of the obtained reaction product on the advancement of the reaction, were confirmed herein. The mechanism of the nanowire formation and the relationship between the morphology and the crystal chemistry was found to be different from the results published to date. A possible reason for the differences found are the applied reaction conditions, like the precursor used or the concentration of the NaOH solution and especially the use of the use of a microwave-assisted synthesis. While these parameters do only have a small influence on the final product of the reaction,[41] there may well be an influence on the reaction mechanism. In order to thoroughly investigate the complete growth mechanism of the sodium titanate nanowires, these influences need to be investigated more intensely.

2.4 Conclusion and Outlook

2.4.1 Conclusion

$NaTi_3O_6(OH) \cdot 2\,H_2O$ nanowires were synthesized *via* a microwave-assisted hydrothermal reaction. The use of the microwave not only accelerated the reaction and led to a more time- and energy-efficient synthesis, but also renders it possible to quench the reaction at any given point, which allows for the investigation of intermediates in the reaction progress and thus an elucidation of the growth mechanism of $NaTi_3O_6(OH) \cdot 2\,H_2O$ nanowires. For that purpose TEM, HRTEM, SAED and XRD were applied after various times during the synthesis. It was found that not only the morphology of the intermediates must be considered to reveal the growth mechanism, the crystal structure and thus composition of the intermediates is of equal importance. Four different stages of growth could be identified. First, the crystalline TiO_2-P25-Precursor is rapidly transformed into sodium titanate nanotubes. These nanotubes mostly form agglomerates and they represent an hitherto unknown phase of sodium titanate, which does have a comparably low amount of sodium incorporated within the structure. The tubes are then partially separated from the unordered agglomerates and they can now form nanowires *via* an oriented attachment mechanism followed by a chemical reaction with the NaOH in the solution. In this process $NaTi_3O_6(OH) \cdot 2\,H_2O$ is the reaction product, a phase containing more sodium, as compared to the nanotubes. The wires grow *via* the same mechanism, their crystal structure remains unchanged during the advancing reaction. This process is related to the so called Ostwald-ripening. The nanowires grow at the expense of the smaller nanotubes. Later in the reaction, the number of isolated nanotubes decreases and thus the reaction progress is slowed down. The remaining agglomerates now only slowly release nanotubes that can be utilized for the continued growth of the nanowires. At the same time the already existing nanowires are sintered in-situ and thus become more ordered during the course of the reaction. However, single crystalline nanowires could not be obtained.

2.4.2 Outlook

A more detailed investigation of the early stages of the reaction will be necessary to elucidate the formation of the nanotubes from the precursor. Along with that, the crystal structure of the sodium titanate nanotubes needs to be determined. Based on this information the formation of sodium titanate nanotubes with the defined diameter of 10 nm might be explained. Additionally, the chemical reaction that is necessary for the formation of the nanowires may be clarified. The influence of the experimental conditions on the reaction mechanism needs to be determined, in order to explain the different findings by several groups. Finally, an investigation of the optical proper- ties of both sodium titanate nanotubes and nanowires will be helpful to determine the usefulness of the synthesized materials, for example for the application in dye-sensitized solar cells.

CHAPTER 3

Dye-Sensitized Solar Cells with Nanoparticle/Nanowire Composite Electrodes: Influence of Different Nanowires on the Preparation of the Photoanode and the Device Performance

3.1 Introduction

In the past two decades dye-sensitized solar cells (DSSCs) have been investigated extensively due to their interesting features, such as high power conversion efficiency (approx. 12 %,[42], low-cost and facile fabrication as well as interesting processing options.[4] In DSSCs the front electrode, or photoanode, consists of conductive glass; commonly fluorine doped tin oxide (FTO); on which a thin film (approx 6-15 micrometers) of interconnected TiO_2 nanoparticles (NPs) is coated. A dye is adsorbed on the surface of the TiO_2 nanoparticles. When excited by visible light, an electron can be injected from the excited state of the dye into the conduction band of the TiO_2. Ideally, the electron then travels through the entire film and reaches the front electrode.

The most widely used type of DSSC is based on a liquid electrolyte, in which case a redox mediator such as I-/I_3- dissolved in acetonitrile is used to reduce the dye back to its ground state [43]. Based on this mechanism the photoanode needs to fulfill two requirements:

1. Large surface area to ensure high dye absorption, leading to high absorption and thus a high short circuit current (J_{sc}).
2. Fast Electron conduction with little losses, to ensure a complete "harvest" of the generated electrons.

These requirements are counteracting, since a large surface area usually leads to a high number of electron traps, e.g. particle-particle boundaries. The use of one dimensional TiO_2 related nanomaterials, such as nanowires (NWs) or nanotubes (NTs), is a possible strategy to overcome this problem [44]. These structures are known to have a larger electron diffusion coefficient and a longer electron lifetime as compared to TiO_2 nanoparticles [45]. However, using nanowires or nanotubes as the only material in a DSSC leads to a decreased current, mostly due to a comparably small surface area and/or low packing density [46]. A possible strategy to circumvent these issues is the use of nanoparticle/nanowire (NP/NW) composite electrodes. In this type of electrode, nanowires (NWs) are mixed with nanoparticles (NPs) in order to benefit from the large surface area of the nanosized particles in combination with the enhanced electron conduction due to the NWs.

In this contribution, we report the fabrication of composite electrodes prepared from TiO_2-P25 nanoparticles and different kinds of nanowires. The nanowires were synthesized via a microwave-assisted hydrothermal reaction, which offers several advantages over the standard hydrothermal treatment in steel autoclaves. The reaction time was significantly reduced from at least 24h in a conventional reaction [29] to 2h in the microwave assisted reaction. Additionally, the cooling and heating cycles are much shorter in microwave-assisted reactions. Heating is rather rapid due to the direct response of the solvent to the microwave radiation, i.e. the reaction vessel does not have to heat up first. Cooling times are reduced due to the low heat capacity of the reaction vessel, compared to conventionally used stainless steel autoclaves. Another noteworthy fact is the smaller environmental impact of microwave assisted reactions, which benefits the energy payback time of the final device. Three different kinds of nanowires, namely sodium titanate ($NaTi_3O_6(OH) \times 2H_2O$) (NaTN), hydrogen titanate (HTN) and TiO_2 nanowires were synthesized in this study and utilized as a material for composite electrodes. The nanowires (NWs) were characterized using X-ray powder diffraction (XRD) and transmission electron microscopy (TEM).

A simplified method for the preparation of the so called semiconducting paste was developed, requiring less processing steps and only small amounts of nanoparticles and nanowires. In the process it was found that both the ratio of nanoparticles to nanowires; i.e. the total amount of nanowires; as well as the chemical nature of the NWs strongly influences the viscosity of the paste. Consequently, tailor made pastes were prepared for the three different kinds of nanowires to ensure high film quality and comparable film thicknesses. The photoanodes were investigated by means of scanning electron microscopy (SEM), Brunauer-Emmett-Teller (BET) analysis, additionally the film thickness was determined by laser microscopy (LM).

First TiO_2 nanowires were used to determine the ideal ratio between nanowires and nanoparticles in a composite electrode. It was found that photonaodes containing 5 wt% NWs yielded the highest current densities and thus the highest efficiencies. In a second step, all three different kinds of nanowires were incorporated into the composite electrodes at the same ratio (5 wt%) and their performance was compared. Interestingly, the use of sodium titanate nanowires lead to an increased open circuit voltage, while the overall performance was inferior, compared to the reference electrode. Hydrogen titanate as well as TiO_2 nanowires on the other hand significantly increased the short circuit current of the DSSCs thus leading to an increased device performance, while the detected changes in open circuit voltage (Voc) were rather small. The use of HTN nanowires led to the highest short circuit currents. The reasons for this behavior were investigated. The photovoltaic performance of the composite electrodes in DSSCs was determined using current-voltage (IV) characteristics and incident photon to current conversion efficiency (IPCE). Further characterizations, such as electrochemical impedance spectroscopy (EIS), intensity modulated photovoltage and photocurrent spectroscopy(IMVS and IMPS), photoelectron spectroscopy and charge extraction measurements were performed in order to further elucidate the differences in device performance.

3.2 Experimental Section

3.2.1 Materials and Synthesis

Materials: All materials were used as received, no additional purification was performed. TiO_2-P25 nanoparticles were purchased from Degussa. The 10 M NaOH solution was made from NaOH pellets (98.5 %, p.A., Acros Organics) and MilliQ water (18 MΩ·cm). Methanol was obtained from J.T. Baker (99.8 %, p.A.). 0.5 M HCl was made from conc. HCl (Analytical reagent grade, Fisher Scientific) and MilliQ water. Ethanol (p.A.) was purchased from Carl Roth and VWR. PEG 400 (BioUltra) and PEG 20000 (BioUltra) were obtained from Sigma Aldrich. A 0.1 M solution of Ti(IV) bis(ethyl acetoacetato)-diisopropoxide (TAD, >95 %, ABCR) was made with 1-butanol (99,5 %, p.A.) obtained from Acros Organics. Chemicals used for the fabrication of solar cells included MPII (1-methyl-3-propylimidazoliumiodide, Sigma Aldrich), LiI (lithium iodide, Sigma Aldrich), I_2 (iodine, Sigma Aldrich), N719 (Solaronix), tBP (4-tertbutylpyridine, Aldrich), and GuSCN (guanidiniumthiocyanate, Sigma). Acetonitrile and t-butanol were obtained from Sigma-Aldrich.

Synthesis: The synthesis was carried out using a MARS Xpress microwave digestion system (CEM Corporation). The procedure derived from the work published by Kasuga *et al.* [27] was modified concerning temperature control and proportions of the substances used, in order to be applicable for the reaction system.

Sodium titanate nanowires: In a typical synthesis 500 mg of TiO_2-P25 powder were mixed with 50 ml of a 10 M NaOH solution by vigorous magnetic stirring for 15 min in a 100 ml Teflon liner. Afterwards the vessel was sealed and subjected to hydrothermal treatment in a microwave oven. The reaction mixture was heated for 10 min until an internal pressure of 20 bar was reached. The pressure was kept constant for 2 h. Due to the technical limitations of the microwave reaction system a direct measurement of the reaction temperature was not possible under these reaction conditions. The maximum energy output was set to 800 W. When the reaction was finished, the mixture was allowed to cool down radiatively for 30 min. Subsequently, the supernatant NaOH solution was removed by centrifugation (9000 rpm, 10 min) and the samples were washed repeatedly with methanol until a neutral reaction of the supernatant solution was reached. Finally, the samples were dried in vacuum overnight.

Hydrogen titanate nanowires: Hydrogen titanate nanowires were synthesized using sodium titanate nanowires as a precursor. The latter were synthesized as described above, but the sample processing was modified. Instead of methanol, the nanowires were washed with 0.5 M HCl until acidic reaction of the supernatant solution. Afterwards the NWs were neutralized by repeated washing with water. Finally the nanowires were dried under vacuum overnight.

TiO_2 nanowires: In this case, hydrogen titanate nanowires were synthesized as described above, and the NWs were calcined at 600 °C for 4 h to ensure a complete conversion from hydrogen titanate to TiO_2.

3.2.2 Materials Characterization

X-ray powder diffraction: X-ray powder diffraction data were collected using a Bruker-AXS D8-Discover diffractometer equipped with a HiStar detector in reflection geometry using graphite-monochromated CuKα radiation. Samples were glued on top of glass and (111) silicon substrates using a VP/VA copolymer (vinylpyrrolidone/vinylacetate).

Electron microscopy: The TiO_2-P25 precursor and the nanowires were characterized by *transmission electron microscopy (TEM)* using a Philips EM420 instrument with an acceleration voltage of 120 kV. Specimens for TEM measurements were prepared from ethanolic suspensions of the samples. One drop of an ultrasonicated suspension was applied onto a Cu grid coated with an amorphous carbon layer. *Scanning electron microscopy (SEM)* was performed on the photoanode films coated on FTO substrates using a FEI Nova nanoSEM in high vacuum mode. The samples were attached to an aluminum stub using adhesive conductive carbon tape and the surface was additionally contacted using conductive copper tape, in order to avoid charging of the samples.

Laser microscopy: TiO_2 film thickness on a FTO substrate was measured with a Keyence VK-8710 laser microscope.

Thermogravimetry was performed using a NETZSCH STA 429 thermal analyzer. Roughly 50 mg of the sample was placed in a ceramic sample holder, which was covered with a ceramic cap. Gases evolving upon heating the sample were released through a hole in the ceramic cap. Data evaluation was performed with the NETZSCH Proteus thermal analysis software (NETZSCH, 2004). The sample was heated from room temperature to 1373 K at a heating rate of 1 K/min.

Dye-loading amount: In order to determine the amount of dye adsorbed within a composite electrode or an electrode consisting of NPs only, the respective films loaded with N719 dye were immersed into 10 mM NaOH for 12 h at 30 °C. Afterwards, the absorption spectra of the respective solutions were measured and the intensity of the peak in the region between 505 - 515 nm was compared to a calibration curve.

Surface area measurements: The surface areas of TiO_2 photoanodes consisting of nanoparticles exclusively or of composite electrodes were evaluated via BET analysis using a QuantaChromeAutosorb 6B instrument applying multipoint BET measurements.

3.2.3 Solar Cell Fabrication

Paste preparation: 300 - 400 mg of TiO_2-P25 nanoparticles or mixtures of these particles and the respective nanowires were mixed with 0.75 - 1.25 ml of EtOH and 30 drops of PEG 400 by magnetic stirring for 15 minutes. Afterwards, the solution was placed in an ultrasonic bath for 1 hour. Subsequently, 1 - 2 drop(s) of PEG 20.000 dissolved in water (5.5 g in 5 mL) was added and the mixture was stirred for another 15 minutes. Before doctor-blading the paste was ground for approx. 5 minutes. Experimental details are found later in the text.

Photoanode: First, a TiO_2 blocking layer of a few hundred nanometers in thickness was coated on the FTO substrates (sheet resistance 8 Ω/sq, Pilkington). A 0.1 M solution of TAD in 1-butanol was administered on the substrate by spin coating, followed by calcination at 450 °C for 30 minutes. All photoanodes were prepared by the doctor-blading method. An appropriate portion of the prepared paste was applied onto the FTO substrate. The anodes were then sintered at 450 °C for 30 min.

Dye loading: The as prepared electrodes were immersed in a 0.3 mM N719 (cis-bis (isothiocyanato) bis(2,2'-bipyridyl-4,4'-dicarboxylato)-ruthenium(II)bis-tetrabutyl ammonium, Solaronix) dye solution in acetonitrile and tert-butanol (1:1 v/v). The samples were kept in the solution for 18 h at 30 °C and then rinsed with acetonitrile and dried in a compressed air flow.

Electrolyte: The electrolyte was composed of 0.1 M LiI, 0.6 M 1-methyl 3-propyl imidazolium iodide (MPII), 0.05 I_2, 0.5 M 4-tert butylpyridine (tBP) and 0.05 M guanidiniumthiocyanate (GuSCN) dissolved in acetonitrile.

Counter electrode:A Pt counter electrode was prepared by the thermal decomposition of H_2PtCl_6. A 0.01 M H_2PtCl_6 solution in isopropylalcohol was spin coated onto a FTO substrate, followed by sintering at 450 °C for 30 min. Two holes in the Pt counter electrode for electrolyte injection were subsequently made using a drill.

Device Assembly: A Surlyn (25 μm, Solaronix) film, used as a spacer, was sandwiched between a TiO_2 photoanode and a Pt counter electrode at 90 °C using a hot press. For the last step of DSSC fabrication, the electrolyte was filled into the gap of the spacer through one of the two small holes in the Platinum counter electrode, which were then subsequently sealed by a Surlyn film and a cover glass.

3.2.4 Solar Cell Characterization

IV and IPCE: The photovoltaic performance of DSSCs based on different composite electrodes was characterized by current-voltage (IV) measurements and incident-photon-to-current conversion efficiency (IPCE). The current-voltage characterization was carried out using a Keithley Model 2400 source meter and a solar simulator with a 300 W Xenon arc-lamp (Newport) under 1 sun illumination (AM 1.5, 100 $mW \cdot cm^{-2}$). The light intensity was calibrated by a silicon solar cell (PV measurements, Inc.). A light shading mask was applied on the residual area of the front side of a FTO substrate except for an active area of 0.25 cm^2, thus preventing the overestimation of power conversion efficiency.

In addition, the quantum efficiency of DSSCs was analyzed by an IPCE device (incident-photon-to-current conversion efficiency, PV measurements, Inc.).

Photoelectron spectroscopy: The analysis of the work functions TiO_2 photoanodes and composite electrodes was performed by photoelectron spectroscopy. An AC2 photoelectron spectrometer (RKI Instruments, Inc., Japan) was used and the measurement was conducted under ambient conditions.

Electrochemical impedance spectroscopy: The interfacial properties of the different photoanodes were analyzed by electrochemical impedance spectroscopy (EIS) using an IM6 (Zahner) under dark conditions. The respective values for the open-circuit voltage were used as a bias potential between the two electrodes. The frequency was varied in a range from 1 MHz to 100 mHz, while the amplitude was fixed at 10 mV.

IMVS and IMPS: The electron diffusion coefficient and electron lifetime were obtained by IMPS (intensity-modulated photocurrent spectroscopy) under short-circuit conditions and IMVS (intensity-modulated photovoltage spectroscopy) under open-circuit conditions as a function of light intensity using a CIMPS (Controlled Intensity Modulated Photo Spectroscopy) system (Zahner). A more detailed explanation for measurements is described elsewhere. [47][48]

3.3 Results and Discussion

3.3.1 Materials

XRD: All synthesized nanowire powders were subjected to XRD-investigation; the corresponding X-ray diffraction patterns are shown in Figure 3.1.

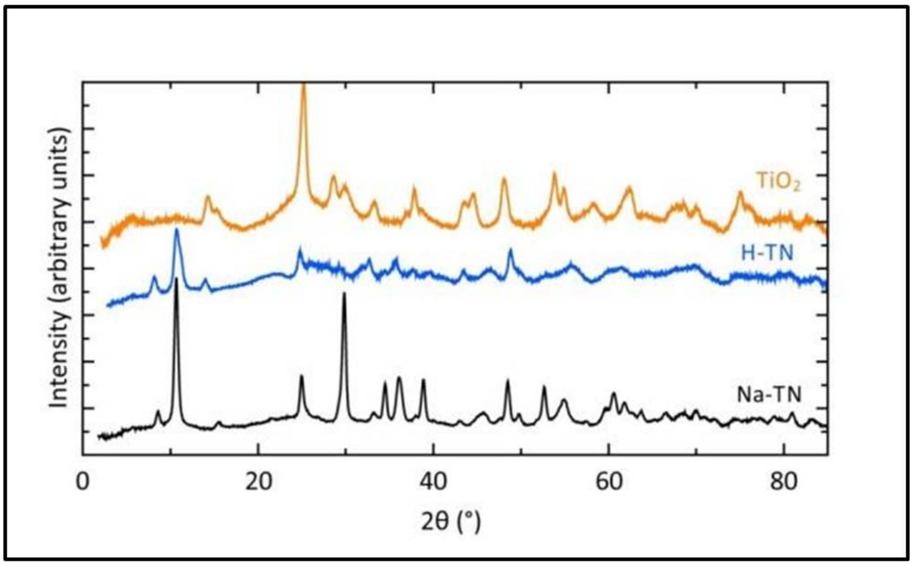

Figure 3.1: X-ray diffraction pattern of sodium titanate nanowires (black), the corresponding hydrogen titanate NWs (blue) and TiO_2 nanowires (orange).

The crystal structure of the sodium titanate nanowires was recently elucidated [31] by means of automated diffraction tomography. The NaTN NWs used in this study were made in the same way and thus possess the same crystal structure as described by Andrusenko *et al.* The composition was determined to be $NaTi_3O_6(OH) \cdot 2\,H_2O$. For clarification, the unit cell of $NaTi_3O_6(OH) \cdot 2\,H_2O$ is shown in Figure 3.2. The structure is built up from distorted $\{TiO_6\}$ and $\{NaO_6\}$ octahedra. The $\{TiO_6\}$ octahedra are connected corner and edge sharing (they can share up to 6 common edges). As a result of this connectivity, $\{Ti_6O_{14}\}^4$- complex ions form corrugated layers. In between the layers sodium ions are situated. The layered structure explains the good ion-exchange properties [26] of sodium titanates; the ions are mobile between the layers. Thus it is easy to exchange the sodium with other ions, such as H^+.

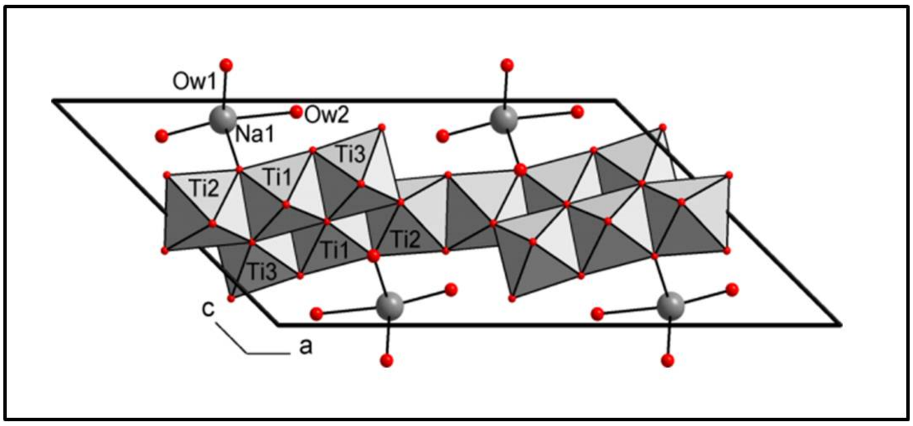

Figure 3.2: Model of sodium titanate $NaTi_3O_6(OH)$ x $2H_2O$ structure (view in [010]). H atoms are omitted for the sake of clarity. Oxygen atoms are represented in red. NaO_6 octahedra are viewed edge-on.

Additionally, electron conduction along the interconnected $\{TiO_6\}$ octahedra (which also represents the growth direction) is expected to be beneficial for electron transport. On the other hand, the NaTN NWs possess a large number of defects, e.g. layer shifts or edge dislocations, which may hinder electron conduction. The as synthesized nanowires are not single crystalline, i.e. borders between crystallites may act as electron traps as well [31]. However, nanowires made by the described method were chosen due to their extremely high aspect ratio (compare next section), which arises from a strongly favored growth in direction of the Ti_6O_{144}-layers. The explanation is the high binding energy of titanium and oxygen, especially compared to the binding energy between sodium and oxygen, which would favor a stacking of layers. The length of the nanowires roughly matches the electrode thickness, i.e. in an idealized case one nanowire can act as an "electron highway" throughout the entire nanoparticular film.

The sintering of the photoanodes during device fabrication leads to a change in the composition of the sodium titanate. The corresponding TG curve is shown in Figure 3.3. At a temperature of 450 °C the sodium titanate has released water, due to a loss of water of crystallization and condensation of titanoyl groups on the surface of the nanorods. Additionally $NaHCO_3$, which is formed due to the uptake of CO_2 from the ambient atmosphere before and after the synthesis, decomposes in this temperature range, leaving behind NaOH. The caustic impurities may be the reason for lowered dye-adsorption of the photoanodes containing sodium titanate (compare below). NaOH solutions are used to detach the dye from the photoanode when the amount of dye loaded onto the TiO_2-film is determined. The byproducts formed due to CO_2 uptake ($NaHCO_3$ and Na_2CO_3) as well as the contamination with NaOH, may also affect the quality of NaTN containing photoanodes; this phenomenon will be discussed in detail later.

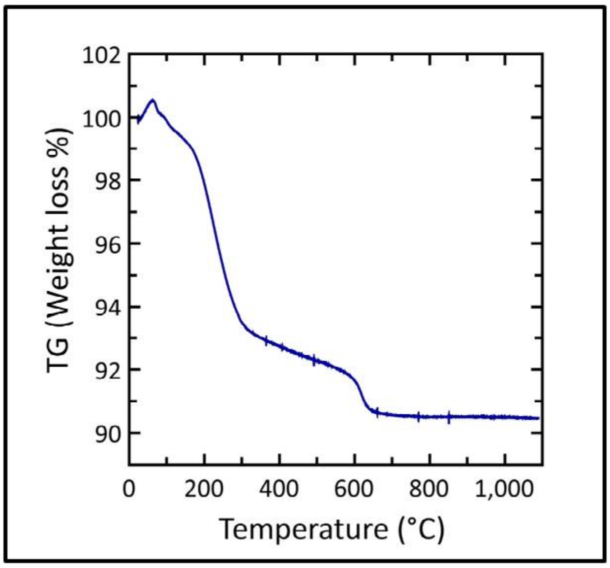

Figure 3.3: TG curve of the sodium titanate nanowires.

The crystal structure of the hydrogen titanate nanowires cannot be identified based on the X-ray diffraction data (see Figure 3.1). However, it is reasonable to assume that the sodium ions are replaced by a hydrated H^+ ion during the washing process of the sodium titanate nanowires that is carried out with diluted HCl. A shift of the reflections at 2θ ˜ 8° and 2θ ˜ 16° towards lower angles indicates a widening of the interlayer distances, which may be due to the high effective radius of H^+ caused by the hydration sphere. Anyway, the hydrogen titanate itself does not influence the cell performance. In course of the previously described cell fabrication the hydrogen titanate is transformed to TiO_2-beta, which can be seen from the X-ray diffraction pattern shown in Figure 3.4. The fact that no crystalline byproduct could be identified *via* XRD supports the hypothesis that sodium is completely exchanged with H_+. Sodium ions remaining in the structure would most likely lead to the formation of a sodium titanate as a crystalline byproduct. However, no trace of any phase other than TiO_2-beta is found. It is noteworthy that the direct incorporation of HTN NWs into the photoanodes allows omitting the final calcination step necessary to obtain TiO_2-nanowires. Among other advantages, which will be discussed below, this further reduces the energy demand for the cell fabrication.

After the calcination process the hydrogen titanate nanowires are transformed into the TiO_2-beta phase, as shown in Figure 3.1. A conversion to anatase- or even rutile phase TiO_2 would have required harsher calcination conditions. A prolonged calcination at higher temperatures has a negative effect on the morphology, i.e. the aspect ratio of the nanowires decreases due to fragmentation. Using the described mild conditions, the morphology was maintained in all three nanowire samples (see below).

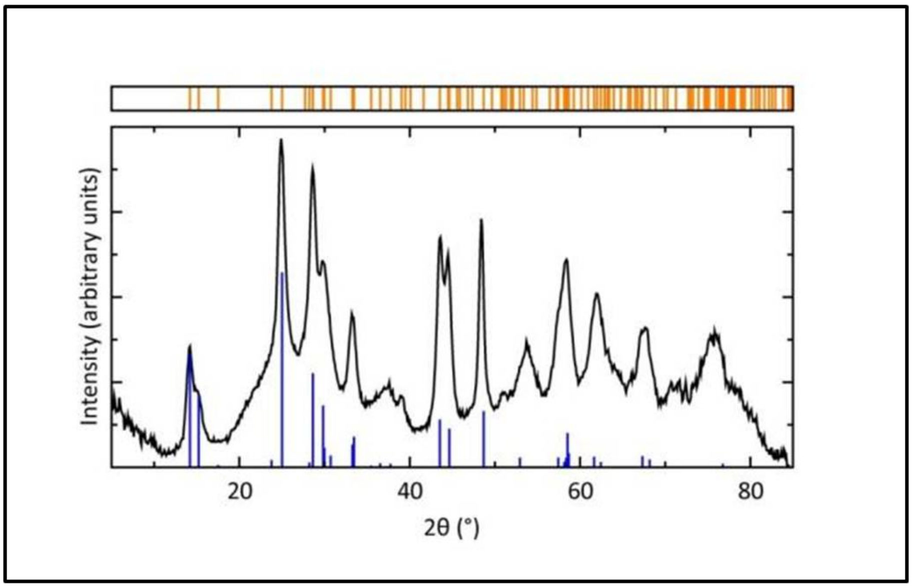

Figure 3.4: X-ray diffraction pattern of hydrogen titanate nanowires (blue) calcined under the same conditions as the corresponding photoanode. All reflections could be assigned to the TiO_2-beta phase (black).

TEM: The nanowires synthesized in this study are very polydisperse in nature (see Figure 3.5). The diameters of the wires range from 50 nm up to 1 μm. The largest diameters are only found if the nanowires agglomerate to form bundles. Single wires reach diameters up to 250 nm. The length of the nanowires also varies strongly, from 100 nm up to 10 micrometer. Some small particles of around 20 - 30 nm in size are found in the sodium titanate samples. They arise from the aforementioned impurities in form of carbonates [31], which is the reason for why they are only present in the NaTN samples. Due to the washing procedure using HCl, the carbonates are removed in the other samples. TEM images of NaTN, HTN and TiO_2-NWs show that the morphology does not change during the different processing steps. The differences in device performance should thus arise from the different chemical composition and/or crystallographic phase of the samples. Furthermore, the influence of the nanowires on the properties of the semiconducting paste contributes to alterations in device performance, as discussed below.

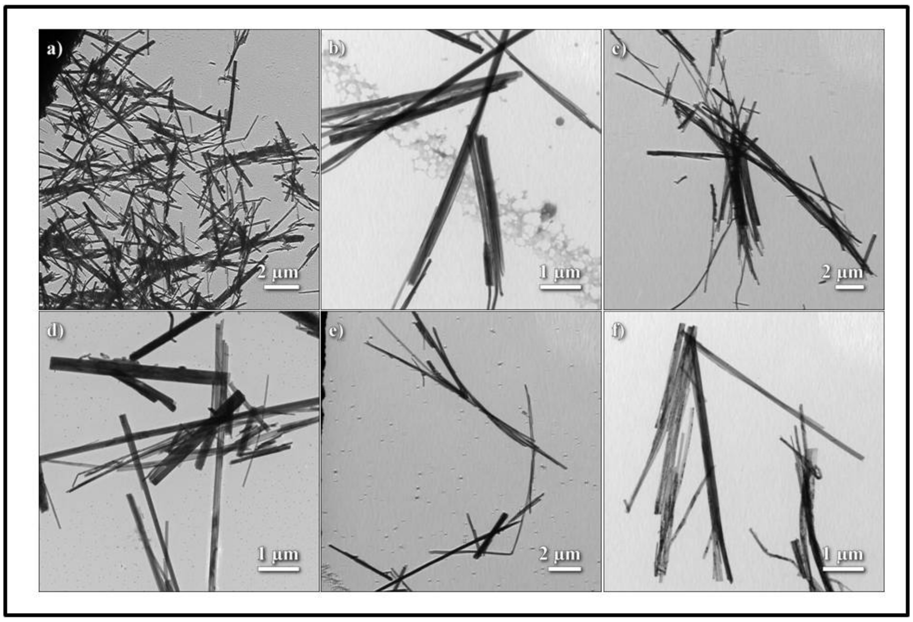

Figure 3.5: TEM images of three different kinds of nanowires: a) and d) sodium titanate, b) and e) hydrogen titanate, c) and f) TiO_2

3.3.2 Photoanodes

"TiO_2 samples": First, the ideal ratio of nanowires to nanoparticles was determined. For that purpose, electrodes with four different amounts of TiO_2 nanowires were prepared, namely 30 wt%, 20 wt%, 10 wt% and 5 wt%. These samples were compared to an electrode consisting of TiO_2-P25 nanoparticles exclusively, which was used as reference.The combined amount of nanowires and nanoparticles used to make the paste was 300 mg. For all samples (reference and samples containing nanowires) 1 ml of Ethanol, 3 drops of PEG 400 and 1 drop of the PEG 20.000-water mixture was added. Adding nanowires into to the paste led to an increase in the pastes' viscosity. While the viscosity change was moderate when 20 wt% nanowires or less were incorporated, a drastic change occurred for the paste containing 30ẇt% nanowires. Due to their size the nanowires are not as easily dispersed in the paste as the small nanoparticles, leading to the observed increase in viscosity.

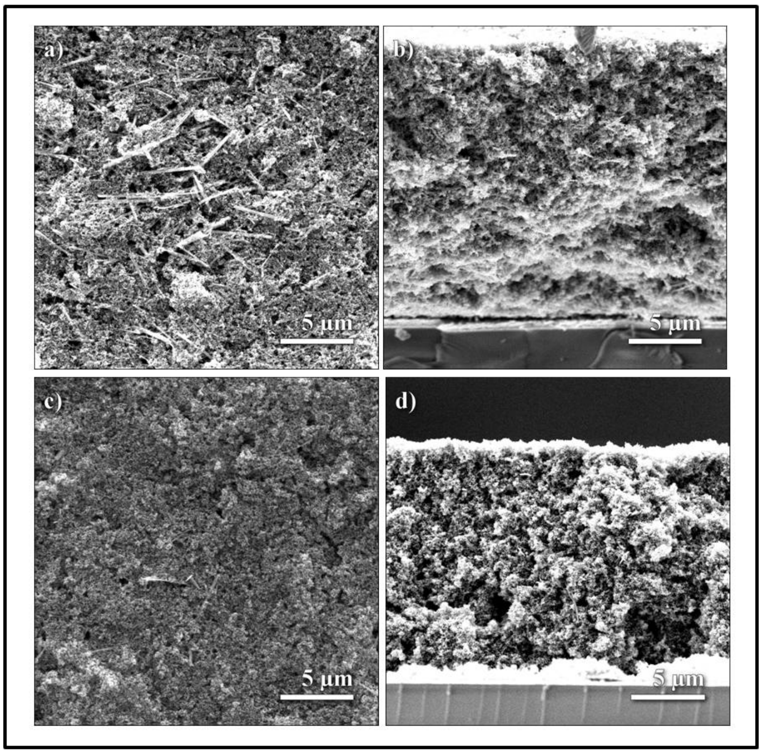

Figure 3.6: SEM images of photoanodes prepared with different amounts of TiO_2 nanowires: a) and b) 30 wt%, c) and d) 5 wt%. Top view images are on the left side, the cross-section pictures are on the right side.

Figure 3.6 shows SEM images of photoanodes with 30 wt% nanowires and 5 wt% nanowires. Images of the other samples are shown in Figure 3.7, the outcome is in line with the results presented in Figure 3.6. The overall film quality is high, the surfaces of the samples are rather even and no significant cracks or voids are visible. Agglomeration of wires on top of the film is observed for the samples containing high amounts of nanowires, shown here for the 30 wt% and 20 wt% sample in Figure 3.6 a and Figure 3.7 a, respectively. These agglomerates on the films' surface are not found for samples with low amounts of nanowires, infact little NWs are found on top these films. Nanowires on the surface of the photoanodes are not desirable since they cannot support electron conduction towards the electrode.

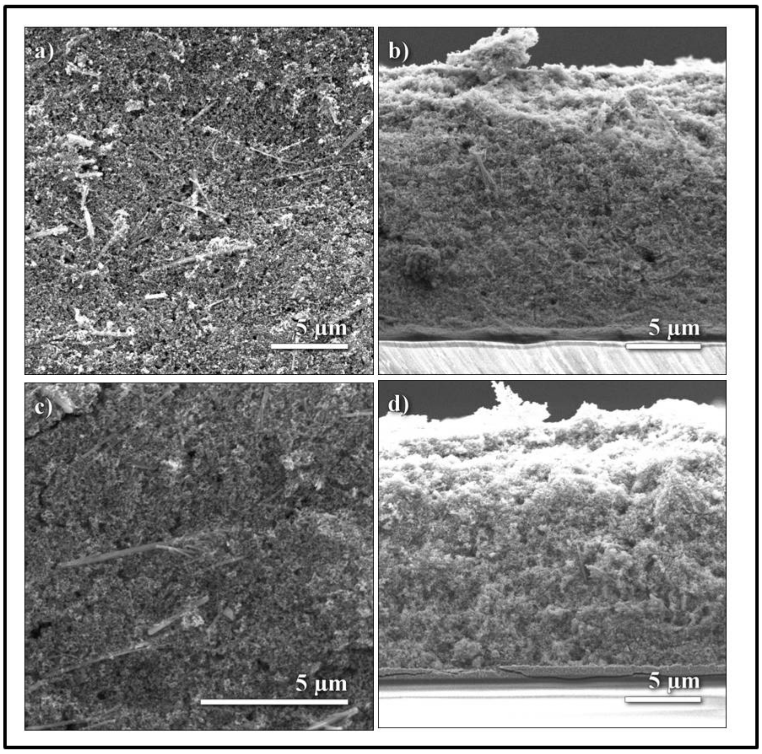

Figure 3.7: SEM images of photoanodes prepared with different amounts of TiO_2 nanowires: a) and b) 20 wt%, c) and d) 10 wt%. Top view images are on the left side, the cross-section pictures are on the right side.

From the cross-section images it can be seen that the films are flat over extended areas and that there are also no voids inside the film. Yet, the films containing TiO_2 nanowires are not completely uniform (compare Figures 3.6 and 3.8); especially with rising amount of nanowires this effect becomes more evident. While the nanowires are nicely distributed within the films in most areas (see Figure 3.6 b and d), agglomeration of nanowires occurs in others, which can be seen in Figure 3.8 b. This observation is made more often for samples containing high amounts of nanowires; additionally agglomerates in these films are larger, they can be up to a few micrometers in size, compared to below one micrometer for the films containing small amounts of nanowires (see Figure 3.8d).It should be noted that the agglomeration of nanowires inside the film cannot be completely prevented even for samples containing only 5 wt% of nanowires (see Figure 3.8d). Yet, agglomerates are rare in these samples. Apparently, the high viscosity of the pastes containing more NWs obstructs an effective distribution of the wires *via* ultrasonication or grinding.

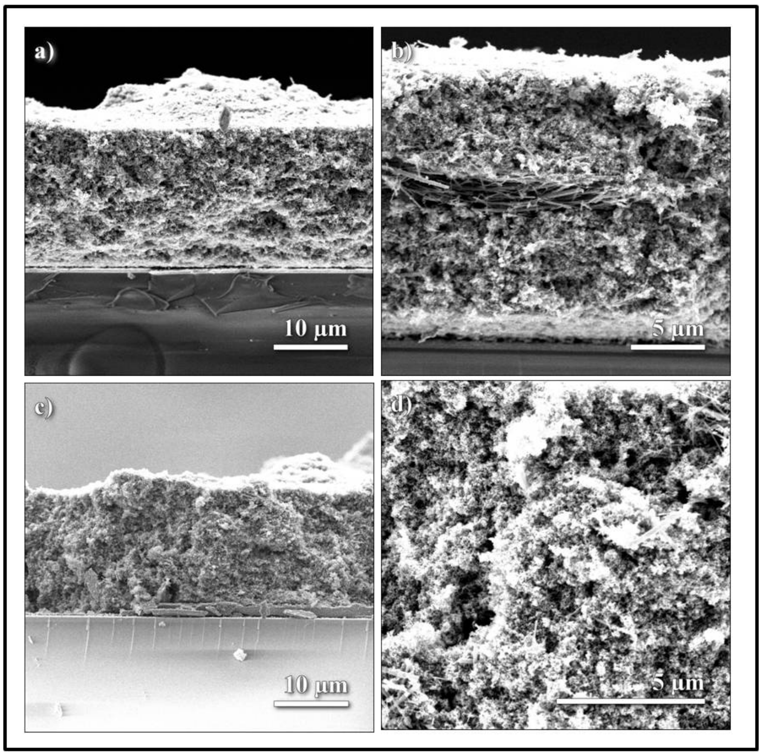

Figure 3.8: Cross-sectional SEM images of photoanodes containing different amounts of TiO_2 nanowires: a) and b) 30 wt%,c) and d) 5 wt%.

In general, it is difficult to disperse the TiO_2 nanowires in any given solvent, while for example hydrogen titanate nanowires are easily dispersed, which is shown in Figure 3.9, where TiO_2 and HTN nanowires are dispersed in ethanol. While the HTN nanowires (left) stay in dispersion for several minutes, the TiO_2 nanowires immediately precipitate. This behavior may be attributed to the calcination process, in which e.g. condensation of titanoyl groups on the surface takes place, i.e. the number of functional groups to interact with a solvent is reduced. Another phenomenon observed in samples containing TiO_2 nanowires is the formation of large "hills" found in parts of all samples (compare 3.6a and c), which is probably due to the same effect. In samples with an inhomogeneous distribution of nanowires the positive effect of the wires on the electron conduction is lowered, compared to a sample with well distributed wires. Additionally, a large amount of nanowires significantly decreases the surface area accessible for dye-adsorption. Performing the described paste preparation, no preferred alignment of the nanowires towards the electrode could be expected: Figure 3.6 and 3.8 indeed show the random orientation of the nanowires.

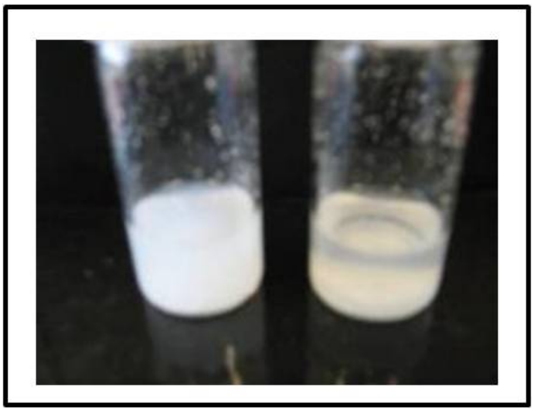

Figure 3.9: Hydrogen titanate- (left) and TiO_2 (right) nanowires dispersed in ethanol.

Different nanowires: In order to compare the performance of the different kinds of nanowires, 5 wt% of each kind was incorporated into the photoanode and compared to a sample consisting of TiO_2-P25 nanoparticles exclusively, which was used as a reference again. The corresponding SEM micrographs are presented in 3.10.

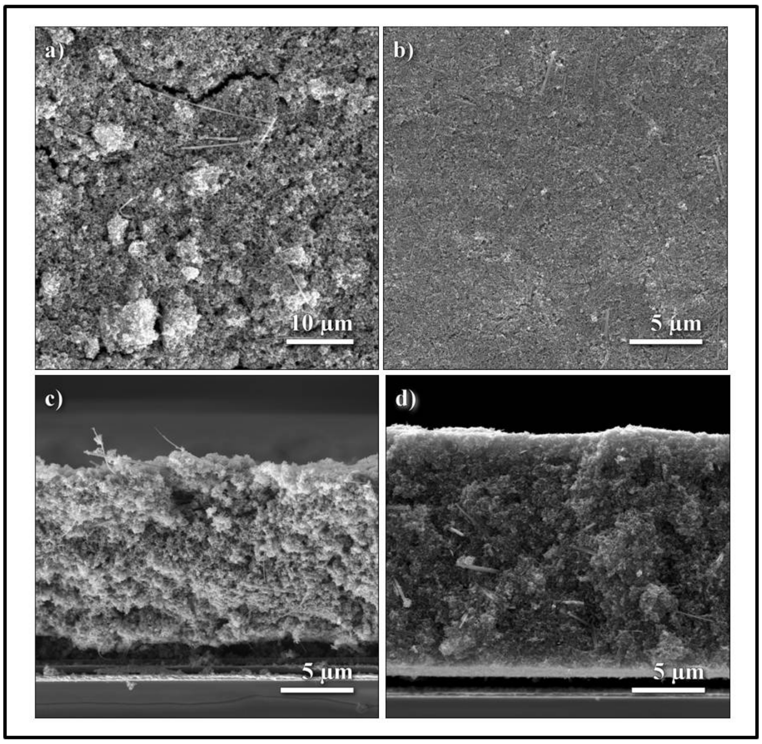

Figure 3.10: SEM images of photoanodes prepared with 5 wt% of different kinds of nanowires: a) and c) sodium titanate nanowires, b) and d)hydrogen titanate nanowires. Top View SEM images are on top, cross-sectional pictures are on the bottom.

For both the reference, as well as the sample containing 5 wt% TiO_2-NWs, 320 mg nanoparticles and nanowires combined, 1 ml of ethanol, 30 drops of PEG 400 and 1 drop of the PEG 20.000-water mixture were used. The SEM micrographs show no significant difference to the samples described above (see Figure 3.6b and d). Incorporating hydrogen titanate and sodium titanate nanowires drastically changes the viscosity of the semiconducting paste, even if only 5 wt% of the respective compound is added. NaTN NWs lead to an increase in the viscosity, which made the paste difficult to doctor-blade onto the FTO substrate. Consequently, NaTN pastes were made with more ethanol (1.25 ml), while the other parameters were kept the same. Despite the seemingly small change, the pastes made with more ethanol were of comparable viscosity as the TiO_2 samples. While facile doctor-blading was possible and film thickness control was achieved, still the surfaces of the NaTN samples are rather rough, as can be seen in Figure 3.10a and c.

Additionally cracks and irregularities are present all over the sample. The effect becomes more obvious when laser microscope images of the surface of a NaTN sample and an HTN sample are compared (see Figure 3.11) and surface profiles are obtained from these images (see Figure 3.12).

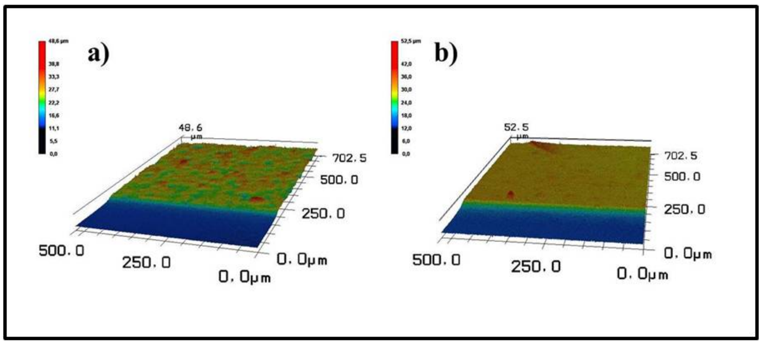

Figure 3.11: Laser microscope images of the surface of samples containing 5 wt% of different nanowires a) sodium titanate, b) hydrogen titanate.

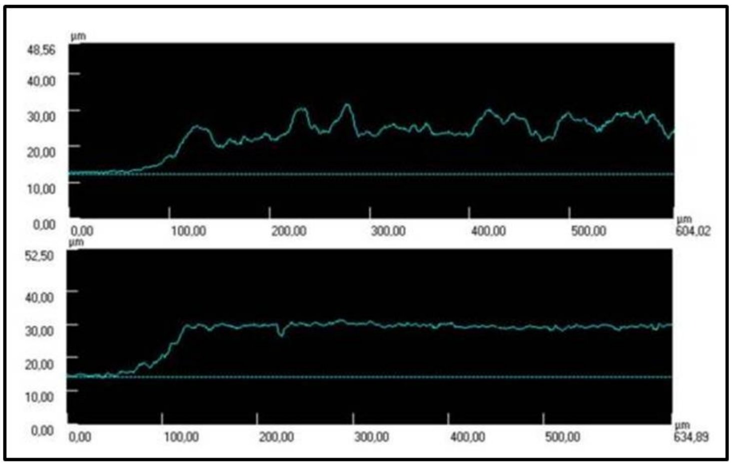

Figure 3.12: Laser microscope images of the surface of samples containing 5 wt% of different nanowires: a) sodium titanate, b) hydrogen titanate.

While the hydrogen titanate sample does have a flat surface without considerable variations in film thickness, the sodium titanate sample exhibits strong variations in thickness and an uneven surface. Immediately after coating the FTO substrate, the NaTN films look smooth and even to the naked eye; they don't show significant differences to the other samples. It is thus likely that the defects in the film arise from the sintering of the paste. A possible explanation is the presence of the aforementioned carbonate and bicarbonate impurities, which may act as "baking powder" and consequently lead to defects in the film. While these impurities could be easily removed by an acidic treatment of the sodium titanate nanowires, this would also lead to partial ion exchange in the wires themselves. In order to be able to determine the behavior of the $NaTi_3O_6(OH) \cdot 2\,H_2O$ as a compound, the acidic treatment was not performed.

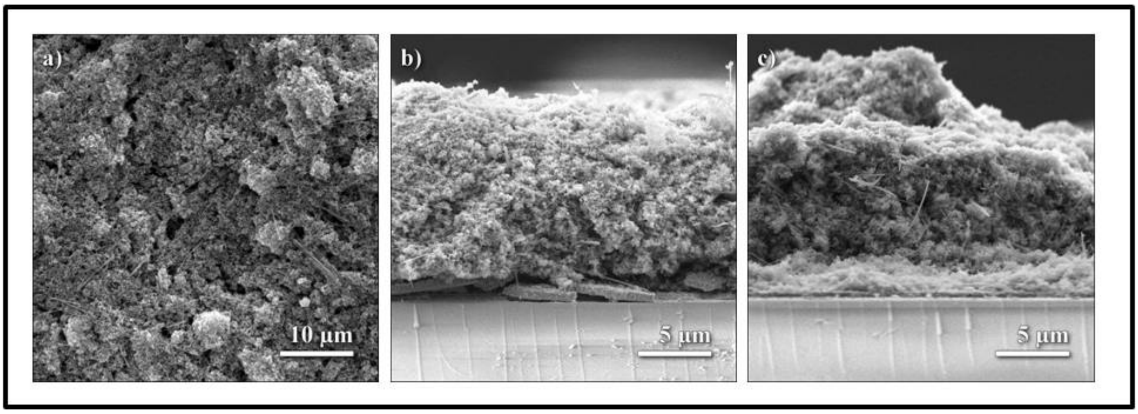

Figure 3.13: SEM images of photoanodes prepared with 20 wt% NaTN NWs: a) top view SEM image, b) and c) and cross-sectional pictures.

To verify that the effect on the film quality is really due the sodium titanate nanowires, samples containing 20 wt% NaTN NWs were prepared. The results are shown in Figure 3.13. It is clearly recognizable that the film quality further suffers from the rising amount of sodium titanate. The irregularities in the films are more abundant and pronounced. Also larger "hills", compared to the TiO_2 samples are now found in the films, which can be seen from the cross-section images. Overall this low film quality will contribute to a lower photovoltaic performance. A complete removal of the impurities before the sintering process would certainly be advantageous. Improvement of the film quality of the sodium titanate samples, while maintaining the original composition of the nanowires, is the topic of ongoing research.

The photoanodes containing hydrogen titanate nanowires possess the highest quality of all films in this study (for clarification these samples are from now on referred to as hydrogen titanate samples); however, since the films were already sintered, the nanowires were transformed to beta-TiO_2). The viscosity of the pastes decreases dramatically upon addition of hydrogen titanate nanowires. The behavior is clarified in Figure 3.14, where a small amount of hydrogen titanate- and TiO_2-paste, made with the same method, is put on two tilted microscopic slides.

Figure 3.14: Comparison of the paste viscosity, upon addition of either hydrogen titanate- (left) or TiO_2 nanowires (right).

While the paste containing hydrogen titanate nanowires flows down the glass slide, the paste containing TiO_2 nanowires remains on the same spot. If the paste is coated on FTO in this low-viscosity state, non-uniform films were obtained. Thus the HTN pastes were preparedusing 380 mg of nanoparticles and nanowires combined, additionally only 0.75 ml of ethanol were used and 2 drops of the PEG 20.000 water mixture were added, while 30 drops of PEG 400 were used as usual. This way a paste with higher viscosity is obtained.

The surface of the films achieved with this method is flat and little nanowires are found on top of the photoanodes (see Figure 3.10 a and b). The wires were nicely distributed inside the film, no agglomerates were found, which can be seen from a magnified cross-section image in Figure 3.15. This can most likely attributed due to the facile dispersion of nanowires within the paste.

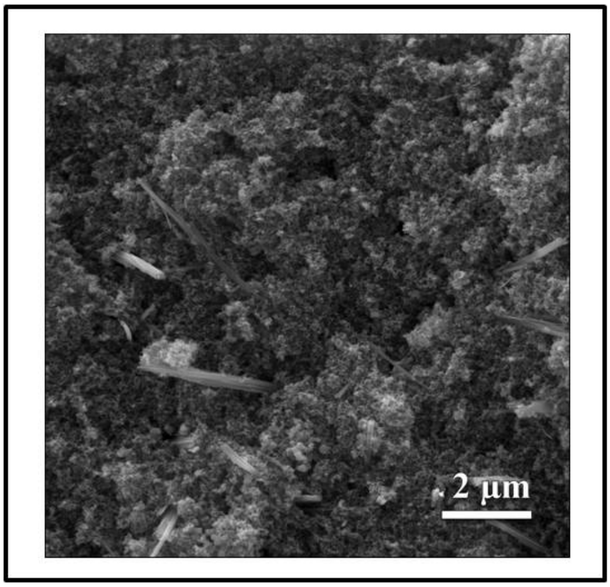

Figure 3.15: Magnified cross-sectional SEM image of a sample containing 5 wt% hydrogen titanate nanowires.

BET and Dye Loading Amount: In addition to the film quality, the surface area of the electrodes is a decisive factor for the device performance, since it directly influences the amount of dye that can be loaded onto the photoanode. BET measurements for electrodes consisting of TiO_2 nanoparticles entirely yielded an average surface area of roughly 50 m^2/g, which is in good agreement with the literature [49]. Photoanodes with 5 wt% nanowires of any kind exhibit values of approx. 47 m^2/g. The value is slightly lower than expected from geometric considerations alone.

Table 3.1: Relative dye loading amount for samples containing 5 wt% NaTN, HTN and TiO_2 nanowires compared to a reference samples containing only TiO_2-P25 nanoparticles.

Sample	Work function (eV)
Reference	1
5 wt% NaTN	0.75
5 wt% HTN	0.92
5 wt% TiO_2	0.90

It is however likely that some TiO_2 nanoparticles are bound to the surface of the nanowires after the sintering process, which causes a decrease of the overall surface area. Based solely on geometric considerations one would expect the dye loading amount to be the same for all samples containing 5 wt% nanowires. Yet, the results shown in table 3.1 reveal that the amount of dye that is adsorbed onto the samples differs from this expectation. The reference sample containing only nanoparticles does have the largest amount of dye on its surface, also the hydrogen titanate and TiO_2 samples do have an equal amount of dye loaded on them, which is slightly lower than the one of the reference. In case of the sodium titanate sample, on the other hand, significantly less dye is absorbed, which cannot be explained by geometric considerations only. Most likely the dye loading is hindered due to basic impurities in the sample. Caustic solutions are used to separate the dye molecules from the surface of the photoanodes. Another explanation is the negative surface charge of the nanowires [34], which aggravates the attachment of the carboxylic acid groups of the dye to the titanoylgroups on the surface of the NaTN nanowires.

3.3.3 Device Characterization

Determination of the ideal ratio of nanowires to nanoparticles The TiO_2 nanowires used for this study were all taken from the same batch, in order to avoid an influence due to possible differences in the synthesis. Figure 3.16 and Table 3.2 summarize the photovoltaic properties of the samples with a varying amount of TiO_2 nanowires.

Table 3.2: Photovoltaic parameters of DSSCs made with different amounts of TiO_2 nanowires relative to a reference cell.

Sample	V_{OC} **(V)**	J_{SC}**(mA/cm^2)**	(FF) Fill Factor	Eff.
Reference	1	1	1	1
30 wt% NWs	1.00	0.86	1.00	0.86
20 wt% NWs	1.03	1.01	0.99	1.01
10 wt% NWs	0.99	1.02	0.97	1.01
5 wt% NWs	0.97	1.15	0.94	1.04

Sensitizer: 0.3 mM N719 dye in acetonitrile and tert-butanol (1:1, v/v)
Electrolyte: 0.1 M LiI, 0.6 M MPII, 0.05 M I_2, 0.5 M tBP, and 0.05 M GuSCN dissolved in acetonitrile
Measured under 1 Sun condition (AM 1.5, 100 mW$\cdot$cm^{-2}) with shading masks, active area: 0.25 cm^2.

No systematic trend for the V_{oc} is visible, concerning the varying amount of nanowires. In principle a smaller V_{OC} is expected for the samples containing nanowires. The band gap of TiO_2-beta (nanowires) is smaller than the one of anatase/rutile (TiO_2-P25 nanoparticles), additionally a narrower band gap is expected due to the bigger size of the nanowires compared to the nanoparticles. However, this systematic trend was not found. The band gap difference is apparently too small to be reflected in the V_{OC} and is overshadowed by other effects. The fill factor (FF) for all samples is high, however, a systematic trend could neither be observed. The difference in FF is probably due to small variations during the device assembly process.

It is noteworthy that despite an overall lower light absorption (see Table 3.1) of the films containing nanowires, the efficiencies of samples containing less than 20 wt% nanowires still improve. Responsible for the improvement of device performance is solely the short circuit current. Due to a more rapid electron conduction in the photoanode (compare Figure 3.18 b), caused by the nanowires, a higher current can be achieved, compared to a reference cell. Hereby, 5 wt% TiO_2 nanowires was found

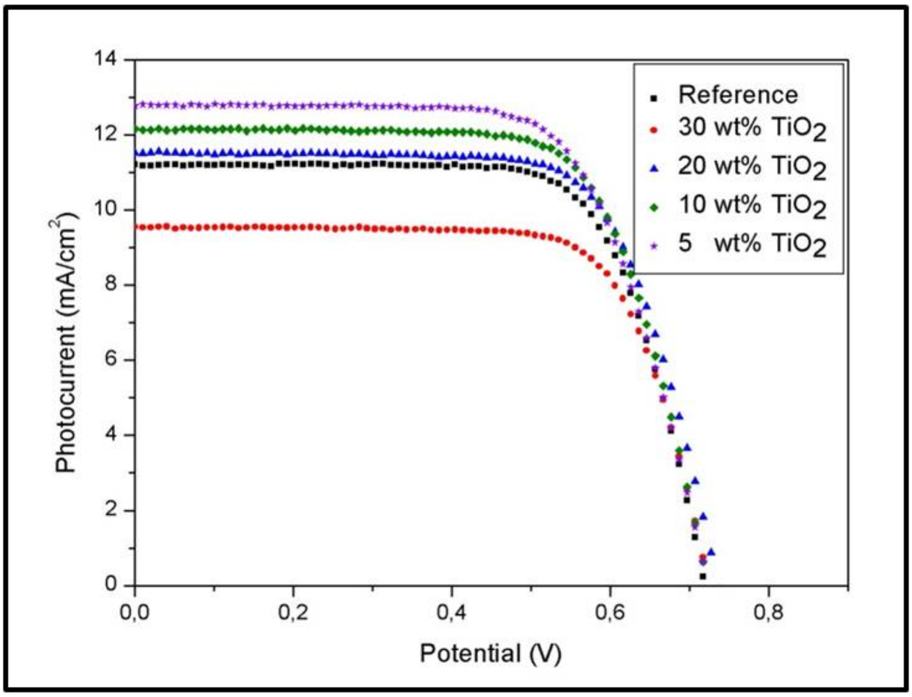

Figure 3.16: IV characteristics of DSSCs employing photoanodes that contain different amounts of TiO_2 nanowires.

to be the best ratio leading to the highest short circuit current. The low J_{SC} of the sample containing 30 wt% TiO_2 NWs can be attributed to both the low surface area of the sample leading to lowered dye-adsorption as well as the agglomeration of the TiO_2 nanowires. In summary, it was found that cells with photoanodes containing 20 wt% nanowires or less exceed the efficiency of the reference cell, while the sample containing 30 wt% nanowires leads to a lowered efficiency. The highest device performance was found for samples containing 5 wt% NWs. When the already discussed factors, such as film quality and wire distribution, as well as the surface area influencing the dye loading amount are taken into consideration, this behavior can be easily explained. These results also confirm findings of other groups [44].

Effect of the incorporation of different nanowires on the photovoltaic performance: After 5 wt% were determined to be the ideal amount of nanowires, NaTN-, HTN- and TiO_2-nanowires were incorporated in this amount. To clarify the effect of the sodium titanate nanowires, additionally a sample containing 20 wt% sodium titanate NWs was investigated. Again, all nanowires used in this study were taken from the same batch. The thickness of the films investigated here ranges from 12.5 to 14.5 μm. Figure 3.17 and Table 3.3 give an overview over the IV-characteristics of samples made with different kinds of nanowires.

Table 3.3: Photovoltaic parameters and of DSSCs made with 5 wt% of different kinds of nanowires (sodium titanate, hydrogen titanate and TiO_2) and 20 wt% of sodium titanate nanowires relative to a reference cell.

Sample	V_{OC} **(V)**	J_{SC}**(mA/cm^2)**	(FF) Fill Factor	Eff.
Reference	1	1	1	1
5 wt% NaTN	1.01	0.64	1.04	0.68
5 wt% HTN	0.99	1.23	1.00	1.22
5 wt% TiO_2	0.99	1.13	1.01	1.11
20 wt% NaTn	1.14	0.22	1.05	0.26

Sensitizer: 0.3 mM N719 dye in acetonitrile and tert-butanol (1:1, v/v)
Electrolyte: 0.1 M LiI, 0.6 M MPII, 0.05 M I_2, 0.5 M tBP, and 0.05 M GuSCN dissolved in acetonitrile
Measured under 1 Sun condition (AM 1.5, 100 mW·cm^{-2}) with shading masks, active area: 0.25 cm^2.

It can be noted that the difference in Voc is very small for the reference cell and the samples containing 5 wt% nanowires of any kind. The reasons for this behavior were discussed in the previous section. For the sample containing 5 wt% NaTN NWs, a more pronounced effect on the V_{OC} was expected, due to the large band gap of NaTN nanowires [Reference]. Again, the amount of incorporated nanowires is too small to see an effect on the V_{OC}, even for a material with a significantly larger band gap, like the NaTN nanowires (approx. 3.3-3.4 eV [50] compared to 3.0-3.2 for titania [51]). However, after increasing the amount of NaTN nanowires to 20 wt%, a significant increase of the V_{OC} is measured, as expected due to the band gap of sodium titanate nanowires. The FF, as previously observed, was not affected by the addition of nanowires of any kind in any amount. The deviations found are random and are most likely due to small variations in the device fabrication, not the materials themselves, i.e. the internal resistance of the cells is small, leading to low parasitic losses and thus a high FF.

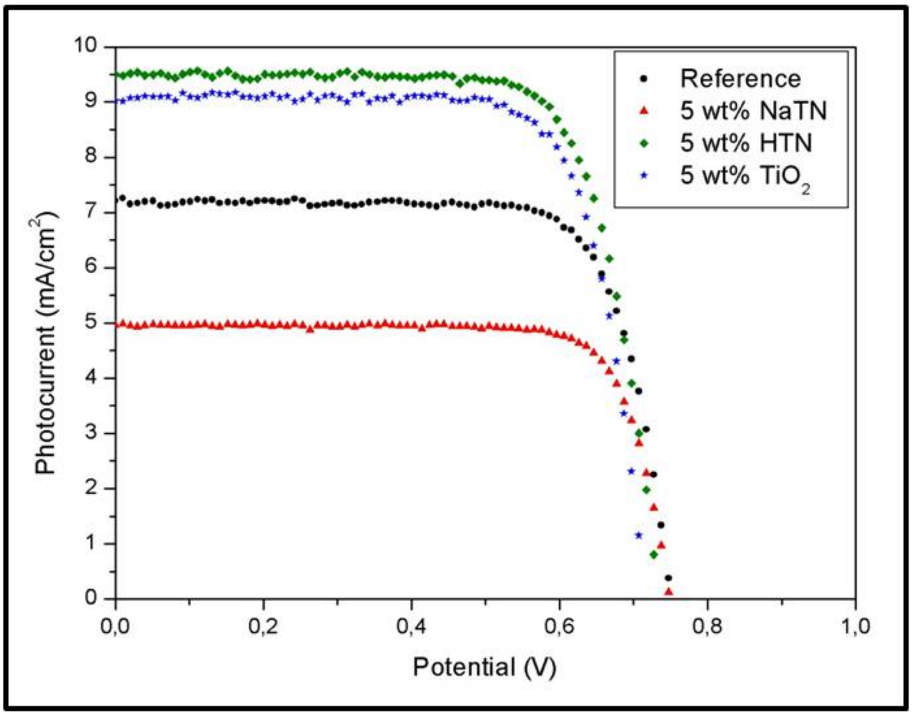

Figure 3.17: IV characteristics of DSSCs employing photoanodes that contain 5 wt% of different nanowires (sodium titanate, hydrogen titanate and TiO_2) compared to a reference cell containing only TiO_2-P25 nanoparticles

The change in efficiency can again be attributed to the change in J_{SC}. In the case of the hydrogen titanate- and TiO_2 samples the J_{SC} rises significantly, leading to a higher efficiency in both cases. The J_{SC} is the highest for the hydrogen titanate samples; the reason for the significant difference compared to TiO_2can be explained by the film quality, wire distribution and the facile processability of the semiconducting paste, as discussed above. For all samples containing sodium titanate the J_{SC} drops, with the effect being more pronounced when a higher amount of NaTN nanowires is used. The behavior can be explained based on considerations such as film quality and lower dye loading amount (compare above). Additionally the large band gap of the sodium titanate nanowires may lead to retarded electron injection from the dye into the conduction band of the NaTN, which is due to a lowered energy gain upon electron injection (see next section). The results of the IV measurements are confirmed by IPCE data shown in Figure 3.18 a.

Work function data for the samples containing different nanowires: The work function data was measured for electrodes containing 5 wt% of the different kinds of nanowires. The data obtained is consistent with the expected band gaps of the materials involved. The work function increases from 5.24 eV for sodium titanate to 5.36-5.39 eV for TiO_2 nanowires and hydrogen titanate, respectively, while the value for the reference cell is in the middle.

Table 3.4: Work functions of DSSCs employing photoanodes that contain 5 wt% of different nanowires (sodium titanate, hydrogen titanate and TiO_2) compared to a reference cell containing only TiO_2-P25 nanoparticles.

Sample	Work function (eV)
Reference	5.32
5 wt% NaTN	5.24
5 wt% HTN	5.39
5 wt% TiO_2	5.34

The relatively low work function of the NaTN sample increases the energy difference between the conduction band of the sodium titanate and the redox potential of the electrolyte, leading to an increased V_{oc}, which were observed in the sample containing 20 wt% sodium titanate nanowires. At the same time this effect may lead to a decreased driving force for electron injection, since the energy the electron gains upon injection into the conduction band of the sodium titanate nanowire is also lowered. The inverted effect is observed for the HTN and TiO_2 samples. It should be noted that the absolute differences in work functions are rather small, i.e. they are not reflected in the measured V_{OC} values because they are overshadowed by other effects.

Effect of different nanowires on the electron transport and lifetime:
The electron diffusion coefficient and the electron lifetime were determined *via* IMPS and IMVS measurements, as well as electrochemical impedance spectroscopy. The electron lifetime was significantly lowered for the samples containing sodium titanate nanowires, as can be seen from Figure 3.18b.

This behavior was attributed to the intrinsic defects of the sodium titanate nanowires themselves, as well the lowered film quality. The electron lifetime of the samples containing hydrogen titanate- and TiO_2 nanowires was slightly higher than the lifetime of the reference sample, yet the difference is rather small. The differences in the J_{SC} of the samples cannot be completely explained by the rather small increase in electron lifetime. In the case of NaTN nanowires on the other hand, the reduced electron lifetime will contribute to the decreased performance significantly. Furthermore, the same trend for the electron lifetimes was found in the electrochemical impedance spectroscopy measurements shown in Figure 3.18c.

The electron diffusion coefficient of all samples containing nanowires was significantly increased as compared to the reference sample (see Figure 3.18d). This result supports the idea behind the incorporation of nanowires, which are supposed to aid (or accelarate) electron conduction towards the electrode. This principle also works for the sodium titanate nanowires. The low performance of devices containing sodium titanate nanowires is attributed to other factors, as discussed above (Film quality, hindered electron injection, lower dye loading amount, internal defects). Improvement of the device performance using NaTN NWs seems possible if the defects in the nanowires can be cured, possibly *via* a sintering step under moderate conditions or longer ripening of the wires in the reaction solution. Additionally, a removal of the impurities in form of carbonates in the sodium titanate samples will likely lead to an improved film quality. Especially the low work function (and thus high V_{oc}) of samples containing NaTN nanowires, makes them an interesting candidate for the use in DSSCs. The highest electron diffusion coefficients were again found for samples containing hydrogen titanate nanowires, followed by the samples made with TiO_2 nanowires. This observation is once again in line with the short circuit current and the device efficiency.

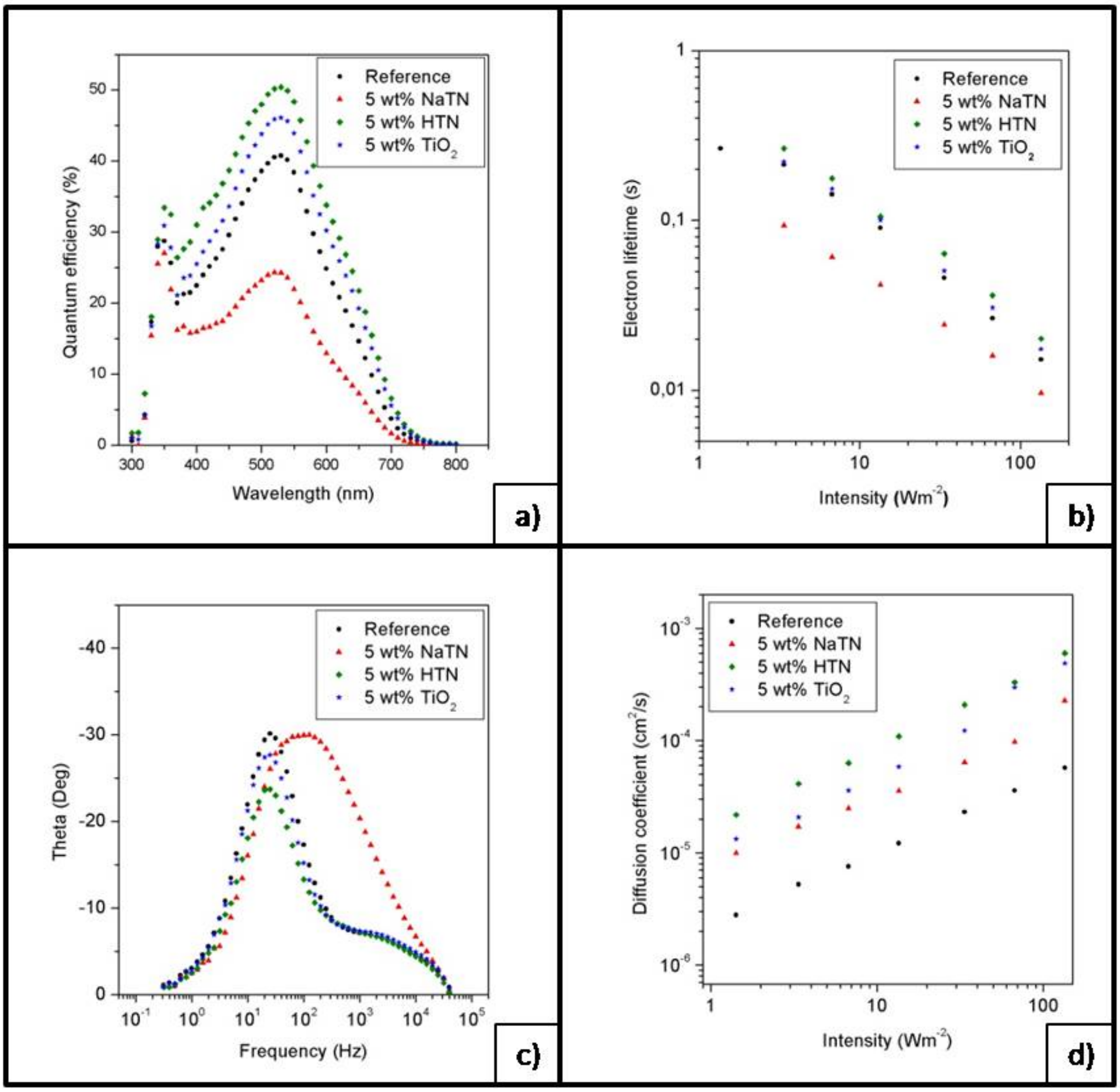

Figure 3.18: a) IPCE curves of DSSCs employing photoanodes that contain 5 wt% of different nanowires (sodium titanate, hydrogen titanate and TiO_2) compared to a reference cell containing only TiO_2-P25 nanoparticles.
b/c/d): Electron lifetime and electron diffusion coefficient of DSSCs employing photoanodes that contain 5 wt% of different nanowires (sodium titanate, hydrogen titanate and TiO_2) compared to a reference cell containing only TiO_2-P25 nanoparticles. b) The data was measured via IMVS and plotted as a function of light intensity.c) The data was measured via electrochemical impedance spectroscopy and plotted in form of a "Bode Plot". d) The data was measured via IMPS and plotted as a function of light intensity.

3.4 Conclusion

Three different kinds of nanowires, $NaTi_3O_6(OH) \times 2H_2O$, the corresponding hydrogen titanate and TiO_2 nanowires, were synthesized using a microwave-assisted hydrothermal reaction. A facile and reliable method to prepare composite electrodes from these nanowires and TiO_2-P25 nanoparticles was developed.

Two different phenomena were investigated in this study. First, TiO_2 nanowires were used to determine the ideal amount of nanowires to be incorporated into a composite electrode. It was found that agglomeration of the nanowires occurs in all experiments conducted, but the effect was most pronounced for samples containing high amounts of nanowires. While the overall film quality was high, in some areas irregularities were found. Comparing all fabricated cells, the best efficiency was obtained using 5 wt% nanowires.

In a second study, all three different kinds of nanowires were incorporated into the photoanodes and their performance in DSSCs was compared. While the incorporation of sodium titanate nanowires led to an increased viscosity of the paste, the effect was inverted for hydrogen titanate nanowires. Thus, the paste preparation was altered, in order to obtain photoanodes of a high quality for each kind of nanowires. Hydrogen titanate NWs were easily dispersible and thus yielded the photoanodes with the best distribution of nanowires and the highest overall film quality. In the case of sodium titanate, on the other hand, the film quality was rather low, which was attributed to the impurities found in the nanowires.

It was found that using both, hydrogen titanate and TiO_2 nanowires led to an increase in device performance, which was due to an improved short circuit current. It is noteworthy that HTN nanowires outperformed their TiO_2 counterparts, mostly caused by a better distribution of the nanowires, leading to a higher film quality. Compared to the photoanode consisting of nanoparticles exclusively, an increased electron diffusion coefficient was observed in all nanowire samples. The effect on the electron lifetime was rather small for the HTN and the TiO_2 samples, while using NaTN leads to a decreased electron lifetime. Incorporation of sodium titanate nanowires lead to an increase in the open circuit voltage, due to the large band gap of the NaTN nanowires. On the other hand, the J_{SC} was significantly lower compared to the other samples.

This was explained by two factors: a) defects in the sodium titanate nanowires lead to electron losses, b) the low film quality caused by impurities in the as-synthesized nanowires. These conclusions agree with the lowered electron lifetime compared to all samples, as well as a lowered electron diffusion coefficient compared to the samples containing hydrogen titanate and TiO_2nanowires.

CHAPTER 4

Synthesis of Ordered Metal Oxide Nanotube Arrays *via* Electrochemical Anodization of Titanium and Vanadium

4.1 General Considerations on the Concept "Electrochemical Anodization"

Anodic oxidation or electrochemical anodization is a versatile tool to form oxidic films on top of valve metal foils. While the technique itself has been known for almost a century, it was found rather recently that ordered arrays of nanotubes or nanopores can also be synthesized *via* anodization, if the experimental conditions such as electrolyte or anodization voltage are adjusted properly.[52] However, under most experimental conditions, solid or compact oxide layers are formed. In order to provide a more profound understanding of the mechanism involved in the electrochemical oxide growth, this introduction contains a brief explanation of the processes occuring during the anodization. This will be exemplarily shown for the case of aluminum, but the principle can be applied to other metals as well. The illustration of the mechanism was taken from Ghicov *et al.*[13]

Compact oxide films are grown *via* a so called high field mechanism. For example, titanium metal is oxidized to Ti^{4+} at the metal-(native)oxide interface and the Ti^{4+} is moved through the oxide layer aided by the the electric field. On the other hand, O^{2-}

anions will be incorporated into the oxide film; they will migrate towards the metal oxide interface. The oxide film can thus grow both at the metal-oxide interface or the oxide-solution interface, depending on the diffusion coefficient of the respective ions. The oxide growth comes to an end, due to the reduction of the electric field (and thus the driving force for the ions) caused by the growing oxide, i.e. the film thickness depends on anodization duration and voltage.

The described process leads to the formation of compact oxides, but it can be modified to yield various morphologies, ranging from random porous structures to aligned and ordered nanotube arrays. The most important parameters, that need to be considered are the electrolyte and its' pH-value, the anodization temperature and voltage as well as impurities in the material. The voltage, for example, mostly controls the tube or pore diameter, when the other experimental conditions are the same.

In the beginning of the anodization the metal is covered with a solid oxide layer. The electric field caused by the anodization voltage is not evenly distributed over the film, morphological differences lead to local fluctuations of the field, which "focuses" the electric field at certain points, resulting in field-enhanced dissolution of the oxide film at these spots. Consequently, the pore growth (i.e. oxide dissolution) reaches an equilibrium with the oxide formation and ordered arrays of nanopores are obtained. It was mentioned that the oxide growth occurs *via* a field supported migration of the respective ions. In order to induce pore growth, the metal ions need to be solvatized. In the case of the amphoteric aluminum, acidic conditions are sufficient for a dissolution of aluminum oxide. Titanium, on the other hand, is not soluble under the same conditions, thus the presence of fluoride ions, which form the water soluble $(TiF_6)^{2-}$-complex, is necessary to start the formation of pores or tubes. This consequently leads to a continuous chemical dissolution (or chemical etching process) of the as-formed oxide layer. In the case of titanium, fluoride ions can also be transported to the solid oxide due to their small size.

It should be emphasized that the presence of an "etchant" or "etching agent" such as fluoride is required for pore formation since it can partially dissolve the oxide layer under conditions that otherwise favor the formation of an oxide. In other words, the experimental parameters need to be adjusted in a way to allow simultaneous growth and dissolution of the oxidic layer. Additionally, an "oxygen source" is needed for the anodization; normally water is utilized. In the case of metals such as vanadium or aluminum, the presence of fluoride ions is not required, thus other etchants can be used. The multiple applications of the ordered arrays of nanotubes will be discussed in sections 4.3 and 4.4.

4.2 Setups for the electrochemical anodization

The design of the setup used for the electrochemical reactions is a very crucial point. While often neglected in the literature, the setup does have a huge influence on the outcome of a reaction. The most important points are the geometry of the setups and the materials they are made of. The material should be inert to the reaction solution to prevent side reactions and it has to be electrically insulating. Another important factor is thermal conductivity of the material. Depending on the setup and the reaction solution, it may not be possible to adjust the temperature of the reaction solution directly; in this case, the setup needs to have a sufficiently high thermal conductivity in order to mediate the temperature. Teflon for example is inert to virtually any reactants, but the thermal conductivitiy is very low, making a temperature control difficult, especially if strongly exothermic reactions are involved. The geometry of the setup, on the other hand, determines the diffusion of the species involved in the electrochemical reaction. Confined spaces in proximity of the anode or cathode lead to obstructed diffusion, thus slowing down or even preventing the desired reaction. Three different setups, which will be introduced in detail, were used in the course of this study.

The first setup consist of two parts (see Figure 4.1). One is a sample holder made out of teflon with a copper contact in the middle. The copper contact is located in a shallow pit, in order to avoid sample movement and to ensure reproducible sample placement. The second part is a teflon-reaction vessel or chamber, which has a 1.5 cm wide and 1 cm long cavity in the middle.

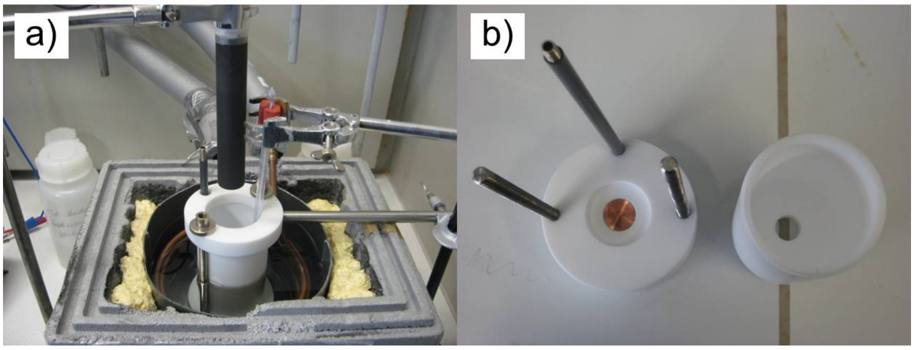

Figure 4.1: Photographs of the "Teflon-Setup" a) While in use and b) the sample holder and the reaction vessel.

The cavity forms a tube, which later leads from the sample to the rest of the reaction vessel, thus limiting diffusion by spatial confinement. After the sample is placed in the shallow pit of the samples holder, the reaction chamber is fixed on top of the sample holder. Subsequently, the desired solution is filled into the reaction vessel and finally the counter electrode is immersed into the reaction solution at a defined distance to the sample. In all setups the counter electrode was centered over the sample. Temperature control is achieved via an outside temperature bath, which is connected to a cryostat. This arrangement leads to relatively long heating and cooling times, but the setup is completely inert towards virtually any reaction solution. For simplicity, this assembly will be referred to as "Teflon-setup".

The second design is quite similar to the first one (compare Fig 4.2). It consist of a solid copper block, on which the sample is centered. A teflon reaction vessel is mounted on top of the sample. This vessel also has a 1.5 cm wide and 0.5 cm long cavity in the middle, so this setup essentially has the same geometry as the first one. Leaking of the solution is prevented with a rubber o-ring between the sample and the rection vessel. While the arrangement of the electrodes and the diffusion in the reaction vessel are very similar to the first setup, temperature control is achieved via a glass coil connected to a cryostat, which is immersed into the reaction solution allowing a rapid temperature control. However, the use of fluoride containing or basic solutions slowly leads to a dissolution of the glass coil. The coil is connected to a cryostat. This assembly will be called "Copper-setup" from now on.

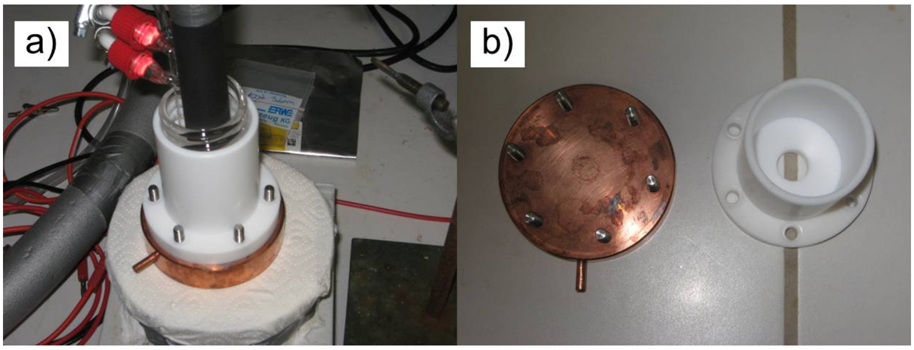

Figure 4.2: Photographs of the "Copper-Setup" a) While in use and b) the sample holder and the reaction vessel.

The third setup is a glass beaker with hollow walls as well as an in- and outlet for a liquid, whose temperature is controlled via a cryostat (as shown on Figure 4.3). The vanadium foil and the counter electrode are also facing each other, but they are arranged in a vertical manner. The distance between the electrodes needs to be controlled manually. The respective solution is filled into the glass beaker. In this case, a quicker temperature adjustment is possible, but solutions containing fluoride ions or caustic solutions cannot be used. Yet, the major difference compared to the other setups is the vertical arrangement of the electrodes and the lack of spatial confinement of the solution around the sample. This leads to unhindered diffusion; additionally debris forming on the sample during a reaction can fall off it, while the aforementioned debris stays on the sample in the other setups. The term used for this setup will be "Glass-setup" from now on.

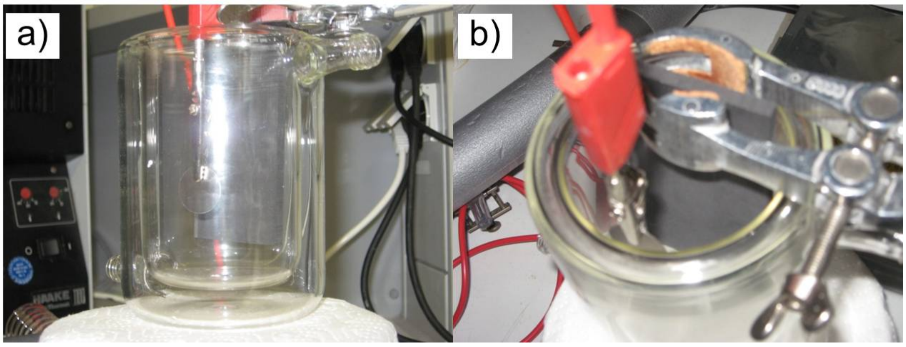

Figure 4.3: Photographs of the "Glass-Setup" a) While in use and b) the sample holder and the reaction vessel.

4.3 Anodization of Titanium

4.3.1 Introduction

TiO_2, both in its bulk form and as a nanomaterial is one of the most intensively studied oxides owing to its wide range of applications, such as photovoltaics (see chapter 3), catalysis,[53] Lithium ion batteries [24] or chemical sensing.[54] However, nanostructured TiO_2 offers even more intersting possibilities in applications owing to factors such as the high surface area, which is important for photovoltaics or catalysis, or short solid state diffusion paths, which can be utilized in batteries. The different pathways towards a synthesis of TiO_2 and related nanomaterials include hydrothermal (see chapters 2 and 3) sol-gel or template assisted synthesis. [55] [56]

However, electrochemical anodization is an additional tool for the synthesis of TiO_2 nanomaterials. As elucidated in section 4.1, self-organized nanotube arrays and other nanostructures can be made when a set of experimental parameters, such as temperature, applied potential, electrolyte nature and concentration is appropriately adjusted.

The synthesis of these nanotube arrays is meanwhile well investigated resulting in multiple applications, one of the most prominent ones is the use in dye-sensitized solar cells. Various architectures of DSSCs can be realized using TiO_2 nanotube arrays. Quantum dots can be used to sensitize the nanotubes, [15] as well as a dye like N719 (see chapter 3). In order to increase the comparably small surface area of the nanotube arrays they can be decorated with TiO_2 nanoparticles and subsequently be sensitized. It is additionally possible to fill the tubular structures with a material like CdTe to obtain an all solid-state device.[16] Finally, TiO_2 nanotube arrays may also serve as a template for the precipitation of $CuInS_2$, which is another way to realize a solid-state nanostructured photovoltaic device (compare chapter 5).

The experimetal work in this chapter was based on the results published by Lee *et al.*. Modifications were necessary since the published results were not reproducible, which is most likely due to the different setups used herein and by Lee *et al.* In course of the study presented herein, titanium metal foils were electropolished in order to provide a flat substrate for the subsequent anodization. It was shown that the electropolishing step is crucial in order to obtain well ordered nanotube arrays. The anodization was carried out as a two-step process, which led to the formation of well aligned nanotubes in relatively short reaction durations. The influence of parameters such as etchant concentration and anodization voltage was investigated. An issue that was caused by the short anodization durations applied herein was the formation of a superlattice on top of the nanotube array. Possible strategies to overcome this problem will be discussed.

4.3.2 Experimental Section

Electropolishing

Electropolishing was performed in order to provide a flat substrate for the following electrochemical anodization. Prior to polishing the titanium foils (Sigma Aldrich, 99.8%, 0.25 mm thick, 2 cm diameter) were cleaned by rinsing them with water and acetone followed by an ultrasonic treatment in acetone for 5-10 minutes. Afterwards the samples were rinsed with acetone again and dried in an air stream. Subsequently, the titanium foils were electropolished in 50 ml of a mixture of perchloric acid (60 wt% in water, Sigma Aldrich), butanol (p.A., Sigma Aldrich) and methanol (p.A., VWR) in a 1:6:9 volumetric ratio [2]. A titanium foil, which was placed at a distance of roughly 1.2 cm from the sample, served as the counter electrode. The samples were subsequently placed in the respective setup and electropolishing was performed under voltstatic conditions at -15 to -20°C. The anodization voltage, the reaction duration as well as the setup were varied in order to obtain the desired result.

Anodization

After the electropolishing and the subsequent measurement in the laser microscope, the titanium foils were again sonicated for 5 minutes, followed by rinsing them with water and acetone. The samples were dried with a stream of compressed air. For the following experiments only the "Teflon setup" was used. 50 ml of the respective solution was filled into the setup; a graphite rod with a diameter of 2 cm was used as a counter electrode. The distance from the titanium foil to the counter electrode was set to roughly 1.2 cm and the anodization was carried out at varying voltages. After the synthesis the samples were again rinsed with water and acetone, followed by drying them in a compressed air stream. The reactions were performed at a controlled temperature of 25°C unless otherwise mentioned. Most of the synthesis were carried out as two-step anodizations. In this case the first anodization was performed for 3 h as described. Afterwards, the TiO_2 layer was removed, using scotch tape. The second anodization was subsequently carried out under the same conditions as the first one, but only for 5 minutes. The solution utilized for the anodization consisted of 0.38 wt% NH_4F (p.A., Sigma-Aldrich) and 1.79 wt% of water (Millipore) dissolved in ethyleneglycole (99%, Chempur), if not otherwise mentioned.[2]

Experimental techniques

Laser microscopy: The surface morphology of the polished samples was checked by recording with a Keyence VK-8710 laser microscope equipped with movable x/y-stage.

Scanning electron microscopy: The surface topography of the samples after anodization was checked using high vacuum mode scanning electron microscopy (SEM). Two different instruments were used; FEI NovaNano FEG-SEM 630 or Quanta 200 FEG, FEI Company, Eindhoven, the Netherlands. The untreated samples were glued to an aluminum stub using conductive carbon tape.

4.3.3 Results and Discussion

Electropolishing of titanium metal foils

Unpolished titanium foil

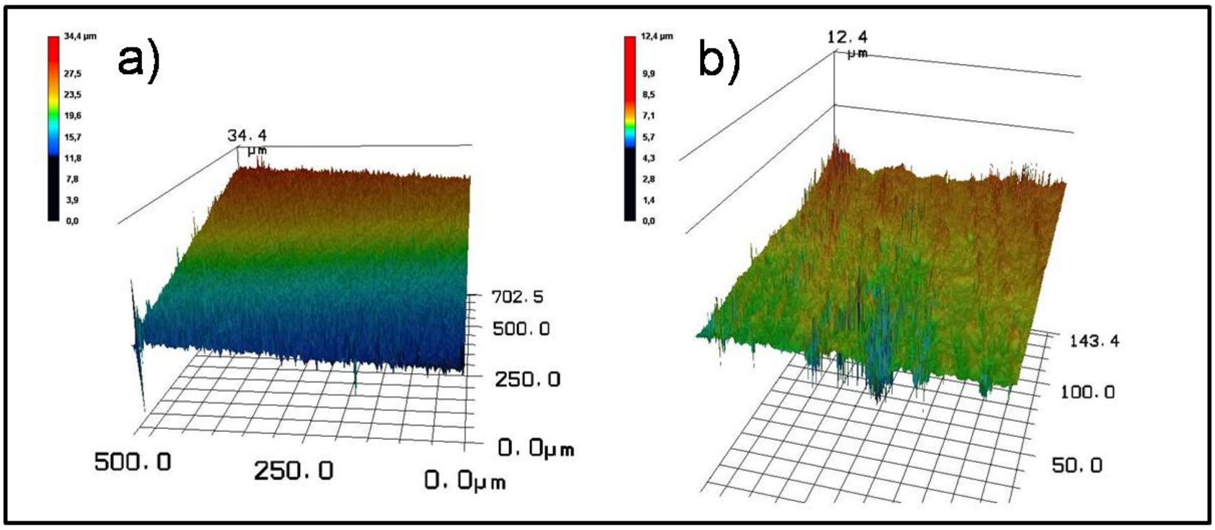

Figure 4.4: Laser microscope images of an unpolished titanium foil in different magnifications.

The surface morphology of the electropolished titanium foils was investigated using laser microcopy. For clarification, the obtained images were extended by factor of 10 on the z-axis (i.e. sample height), making the changes in the morphology of the surface more easily traceable.

The unpolished titanium foil was subject to a laser microscope investigation in order to be able to evaluate the chages upon electropolishing. In Figure 4.4 laser microscope images of the surface of an unpolished titanium foil are shown. It can be seen that the surface is strongly corrugated, multiple scratches and surface irregularities are observed. The spikes visible in the laser microcopy images are indications for the presence of unwanted particles on top of the metal foil. In Figure 4.4 a a slope of the titanium foil itself can be seen. This was only observed on the outer parts of the sample and was thus attributed to mechanical stress of the sample.

Electropolished titanium foils

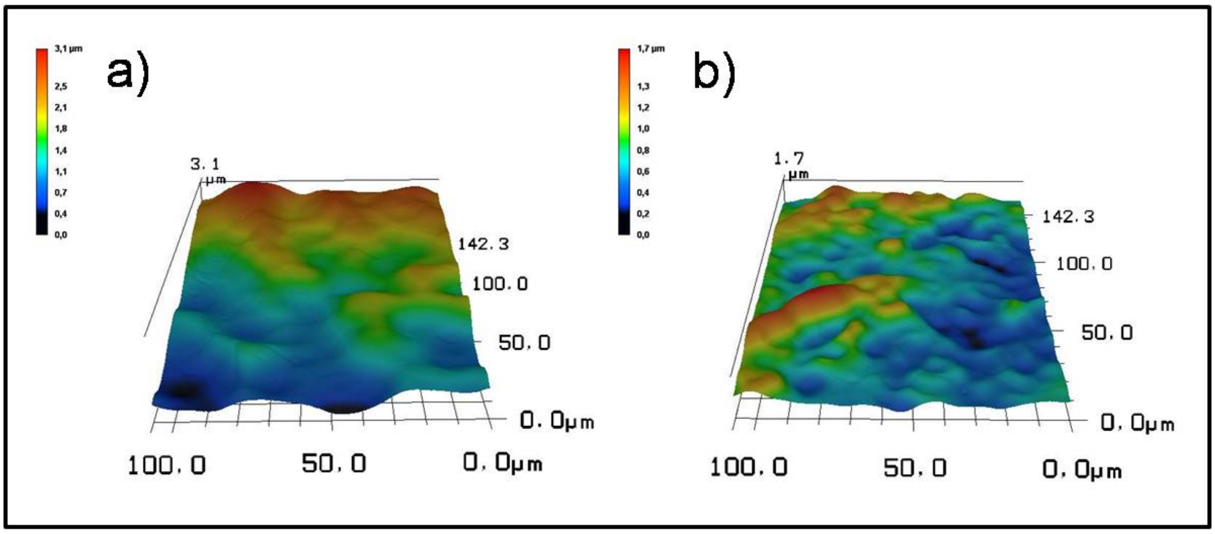

Figure 4.5: Laser microscope images of titanium foils polished at 30 V for different durations in the "Teflon-setup": a) 5 min and b) 15 min.

In Figure 4.5 a laser microscope image of a titanium foil polished under the conditions used by Lee *et al.* is shown (30 V, 5 min). A direct comparison between Lee's results and the ones presented here is difficult, since only a $5 \cdot 5$ µm section measured with an AFM was shown by Lee *et al.* However, the surface of the titanium foil is clearly smoother after the electrochemical treatment. No unwanted particles, indicated by spikes in the laser microscope image (compare 4.4), can be found anymore. Additionally, no scratches are observed on the surface of the foil. An almost completely flat samples was not obtained, though. Smooth "hills" of several micrometers in size are found on the samples' surface. If the anodization is carried out for 15 minutes the results are similar, however the size of smooth "hills" decreased, while their number increased, as compared the sample treated for 5 minutes. A problem concerning the reproduction of the work published by Lee *et al.* is the missing description of the setups used therein. The setup has a huge influence on the outcome of the electropolishing, but also for the anodization, as will be shown below and in the chapter concerning the anodization of vanadium (compare section 4.4).

In order to improve the results obtained so far, the voltage used for the electropolishing was altered. A stronger polishing effect is expected for higher voltages, since also the current will be higher leading to skimming of some material from the sur-

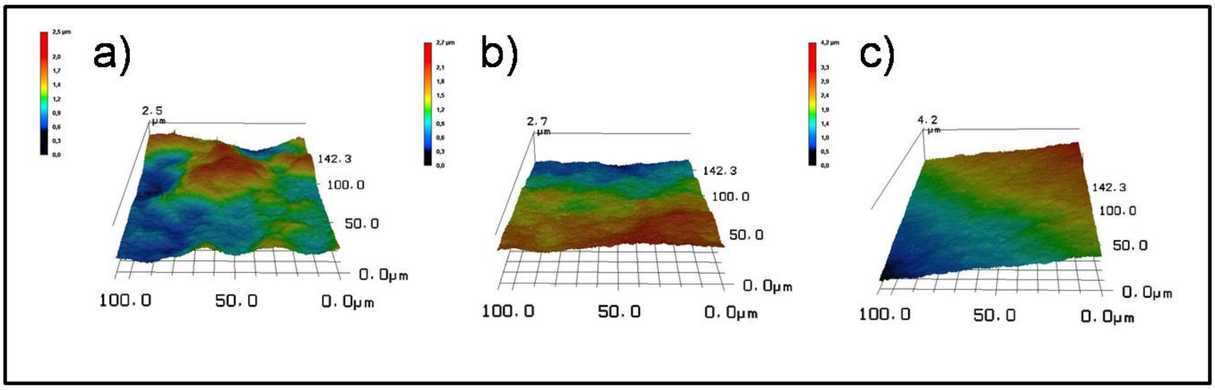

Figure 4.6: Laser microscope images of titanium foils polished for 15 minutes at different voltages in the "Teflon-Setup": a) 40 V, b) 50 V and c) 60 V.

face. If the voltage is too high, on the other hand, this will lead to strongly exothermic reactions and ultimately inhomegeneous polishing results due to the increased temperature. The results are shown in Figure 4.6. Indeed, an increasing voltage led to better polishing results, i.e. the hills observed in the samples shown in Figure 4.5 were diminished until an almost completely flat sample was obtained at 60 V. On the other hand, the surface of the samples was not as smooth as seen for the samples polished at lower voltages. It was additionally observed that electropolishing at voltages higher than 30 V led to a temperature increase in the reaction solution, despite active cooling. For the samples treated at 40 V or 50 V the increase was moderate, i.e. roughly 1°C and 3°C, respectively. If electropolishing was carried out at 60 V, the reaction had to be interrupted after 10 minutes because the temperature was already higher than 30°C. Possibly the exothermic nature of these reactions led to the rougher surface by inducing local temperature, and thus, solubility fluctuations.

Finally, electropolishing was carried out in the "Copper-setup" at 30 V for 15 minutes. The glass coil, which is used for active temperature control in this case (see section 4.2) could not be utilized since high amounts of water condensated on the coil and subsequently dropped into the electropolishing solution. For this reason the solution was pre-cooled to a temperature of roughly -18°C in a freezer; no active cooling was applied during the synthesis. The results are shown in Figure 4.7 a. completely flat and smooth sample was obtained. Very few spikes observed in the laser microscope image indicate the presence of unwanted particles, which could not be removed in the ultrasonic bath. For comparison, a sample was treated under the

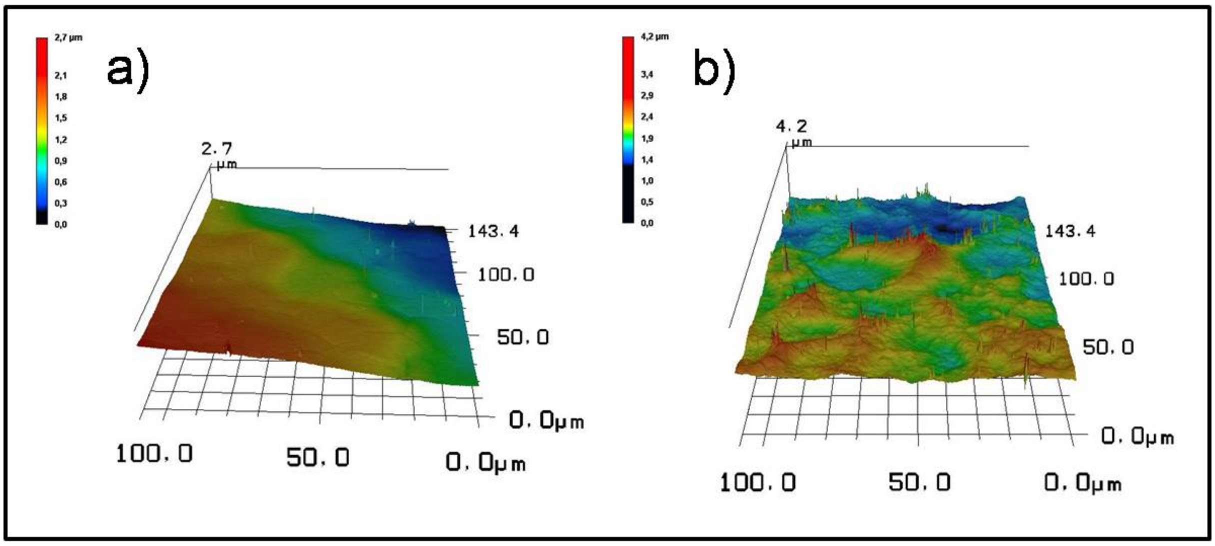

Figure 4.7: Laser microscope images of titanium foils polished at 30 V for 15 minutes in different setups: a) "Copper-setup" and b) "Teflon-setup".

same conditions in the "Teflon-setup", the results can be seen in Figure 4.7 b. The surface is neither flat nor smooth. These results nicely demonstrates the influence of the setup on electrochemical reactions.

Anodization of titanium metal

The effect of the electropolishing step

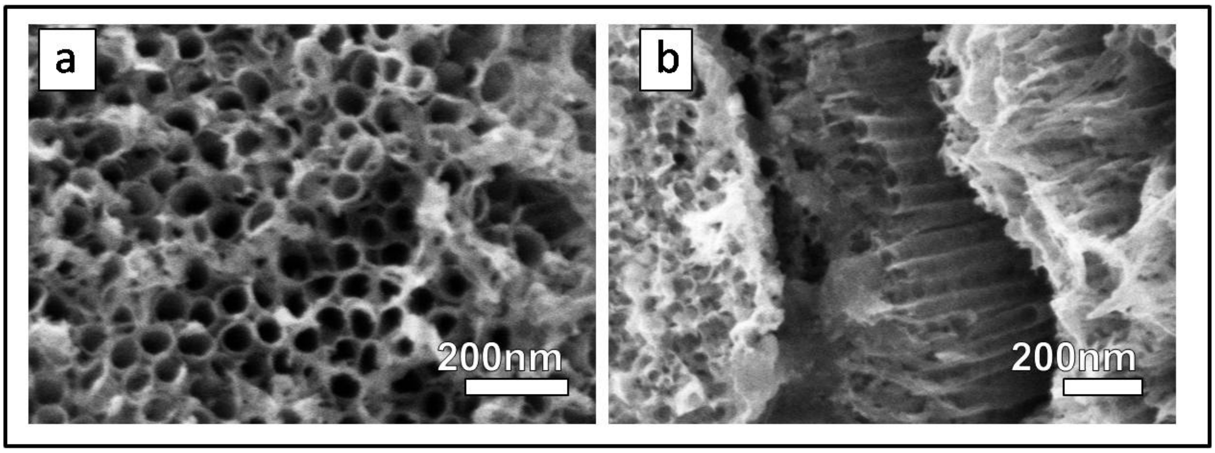

Figure 4.8: SEM images of oxidic nanotubular structures obtained after the first anodization at 30 V for 3 h on an unpolished titanium foil.

In order to clarify the influence of the electropolishing step on the final sample, unpolished titanium foils were anodized; Figure 4.8 shows nanotubes obtained after the first anodization at 30 V for 3 h. While the formation of nanotubes was successful, they were neither well ordered, monodisperse nor completely round. (see Figure 4.8 a). Additonally, debris was found on top of the foils to large extent. Figure 4.8 b shows a crack observed in the nanotube array, leading to tilted tubes. Even though not desirable, the image nicely shows the formation of isolated nanotubes that are attached to each other to form a layer. The same image also shows the presence of closed tubes (right part of Figure 4.8 b). Furthermore, parts of the sample were apparently not affected by the anodization and thus no tubes were found on these parts (image not shown).

Figure 4.9 shows nanotube arrays that were obtained under the same conditions as the ones described above, but after two subsequent anodizations for 3 h and 5 minutes, respectively. The outcome was fairly similar to the sample obtained after only one anodization. Large parts of the foils' surface were covered with roundish unordered nanotubes (see Figure 4.9 b). In the same image it can be seen that the surface was by no means flat, in the lower left part of Figure 4.9 b a layer above the nanotubes, which does exhibit a tubular morphology, can be seen. This phenomenon

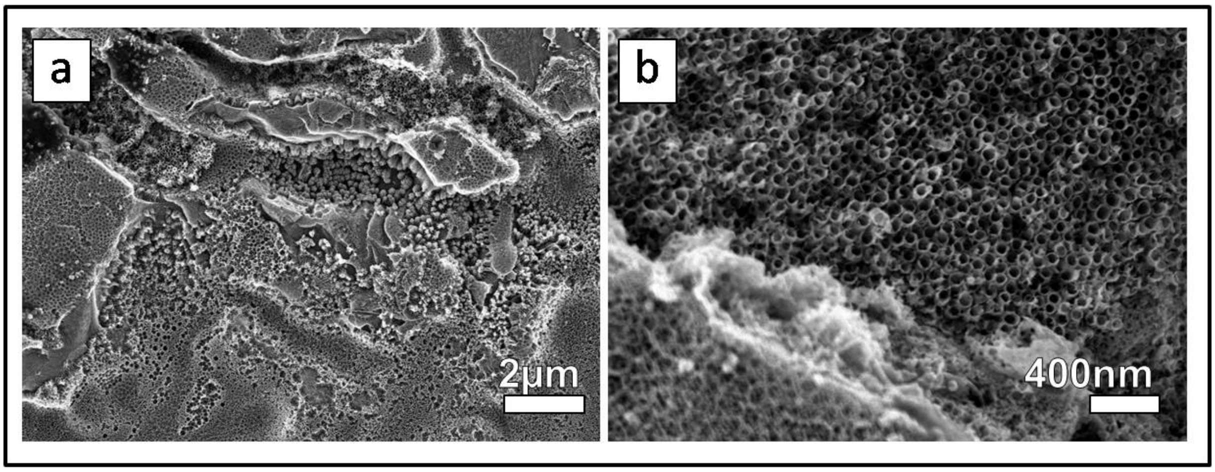

Figure 4.9: SEM images of oxidic nanotubular structures obtained after the second anodization at 30 V for 5 min on an unpolished titanium foil.

will be discussed later. From Figure 4.9 a it can be seen that the sample is not uniform at all, and also structures other than tubes are observed. Some of the tubes nanotubes collapsed and formed bundles.

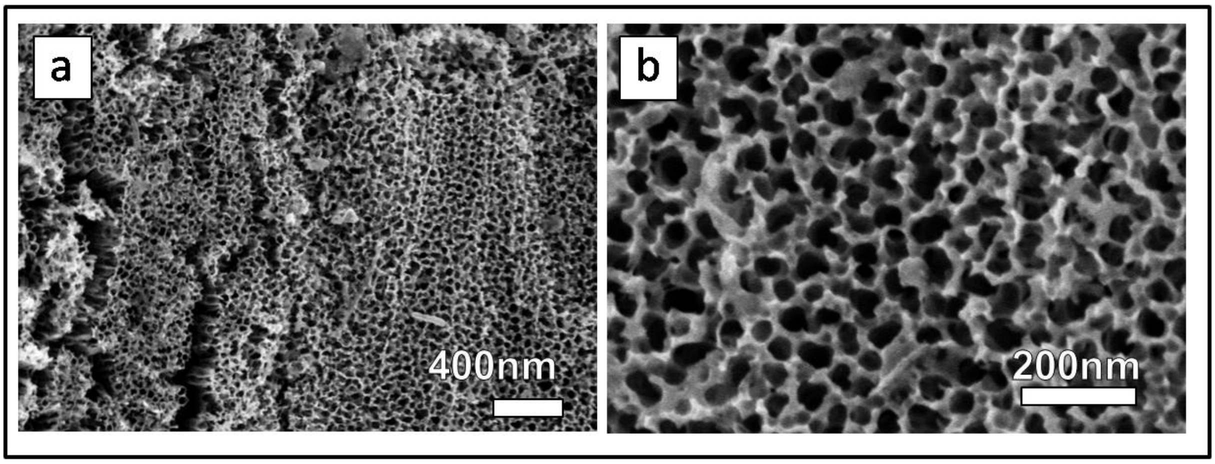

Figure 4.10: SEM images of oxidic nanotubular structures obtained after the first anodization at 30 V for 3 h on a poorly polished titanium foil (compare Figure 4.5b).

Furthermore, an anodization was conducted on a poorly polished sample (compare Figure 4.5). The surface of this sample is rather flat, but cracks and voids are observed in the nanotube array (compare Figure 4.10 a). The shape of the pores is completely irregular and they are rather polydisperse (as shown in Figure 4.10 b). It can also be seen that the walls seperating the pores from each other disappeared in some cases. The surface of the nanotube array is completely covered with a porous oxide layer. A similar surface layer was observed in the sample after the second anodization on an unpolished foil. The results clearly demonstrate the necessity of an effective polishing step, especially when compared to the results shown below.

The effect of the second anodization

Only well polished (compare Figure 4.7) titanium foils were used for the anodizations described from now on. In the experimental section it was described that the anodization was carried out in two steps; one rather long (3 h) subsequently followed by a short (5 min) anodization. The first anodization is supposed to provide a well ordered pattern of nanoindentations on the samples' surface on which the nanotubes grow in an ordered fashion during the second anodization. This enables one to utilize extremely short reaction durations and still obtain an ordered array of nanotubes; a process that normally takes hours (compare the growth mechanism of oxidic nanotubes in section 4.1).

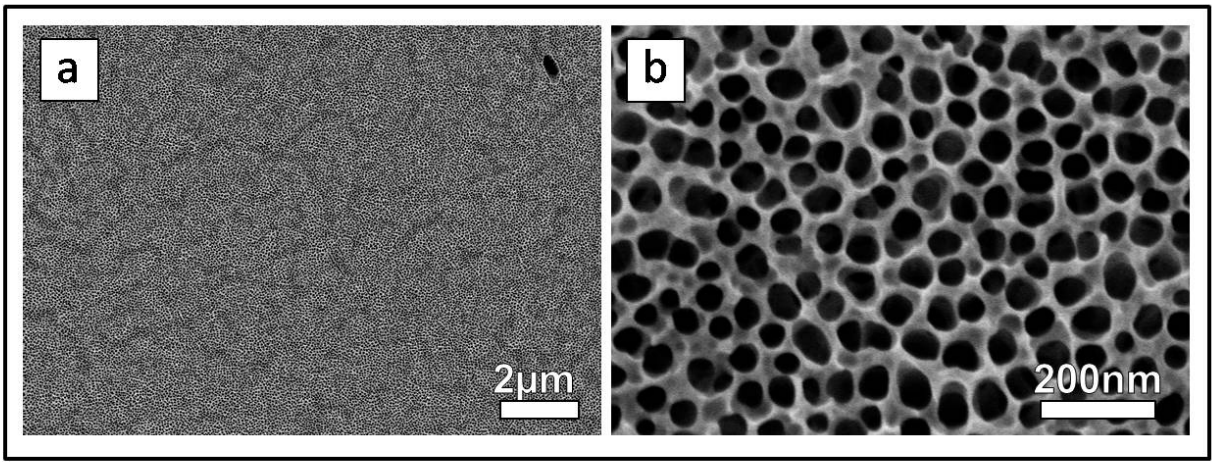

Figure 4.11: SEM images of oxidic nanotubular structures obtained after the first anodization at 30 V for 3 h on a well polished titanium foil (compare Figure 4.7a).

Figure 4.11 shows the nanotubes obtained after 3 h of anodiazation on a well polished substrate at 30 V. The surface of the sample is completely flat and it is also uniform. The porous layer on top of the nanotube array is not well ordered and the pores differ in diameter from each other. While this results is an improvement compared to the samples obtained on un- or poorly polished titanium foils, no ordered array of nanotubes was obtained so far.

As described in the experimental section the oxide layer can easily be removed from the metal foil after the first anodization. A piece of scotch tape is attached to the metal foil and subsequently peeled off. Due to the poor attachment of the oxide

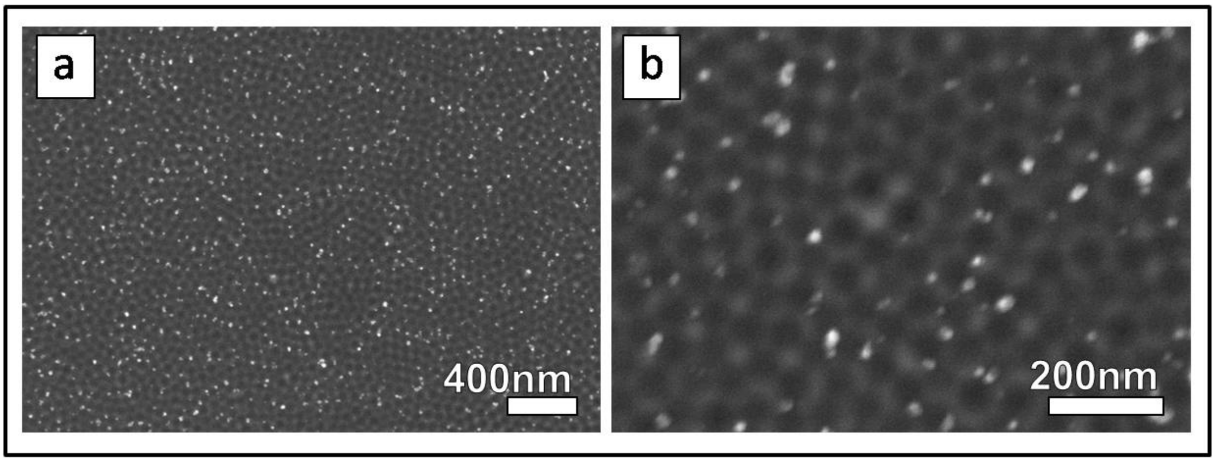

Figure 4.12: SEM images of oxidic nanotubular structures obtained after the removal of the oxide layer formed after the first anodization at 30 V for 3 h.

layer on the metal, it can be completely removed by this simple process. Figure 4.12 shows the surface of a titanium foil after the removal of the nanotubular layer. It can be seen that the sample is completely uniform and a high number of particles is found on the titanium foil. A magnified image of the samples' surface (seen Figure 4.12 b) reveals that an ordered array of nanoindentations is imprinted into the metal after the removal of the oxide layer. The array serves as a template for the pore growth in the subsequent anodization.[2]

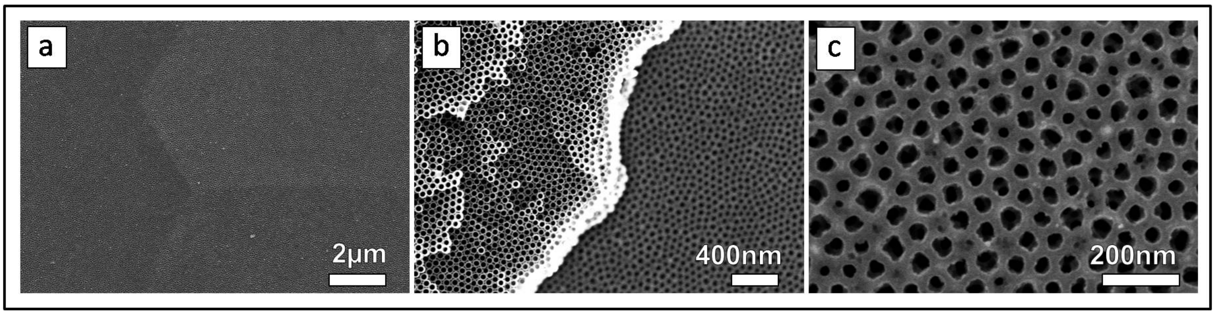

Figure 4.13: SEM images of oxidic nanotubular structures obtained after the second anodization at 30 V for 5 min.

Figure 4.13 shows the surface of a nanotubular layer on top of a titanium after the second anodization for 5 minutes at 30 V. From the overview image in Figure 4.13 a it can be seen that the surface is nearly completely flat and uniformly covered with ordered nanopores. Figure 4.13 b shows one of the few defects on the samples' surface. Most likely caused by a coincidental removal of the upper porous layer, nicely ordered and monodisperse nanotubes are observed. Also the aforementioned porous layer consists of uniform and ordered pores with diameter of roughly 30 nm (see right part of Figure 4.13 b). Figure 4.13 c reveals that not all parts of the surface are as well ordered as the ones described above. Irregularly shaped, polydisperse pores were also found. However, these pores were only found in small parts of the sample. In summary, the beneficial effect of the second anodization was demonstrated in this section. All samples shown from now on were prepared using two subsequent anodizations.

The effects of anodization voltage and fluoride concentration: Pore size tuning

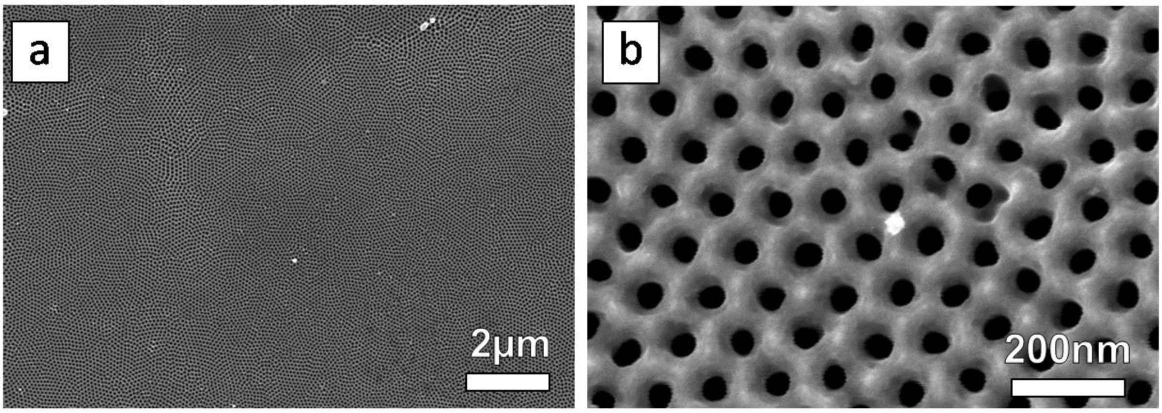

Figure 4.14: SEM images of an ordered array of TiO_2 nanotubes obtained after the second anodization at 50 V for 5 minutes.

In the description of the reaction mechanism it was mentioned that, under otherwise similar conditions, the anodization voltage determines the pore diameter. Thus it was expected that an increase of the anodization voltage to 50 V leads to a diameter higher than 30 nm, which was obtained at 30 V. The expected behavior was indeed found, the pore diameter was increased to roughly 40 nm when a titanium foil was anodized at 50 V (see Figure 4.14). It is also noteworthy that the sample obtained under these conditions was completely uniform and the nanopores were well ordered and monodisperse. Only few defects were observed (compare Figure 4.14 a). This result is rather surprising since the voltage was not expected to have an influence on the order and uniformity of the sample. While the reasons for this behavior remain unclear, it can be noted that the influence of the anodization voltage is more complex than simple size tuning.

Figure 4.15 shows SEM images of a sample anodized at 20 V. As expected, the pore size significantly decreased to roughly 20 nm, but the pores were neither ordered nor monodisperse (see Figure 4.15 b). Furthermore, it seems that there is a superlattice on top of the anodic oxide. The pores with a diameter of around 20 nm are located in shallow pits with a diameter of roughly 50 nm. These observations clearly show once more that voltage does not simply determine the pore diameter, at least under the conditions applied here. However, the sample in general was uniform, only some small particles were found on the surface (as shown in Figure 4.15 a and b).

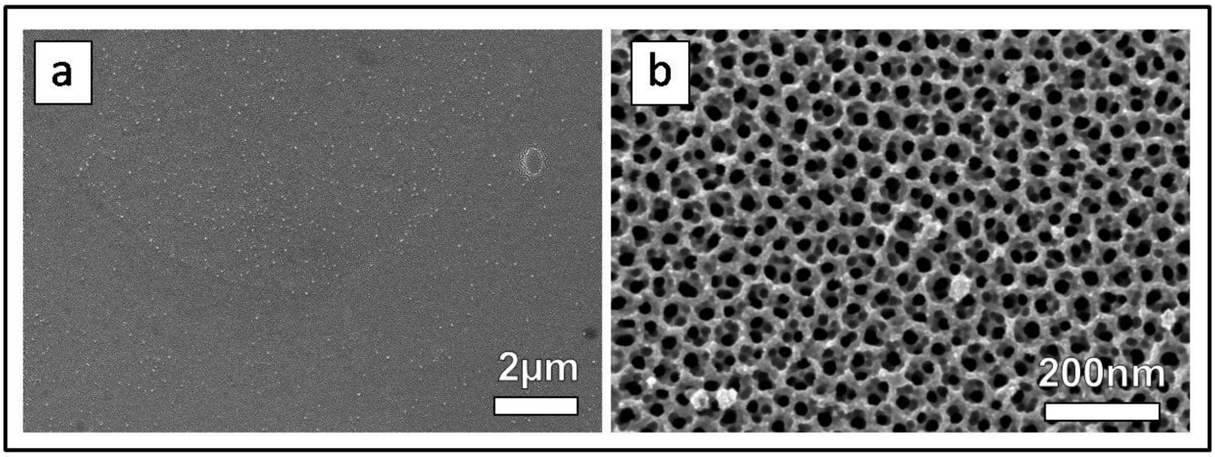

Figure 4.15: SEM images of TiO_2 nanostructures obtained after the second anodization at 20 V for 5 minutes.

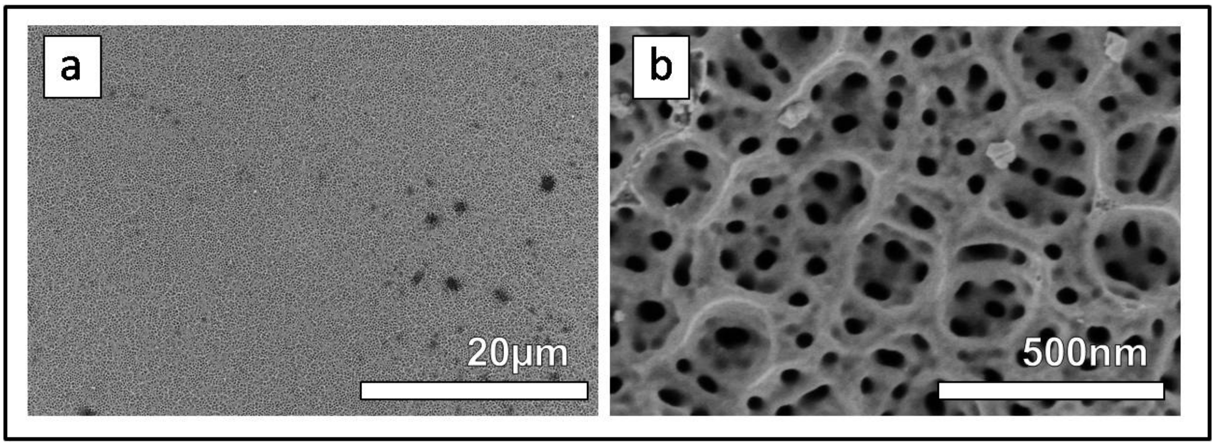

Figure 4.16: SEM images of TiO_2 nanostructures obtained after the second anodization at 80 V for 5 minutes.

SEM images of a titanium foil anodized at 80 V are shown in Figure 4.16. While the surface of the sample is flat and uniform (see Figure 4.16 a), an ordered array of nanopores and nanotubes was not obtained (compare 4.16 b). The observations were similar to the sample anodized at 20 V, smaller pores were located in large pits that form a superlattice. The diameter of the pores was increased to 30 nm, while the pits exhibit a diameter of 100- 200 nm, i.e. as expected the pore size was increased as compared to the sample anodized at 20 V. Due to the different nature of the oxide layers on the "20 and 80 V sample" a direct comparison to the "50 V sample" was not possible.

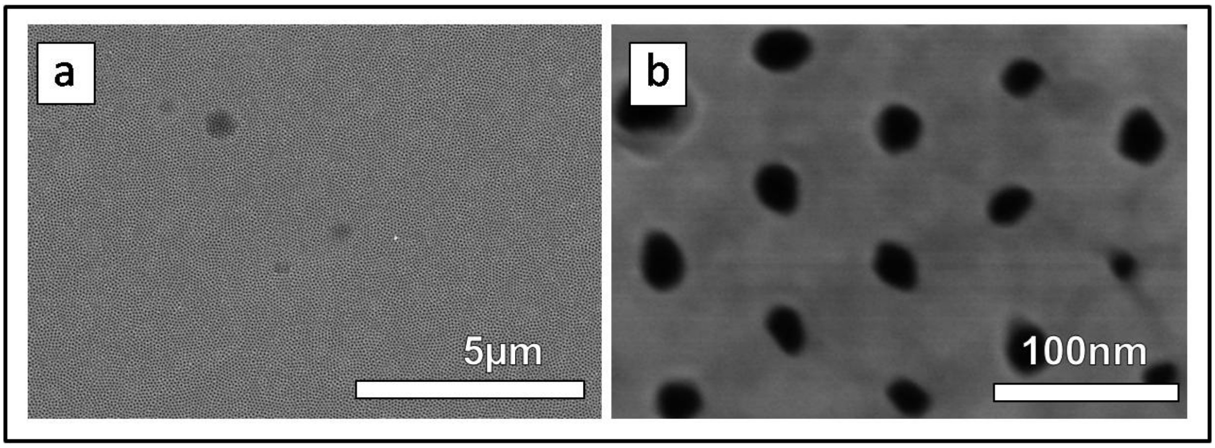

Figure 4.17: SEM images of nearly ordered TiO_2 nanotubes obtained after the second anodization at 30 V for 5 minutes with lowered fluoride concentration (0.2 wt%).

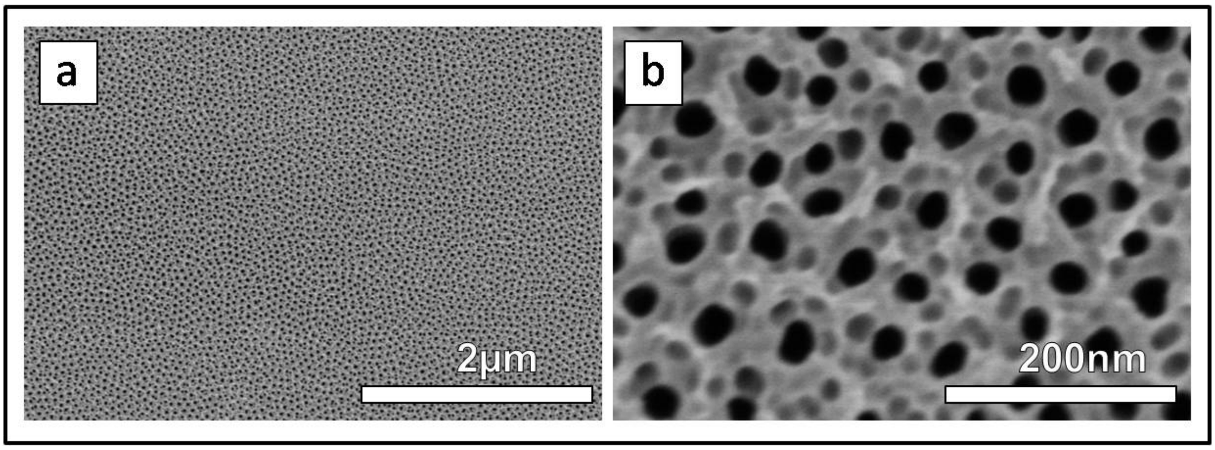

Figure 4.18: SEM images of TiO_2 nanotubes obtained after the second anodization at 30 V for 5 minutes with increased fluoride concentration (0.5 wt%).

Another way to tune the size of nanopores in the anodic oxides is a variation of the fluoride concentration. Fluoride ions are used to etch the pores into the solid TiO_2 layer. When anodized at the same voltage, a nanoporous film prepared with a lowered fluoride content will exhibit a smaller pore density, i.e. the pore walls will be thicker. Figure 4.17 shows the SEM image of a sample anodized at 30 V with a

NH_4F concentration of 0.2 wt%. The sample was uniform and no superlattice or significant defects were found. As expected, the pore size was decreased to 20 nm or decreased, as compared to 30 nm for a sample anodized with a fluoride content of 0.38 wt%, and the pore density was also lower. However, while the pores were nicely ordered, the pores size was not uniform.

Figure 4.18 shows SEM images of a sample anodized with a fluoride concentration as high as 0.5 wt%. The higher concentration of NH_4F in the anodization solution should lead to enhanced etching, thus resulting thin pore walls and consequently a higher pore diameter, as compared to the 30 nm pores on a titanium foil anodized with 0.38 wt% NH_4F (compare 4.13). However, the pores did not exhibit an increased diameter. They were rather unordered and irregularly shaped. Shallow, smaller pores or indentations were found on the walls in between the pores (see Figure 4.18 b). The higher fluoride concentration led to random etching on the outer part of the oxide, rather than tube growth.

The thickness of the oxide layer and the "superlattice"

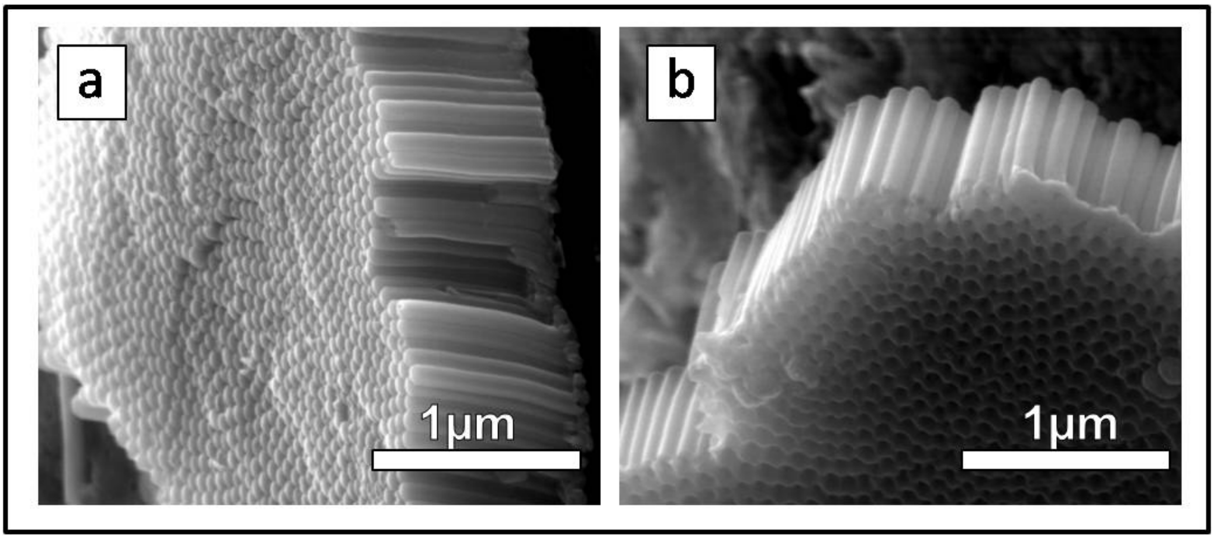

Figure 4.19: Cross-sectional SEM images of TiO_2 nanotubes obtained after the second anodization at 50 V for 5 minutes.

The cross-sectional SEM images shown in Figure 4.19 were obtained by scratching the surface of an as-anodized foil (50 V, second anodization) with a diamond cutter. Parts of the tubular layer were randomly detached and could be investigated by means of SEM. It was found that the oxide layer was roughly 1 μm thick consisted of isolated nanotubes that were attached to each other and the bottom of the pores was closed. It can be seen from Figure 4.19 b that the pores are covered by a porous, yet continuous oxide layer. This layer is the reason why tubes were rarely seen when the surface of the samples was investigated.

According to Macak *et al.* [57] the origin of this continuous oxide is a very stable rutile layer that is found on the bare titanium foil. Owing to its stability, the layer can only be removed by prolonged etching of the layer in anodizations with a longer reaction duration. In principal it should also be possible to etch this layer away using HF. This process is already established as a way to open the bottom of the pores.

Typical current-time curves for the first and second anodization

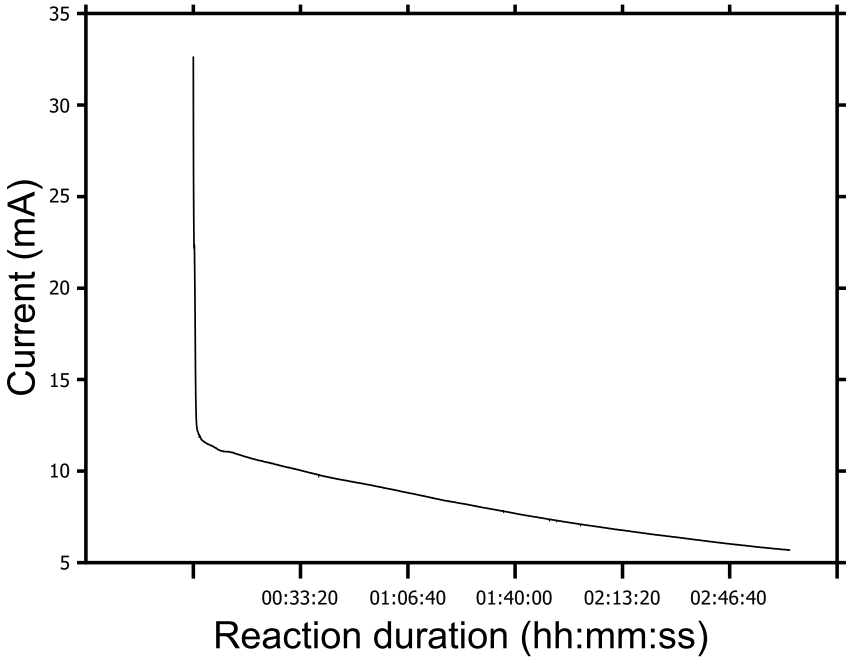

Figure 4.20: Typical current-time curve for the first anodization of a titanium foil at 50 V for 3 h.

Current-time curves were recorded using a multimeter with automated data acquisition. The results are shown in Figure 4.20 for the first anodization and in Figure 4.21 for second anodization. Lee *et al.* obtained similar current-time curves and interpreted the results as follows: [2]

The electric field is built up rapidly and the current quickly rises to its maximum value, thereby initiating the formation of the anodic oxide. Owing to technical limitations of the recording device, the rise of the current could not be monitored, a current value can only be measured after two seconds. Due to the formation of the oxide the current quickly decreases into a minimum. Assisted by the electric field, the etching involving fluoride ions starts at that point, which leads to a decrease of the oxides' thickness and thus an increase of the current. Afterwards, an equilibrium between oxide formation and dissolution is established, leading a slow decrease of the current.

This behavior was found for the second anodization (see Figure 4.21), while in case of the first anodization the onset of the etching process is hardly visible and it is followed by a strong decrease of the current until the end of the anodization. The different current-time behavior can be attributed to the prolonged anodization. In an anodization with a reaction duration of 3 h the increasing thickness of the oxide layer leads to a decrease of the current, until the oxide formation comes to a halt.

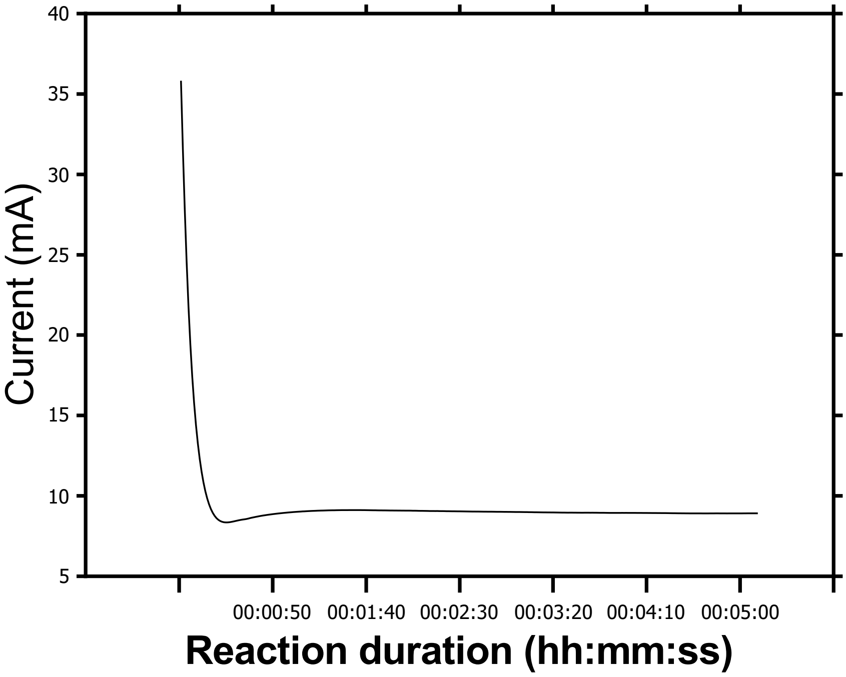

Figure 4.21: Typical current-time curve for the second anodization of a titanium foil at 50 V for 5 min.

4.3.4 Conclusions and Outlook

Conclusions

Ordered arrays of TiO_2 nanotubes were successfully prepared *via* a two-step anodization. The thickness of the obtained oxide layer was found to be 1 μm after 5 minutes of anodization. The study in here was based on the work of Lee *et al.*, however, their results could not be reproduced without modifications to the procedure. This was attributed to the missing about the setup used in their study. While as-purchased titanium metal foils were successfully electropolished using the "Copper-setup", i.e. the surface of the samples was flat and smooth after the treatment, it was found that the setup has a decisive influence on the outcome of the electropolishing experiments. The effect of the polishing step on the subsequent anodization was shown. Poorly or unpolished samples led to the formation of uneven oxide films with cracks and voids. It was furthermore demonstrated that introducing a second anodization step led to a significant improvement in the samples' uniformity and also had a positive effect on the pore ordering. As expected, the anodization voltage did have an influence on the pore size, but also on the ordering of the pores, which was not to be foreseen. However, nicely ordered monodisperse pores were obtained with an anodization voltage of 50 V. By lowering the content of fluoride in the anodization solution, smaller pores with thicker pore walls were obtained. In all samples anodized for only 5 minutes (after the second anodization) a continuous, porous layer was found on top of the nanotubular film. This layer originates from the native oxide film on the titanium foil and is thus rather stable.

Outlook

The next step will be the removal of the continous oxide layer from the top of sample anodized for relatively short reaction durations. Possibilieties to achive this were discussed. In order to obtain a stable membrane for the subsequent applications of the nanotubular film, careful sintering of the as obtained anodic oxide film will be systematically investigated. In this process also the crystallographic phases of the anodized films will be investigated and they can hopefully be tuned *via* adjusting the sintering conditions.

A stable membrane of TiO_2 can be used in numerous applications, as discussed before.

4.4 Anodization of Vanadium

4.4.1 Introduction

The various oxides of vanadium have received a considerable amount of attention owing both to their chemical and mechanical stability, as well as intriguing properties, such as variable oxidation states [58] or the metal insulator transition in VO_2.[59] Especially vanadium oxide nanoparticles or other nanoarchitectures, such as wires, are being thoroughly investigated due to their wide range of possible applications. The most prominent examples are the use in lithium ion batteries,[60] supercapacitors,[61] photocatalysis [62] or chemical sensors.[63] The interest in vanadium oxide nanostructures arises from the size and shape induced properties, as well as the possibility to create complex architectures.[64] An example is the use of vanadium oxide as a material for lithium ion batteries. Using an anode material in the nano-size regime leads to higher power densities and shorter lithium diffusion lengths, as compared to a bulk material.[65] Vanadium oxide nanomaterials can be made using a variety of techniques, including hydrothermal-,[66] surfactant assisted-,[67] sol-gel-,[68] or template assisted synthesis.[69]

While it is possible to synthesize vanadium oxides nanoparticles or other nanostructures using these techniques, there are several drawbacks to them. Mostly high temperatures are required and the syntheses involve multiple steps. Additionally, the properties of vanadium oxide depend on the oxidation state, which is often influenced by the reactants present in the solution.[66] The synthesis of vanadium oxide nanotubes, for example, requires the use of organic spacers/inorganic ions, both of which have an influence on the properties of vanadium oxides.[70]

Thus a simple, low temperature method to synthesize vanadium oxide nanostructures would be a great asset to the existing approaches. A synthetic option not only meeting these requirements, but also facilitating the possibility to synthesize ordered arrays of vanadium oxide nanotubes is the electrochemical anodization or anodic oxidation. Ordered arrays of transition metal oxide nanotubes or nanopores can be made *via* this technique. The most salient examples are the anodization of aluminum [52] and titanium [71], but also a variety of other metals can be anodized, for example zirconium, [72] hafnium, [73] niobium, [74] tantalum, [75] iron [76] or tungsten.[77] To the authors best knowledge, no ordered arrays of vanadium oxide nanotubes have been synthesized so far. In principle all metals forming stable oxides with an anisotropic crystal structure, so called "valve metals" can be anodized to form ordered arrays of nanotubes.[13] While vanadium meets these requirement, its' oxides are soluble in most commonly used electrolytes. [78][79]

Schmuki *et al.* recently synthesized an ordered array of V_2O_5-TiO_2 nanotubes *via* anodic oxidation, using titanium-vanadium alloys with a vanadium content of 18$\%$ at most.[80] However, the electrolyte and other experimental parameters used for the electrochemical synthesis were similar to the ones utilized for the anodization or pure titanium metal, i.e. the titanium metal metal caused the formation of nanotubes, vanadium was merely an "impurity". Stefanovich *et al.* were able to grow solid vanadium oxide films *via* anodic oxidation of vanadium foil using an electrolyte consisting of acetone, sodium tetraborate and benzoic acid. [79] Vanadium oxides neither dissolve in electrolytes consisting of acetic acid, small amounts of water and sodium tetraborate.[81] While the growth of solid films was succesful using these electrolytes, no nanostructured ones were obtained.

In course of this study, the electrochemical anodization of vanadium to obtain ordered arrays of vanadium oxide nanotubes was investigated intensively. The vanadium foils were first electropolished in order to provide a flat and smooth substrate for the subsequent anodic oxidation. [82] Multiple experimental parameters were varied to determine a pathway for the fabrication of such a substrate. The as-purchased vanadium foils are rather rough and their surface is uneven, leading to inhomogeneous growth of the vanadium oxide films. Additionally, impurities on the metals' surface, such as oil or grease, that arise from the processing of the foil are removed by electropolishing. In a second step the anodization itself was investigated using multiple different electrolytes and other experimental conditions. A series of well designed experiments led to the conclusion that an electrolyte composed of diethylene glycol, boric acid, water and oxalic acid is the most promising reaction solution leading to well ordered arrays of vanadium oxide nanopores. However, not only the composition of the solution plays an important role, also the design of the experimental setup was found to have a crucial influence on the result of the anodization.

It is noteworthy that the materials obtained herein are suitable candidates for the use in photovoltaic devices. The use of ordered arrays of TiO_2 nanotubes was already investigated,[83] and it was found that highly efficient dye sensitized solar cells (DSSCs) could be made based on this anode material. Due to the dissolution of vanadium in common electrolytes, a use in liquid type DSSCs would not be desirable, but the band gap of 2.8 eV [64] and the good electron conduction of V_2O_5 makes it a suitable candidate for photovoltaic applications. Additionally, a photovoltaic effect in V_2O_5 was found [84] and it was already used a hole conducting material in inverted tandem solar cells. [85] Depending on the dopants, vanadium oxide can be obtained as an electron or hole conducting material; i.e. n- or p-type semiconductor, which opens up interesting options for the design of devices based on vanadium oxide nanotubes.

4.4.2 Experimental Section

Experimental Procedure: Electropolishing

Electropolishing is performed in order to provide a flat substrate for the following electrochemical anodization. Vanadium foils (ABCR, 99.8 % pure, 0.127 mm thick, 2 cm diameter) were treated electrochemically employing different experimental conditions in order to find a suitable way to polish the substrate for the subsequently following anodization. First the vanadium foils are cleaned by rinsing them with water and acetone, followed by ultrasonication of the samples in acetone for 5-10 minutes. Afterwards, the samples are once again rinsed with acetone and dried using compressed air. The samples were then placed in either the "Glass-setup" or the "Copper-setup" (details will be mentioned later in the text) and subjected to electropolishing. The distance from the sample to the counter electrode was set to 1.5 cm. Depending on the setup, counter electrodes of a different geometry were used. In case of the "Copper-setup" a graphite rod with a diameter of 2 cm was employed, while a graphite plate (10 x 5 cm) was utilized in the "Glass-setup", owing to its geometry.

The electropolishing was carried out using 50 ml of different solutions. The first ("Polishing solution 1") consists of perchloric acid (60 wt%, Sigma Aldrich), butanol (p.A., Sigma Aldrich) and methanol (p.A., VWR). The reagents were mixed in a 1:6:9 volume ratio.[2] The second solution ("Polishing solution 2") is composed of 20 vol% sulfuric acid (96-98%, VWR) and 80 vol% Methanol (p.A., VWR); additionally 5 ml water were added per 400ml of the sulfuric acid/methanol mixture.[86] The exact experimental conditions, such as temperature, polishing voltage or current and reaction duration are noted later in the text.

Experimental Procedure: Anodization

After electropolishing, the samples were again sonicated for 5 minutes, followed by rinsing them with water and acetone. The samples were dried with a stream of compressed air. For the anodization experiments all setups were used, details will be mentioned later in the text. The same counter electrodes as described above were used, depending on the setup. The graphite rod was employed in both "Copper-" and "Teflon-setup". The distance from the vanadium foil to the counter electrode was set to 1.0 cm in the "copper-setup". For the "Teflon-" and the "Glass-setup" the distance had to be changed to 1.5 cm, which was due to the geometries of these setups. After completion of the anodization, the samples were again rinsed with water and acetone, followed by drying them in a compressed air stream. The reactions were performed at a controlled temperature of 25°C unless otherwise mentioned.

The reactions performed to synthesize an array of vanadium oxide nanotubes can be separated into 3 Phases, using 4 different solutions and variations thereof. Parameters like voltage or reaction duration were varied in course of this study, hence the exact experimental conditions are given later in the text.

- Phase I: Pre-Tests
  Anodization Solutions 1:[79] 22 g of benzoic (purity, supplier) acid were dissolved in 1L of acetone (p.A., Supplier) and 50ml of a saturated, aqueous borax (purity, supplier) solution were added to the mixture.
  Anodization Solution 2:[2] The solution consisted of 0.38 wt% NH_4F (p.A., Sigma-Aldrich) and 1.79 wt% of water (Millipore) dissolved in ethyleneglycole (99%, Chempur).

- Phase II: Saturated, aqueous Boric Acid Solution
  A saturated, aqueous boric acid (purity, supplier) solution was prepared. For some experiments 0.5 wt% of either NH^4F (p.A., Sigma-Aldrich) or oxalic acid (p.A., supplier) were added to the solution.

- Phase III: Organic solvents
  The respective solvent was saturated with boric acid (purity, supplier) by stirring over night (Ethylene glycol (EG): 0.25 g/ml; Diethylene glycol (DEG): 0.2 g/ml; 1:1 volumetric mixture of Tetraethylene glycol (TEG) and ethylene glycol: 0.25 g/ml; Tetraethylene glycol: 0.15 g/ml; Polyethylene glycol: 0.1 g/ml). The remaining solid was separated from the solution by centrifugation. Water and either ammonium fluoride (p.A., Sigma-Aldrich) or oxalic acid (p.A., supplier) were added to the saturated solution, to yield a final composition of 2 wt% water, 0.5 wt% NH_4F or $H_2C_2O_4$ dissolved in saturated boric acid. Possible deviations are mentioned later in the text.

Experimental: Techniques

Laser microscopy (LM): The surface morphology of the polished samples was checked by recording with a Keyence VK-8710 laser microscope equipped with movable x/y-stage.

Scanning electron microscopy (SEM): The surface topography of the samples after anodization was checked using high vacuum mode scanning electron microscopy (SEM). Two different instruments were used; FEI NovaNano FEG-SEM 630 or Quanta 200 FEG, FEI Company, Eindhoven, the Netherlands. The untreated samples were glued to an aluminum stub using conductive carbon tape.

X-ray Photoelectron Spectrocopy (XPS): The oxidation state on the sample surface was determined by means of a X-ray photoelectron spectrometer (XPS, PHI 5600 ci, Physical Electronics, MN, USA). The instrument was equipped with a standard Mg Kα X-ray tube and an Al Kα monochromator X-ray source (14 kV, 300 W). Survey scans were performed using the Mg Kα X-ray tube; the pass energy was set to 187.85 eV. The measurements of the vanadium peaks were carried out using the Al Kα monochromator source; the pass energy was set to 58,7 eV. Measurements were performed for 6-8 h. The pressure in the analysis chamber was maintained at below 10^{-7} Pa during analysis.

Automic Force Microscopy (AFM): The pore depth of chosen anodized samples was measured using a Dimension 3100 AFM with NanoScope IIIa controller manufactured by Veeco. The AFM was operated in tapping mode under ambient conditions. The cantilever PPP-NCLAuD with a tip radius of typically 2 nm and a tip height of 10-15 μm was utilized.

4.4.3 Results and Discussion

Electropolishing of Vanadium

Unpolished Vanadium Foil:

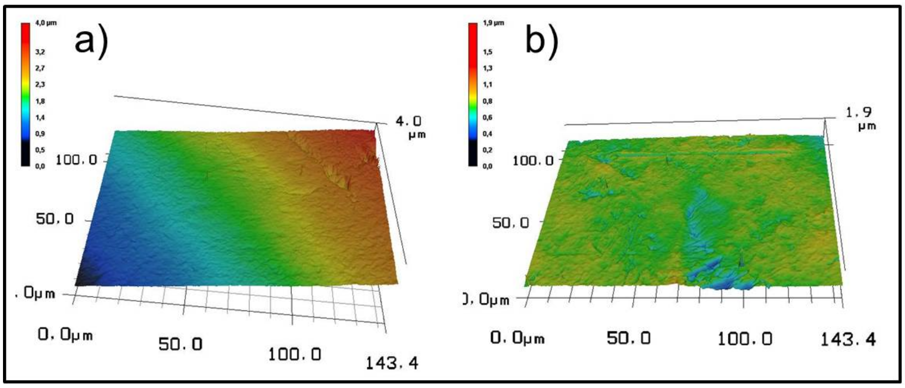

Figure 4.22: Laser microscopy images of an unpolished vanadium foil.

The surface morphology of all electropolished samples was tested using laser microscopy. For clarification, the obtained images were extended by factor of 10 on the z-axis (i.e. sample height). This way, the changes in the morphology of the surface can be followed more easily.

In Figure 4.22 laser microscopy images of an unpolished vanadium foil were measured. The unpolished foil serves as a standard in order to determine whether or not the electropolishing was successful, i.e. provided a smooth and even surface for the subsequent anodization.

In Figure 4.22 a slope is visible on the foil itself. This slope is due to the manufacturing process of the vanadium foil. It was observed in all samples. However, this slope in the material does not influence the roughness of the surface and was thus neglected. In both Figure 4.22 a and b scratches are visible on the surface, as well as irregularities. However, compared to the purchased titanium foil, these samples were rather flat from the beginning (compare section 4.3).

"Polishing solution 1"

The laser microscope images in Figure 4.23 were taken from samples treated with "polishing solution 1" at a temperature of -15 to -20°C and a voltage of 30 V for different durations. The conditions were very similar to ones described by Lee *et al.*,[2] who polished titanium foils under the same conditions. In a first step, the "Teflon-setup" was used.

The surface roughness for none of the samples shown in Figure 4.23 was lowered, as compared to the unpolished vanadium foil. On the contrary the polished foils did exhibit a more irregular surface than the unpolished ones. The sample treated for 5 minutes (4.23 a) exhibits a rugged surface, but no cracks or particles on top of the foil are visible. The samples treated for 10 and 15 minutes (4.23 b and d) were even more corrugated. The vanadium foil that was subjected to a 20 minute treatment was rather flat; on the other hand, scratches were observed in the foil, that were not present in the other samples. After a 30 min treatment the sample (4.23 f) exhibited large scratches and the spikes on its' surface, which indicate the presence of unwanted particles. A treatment of the vanadium foils for 2 x5 minutes was also performed. After 5 minutes the solution was exchanged and a fresh one was used for the second polishing step. The sample was also rinsed with water and acetone in between. Treating a sample twice for a shorter reaction time yielded a result very different from the one obtained for a sample treated for the same duration, but in one step. The surface was smoother in case of the 2 x5 minute sample, as compared to the 10 minute sample (see 4.23 c and b). However, the surface roughness was not decreased compared to the unpolished vanadium foil.

The aforementioned reaction conditions did not yield samples with the desired flat surfaces, regardless of the reaction duration. Longer reaction times were not tested, since the current measured at the constant voltage of 30 V decreases strongly with proceeding reaction time. This leads to a decreasing effect of the current, i.e. no more "electropolishing" is performed, but in fact "chemical" polishing. The latter is a random, diffusion based process and does not lead to smooth and even samples. [87]

The samples in Figure 4.24 a and b were treated for 10 and 15 minutes, respectively, at an increased voltage of 40 V, under other wise similar experimental conditions as described above. A higher voltage enhances the dissolution of vanadium, thus leading to a stronger electropolishing effect. However, the samples are by no

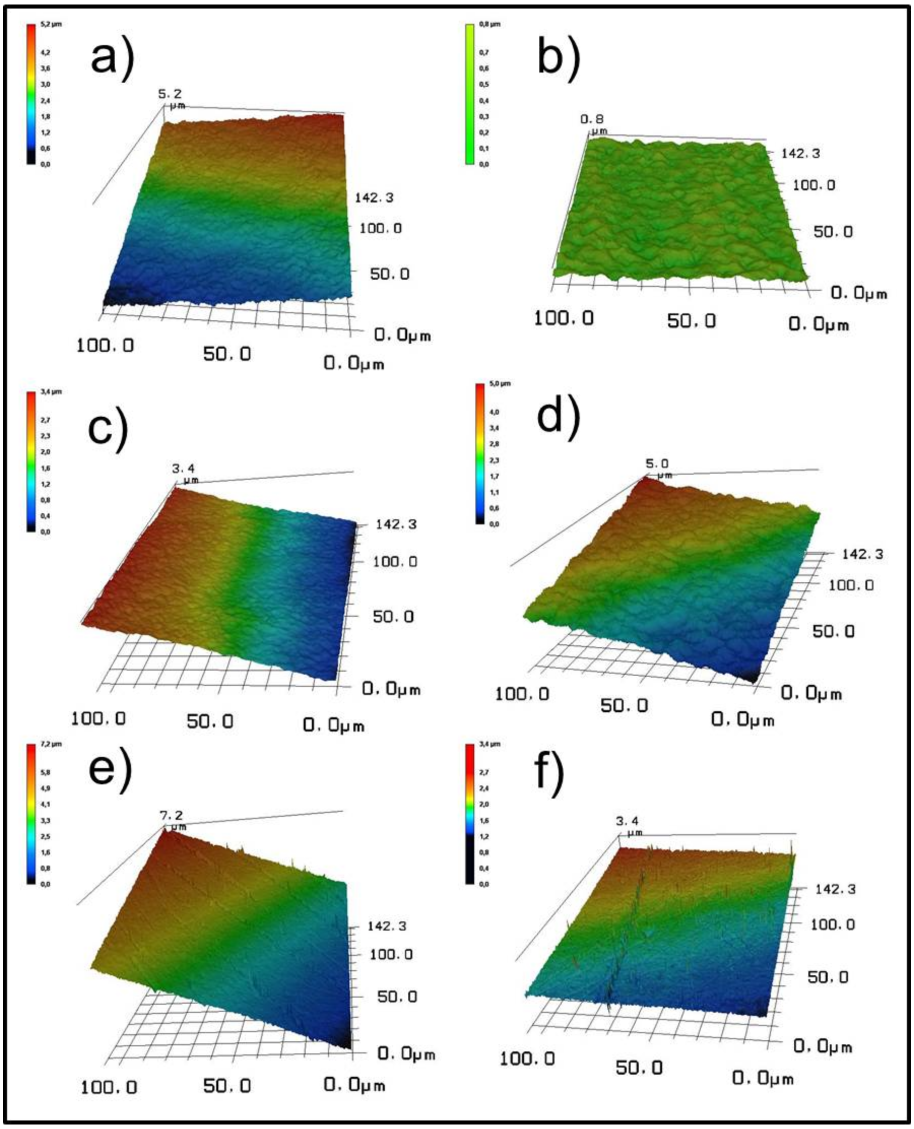

Figure 4.23: Laser microscopy images of vanadium foils polished with "Polishing solution 1" at a temperature of -15 to -20°C and a constant voltage of 30 V for different durations: a) 5 minutes b) 10 minutes c) 2x5 minutes d) 15 minutes e) 20 minutes f) 30 minutes.

means flat, the surface of both samples is rather irregular. A high number of spikes on the samples treated for 10 minutes indicates the presence of unwanted particles on its surface, while the foil subjected to a 15 minute treatment exhibits corrugated structures on top of it. An increase of the voltage did not have a positive effect on the roughness of the samples.

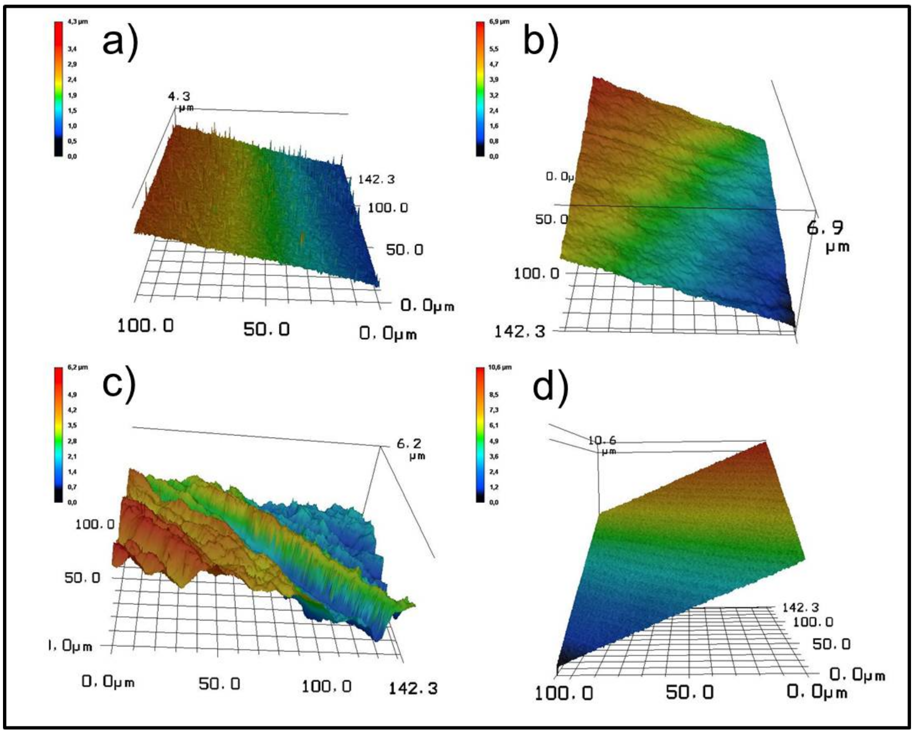

Figure 4.24: Laser microscopy images of vanadium foils polished with "Polishing solution 1" at a temperature of -15 to -20°C. Polished at a constant voltage of 40 V for different durations: a) 10 minutes b) 15 minutes. Polished in the "Glass-Setup" at a constant current of 750 mA for different durations: c) 10 minutes d) 15 minutes.

A final study using "polishing solution 1" was conducted in the "Glass-Setup". Using a constant voltage of 30 V was not possible, because the solution was heated from -15 to -20°C to room temperature within a few seconds, after which the reaction was aborted. Owing to this behavior, a galvanostatic approach was used; the current was set to 750 mA. The other experimental conditions were as described above. A disadvantage of the "Glass-setup" is the condensation of water inside the setup, which is due to the its' comparably wide opening.

Laser microscope images of a sample polished for 10 minutes under galvanostatic conditions in the "Glass-setup" are shown in Figure 4.24 c and d. While parts of the sample were rather flat; only thin and shallow channels were observed; large scratches were found in other parts of the vanadium foil. The well and badly polished areas were distributed randomly over the sample. Different reaction durations were also tested, but the outcome was similar. Despite the flat and nicely polished areas of the sample, the resulting inhomogeneity could not be prevented and thus the method can also not be used for electropolishing of vanadium foils.

"Polishing solution 2"

For all the reactions described in this section the "Copper-setup" was used. The solution was refrigerated before, but not actively cooled during the reaction. Active cooling in this assembly can only be achieved *via* a glass coil that is partially immersed into the reaction solution. At low temperatures this leads to condensation of high amounts of water onto the coil, which is not controllable and thus aggravates reproducible reactions. However, the setup is easy to assemble and the geometry is comparable to the "Teflon-setup". The reactions were conducted for 5 minutes or less, due to the generation of heat during the polishing process.

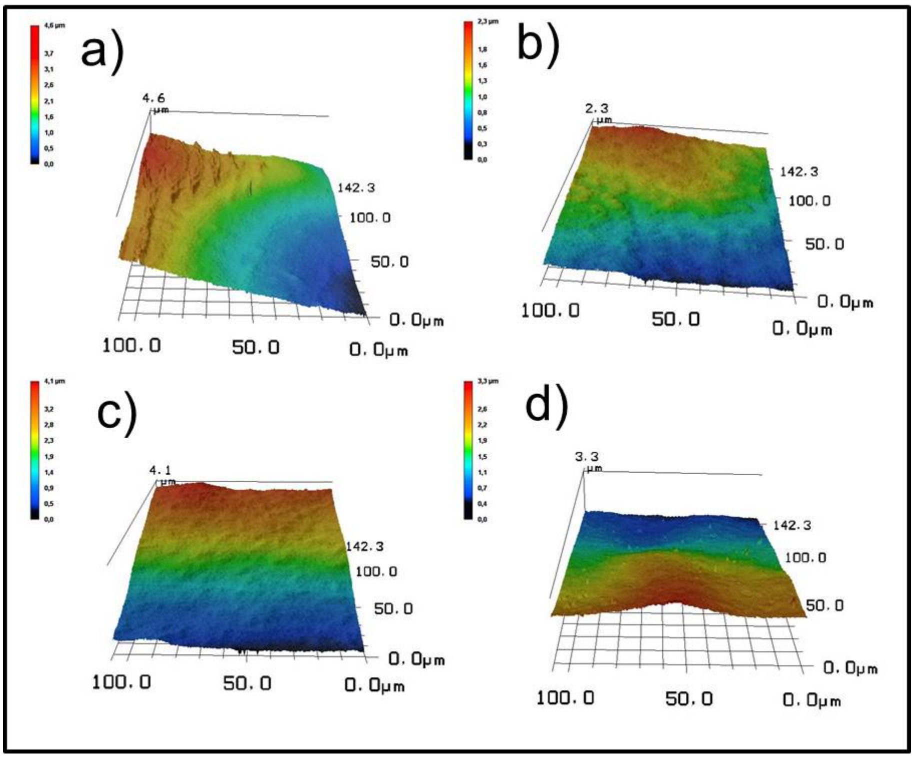

Figure 4.25: Laser microscopy images of vanadium foils polished with "Polishing solution 2", which was refrigerated before the reaction. Samples were polished for 5 minutes at different voltages: a) 10 volt b) 15 volt c) and d) 20 volt.

The images shown in Figure 4.25 were taken from samples treated with "Polishing solution 2" at different voltages for 5 minutes. With rising voltage the samples' roughness was decreased. While the sample treated with 10 V still exhibited some larger scratches (see Figure 4.25 a), the vanadium foil polished at 20 V (Figure 4.25 b) was nearly flat, only some smaller irregularities are observed. When electrochemically treated at 15 V, no scratches were observed on the foils' surface, however, the irregularities were larger, as compared to the 20 V sample. Figure 4.25 d shows an elavation that was formed during the electropolishing process; a phenomenon observed in all three samples. The origin of this irregularity could not be identified. However, these results were the most promising so far.

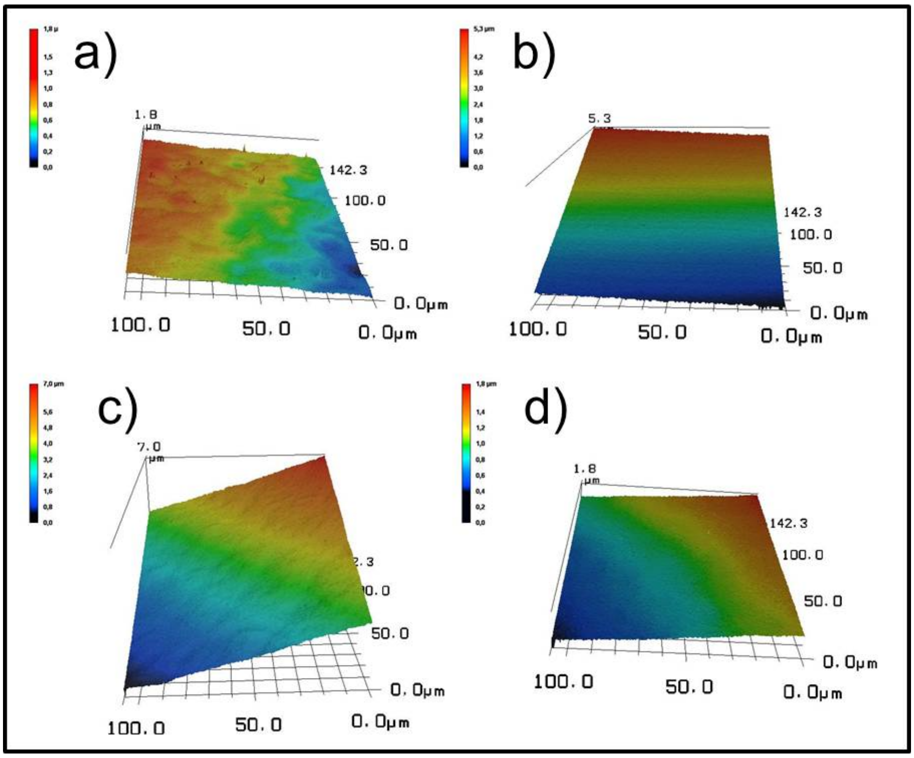

Figure 4.26: Laser microscopy images of vanadium foils polished with "Polishing solution 2", which was refrigerated before the reaction. Sample a) was polished for 5 minutes at 20 volt. The other samples were treated for 4 minutes at different voltages: b) 20 volt c) 15 volt and d) 10 volt.

In order to verify these results, another sample was treated at 20 V for 5 minutes (see Figure 4.26). Surprisingly, the results were quite different from the first experiment. While the smaller irregularities and rather steep elavations disappeared, they were replaced by large flat areas that seem to be arranged in layers. However, the only difference to the first experiment was the reaction solution, which was left standing outside the freezer for 2 days in between the experiments.

Another study was conducted to investigate the influence of the reaction duration on the polishing results. For that purpose, the same reaction conditions as used above were applied; i.e. three different voltages were used; only the duration was reduced to 4 minutes. Again the results were very different from the experiments presented in Figure 4.25. Regardless of applied voltage, all samples were extremely flat and completely homogeneous, no significant irregularities were observed (see Figure 4.26 b, c and d). Surprisingly, the difference between the samples shown in Figure 4.26 a compared to b, c and d is relatively large, while the latter samples are quite similar to each other. Apparently, the applied voltage did not make a significant difference. It should be noted that the solution was left outside the fridge for another two days before the samples shown in Figure 4.26 b, c and d were prepared. These observations led to the conclusion that in fact the age of solution is a decisive factor, while the influence of the applied voltage seems to be limited.

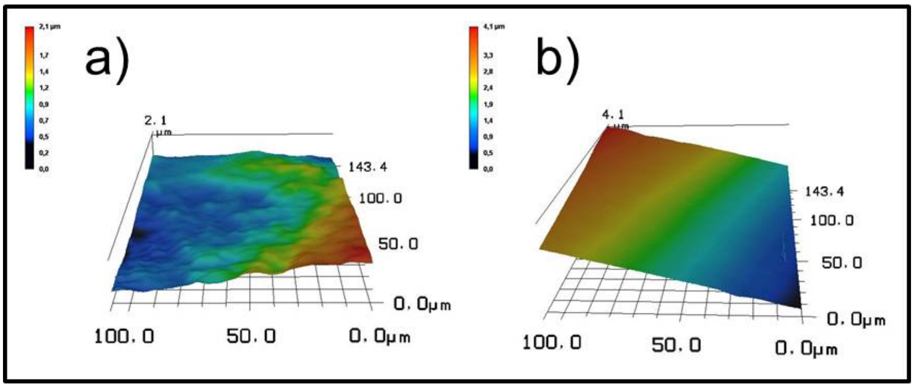

Figure 4.27: Laser microscopy images of vanadium foils polished with "Polishing solution 2", which was refrigerated before the reaction. Both samples were polished under the same conditions (4 minutes, 10 V) but with a) a freshly prepared solution and b) a solution that was left in the lab for four days.

In Figure 4.27 a and b two samples polished under the same conditions (10 V, 4 minutes) using a freshly prepared and an "old solution", respectively, are shown. The solution used for sample a was left outside the freezer for four days. It is clearly evident that the aging of the solution has a tremendous influence on the result of the electropolishing. While the samples polished with a fresh solution was rather irregular, the sample polished with old solution was perfectly flat and thus suitable for the subsequently following electrochemical anodization. The reason for this behavior is the topic of ongoing research.

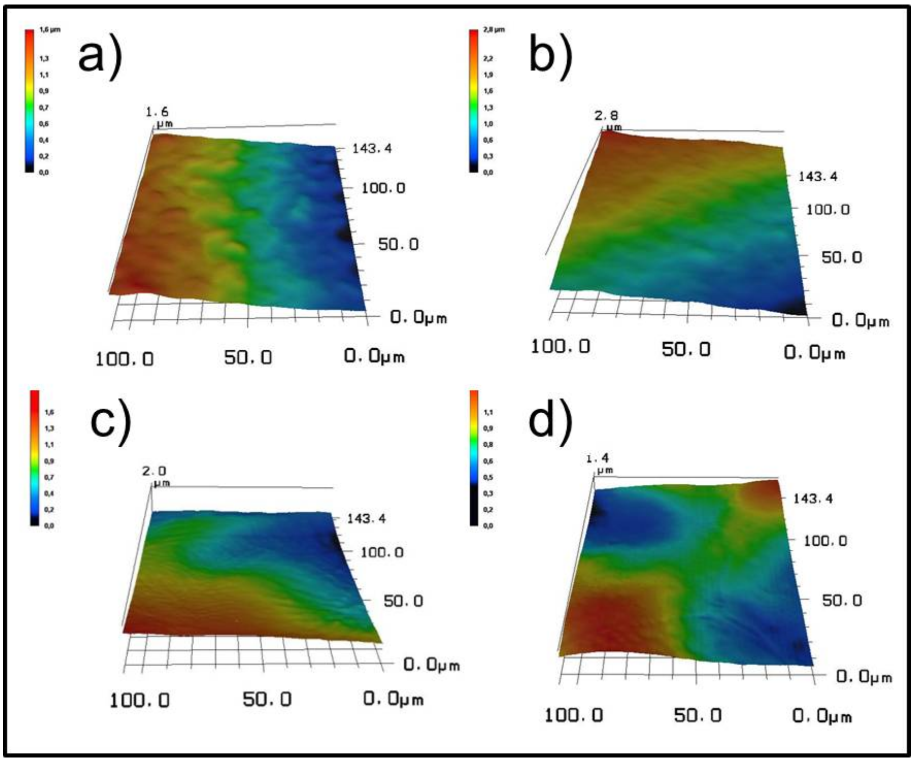

Figure 4.28: Laser microscopy images of vanadium foils polished with "Polishing solution 2", which was refrigerated before the reaction. Samples a) and c) were treated for 4 minutes at 10V using the same solution, only on different days. Sample d) was subjected to a 2nd polishing step for 30 seconds at 10 V and sampled b) was treated using the used solution from sample a).

Two additional experiments were conducted under the same conditions and with the same solution as used above. The mixture was left standing outside the freezer for one and two days, respectively (see Figure 4.28 a and c). An improvement of the polishing results towards a smooth and even surface is clearly evident. This change can be directly attributed to the aging of the polishing solution.

Finally, it was tested whether the aging of the solution can be artificially accelerated or if a second polishing step can be used instead. Accordingly, the same solution used to polish the sample shown in Figure 4.28 a was used again for the electropolishing of another vanadium foil (see Figure 4.28 b). While the surface of the sample is not as flat as seen in Figure 4.27 b, a positive effect of the artificially aged solution is clearly visible. The effect of a second polishing step for a shorter duration was also tested (see Figure 4.28 d). The sample shown in 4.28 c was subjected to a second treatment for 30 seconds at 50 volt. The high voltage was used to initiate a "break-down" of the irregular areas. However, no significant difference was observed due to the second polishing step.

Anodization of Vanadium: General Remarks

There is one general difference between the anodizations of vanadium and titanium. In the case of titanium, a detachable oxide layer is formed after a 3 h anodization. The oxide layer formed during the anodization can be removed due to a lattice mismatch between the oxide and the underlying metal.[2] In the case of longer anodizations (in general 12 h or more), a removal is not possible anymore; due to the long reaction duration the lattice mismatch is compensated. For the anodization of vanadium, on the other hand, a loose precipitate, which consists of platelets and normally has an orange color, is formed on the vanadium foil. After drying, the precipitate turns black, which is most likely due to a reduction from V^{5+} to V^{4+}). When investigated *via* SEM, the dried precipitate seems compact in nature, no pores are found. It is noteworthy that the precipitate can easily be washed away and is undergoing a color change from orange to green in the process, which is most likely caused by a reduction process to V^{3+}.

Anodization of Vanadium Part I: The First Steps

In a first step the anodic oxidation of vanadium described by Stefanovich *et al.* was reproduced ("Anodization solution 1"). They claimed to obtain a solid vanadium oxide film, however, due to the differing focus of their study, no SEM images of the as-obtained films were shown. Herein, the experiments were conducted at a voltage of 60 V for various reaction durations. The reactions were carried out in the "Copper-setup".

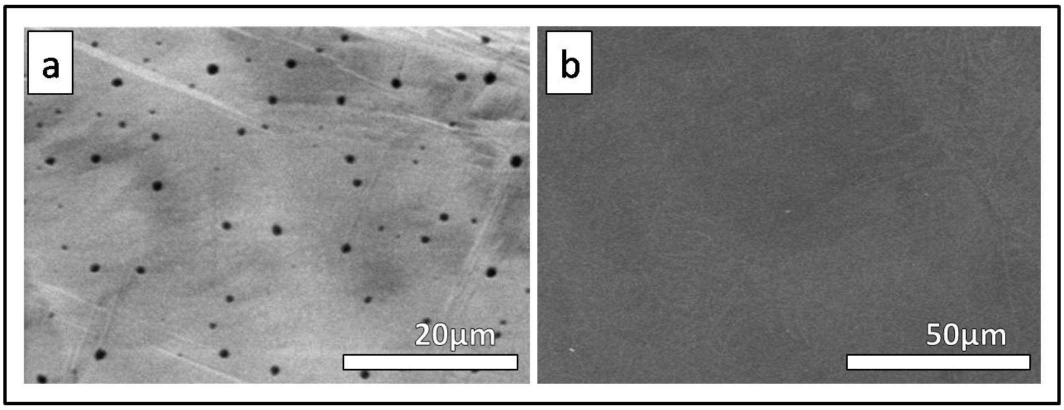

Figure 4.29: SEM images of vanadium oxide films obtained by the method of Stefanovich *et al.*. The experiments shown here were conducted at 60 V for a) 15 h and b) 5 minutes.

When the vanadium foil was anodized for 15 h, a rather solid vanadium oxide film was obtained. On the surface of the film few randomly distributed holes were observed (see Figure 4.29 a). The sample looked whitish to the naked eye, indicating the formation of an oxide layer on the metal. For shorter reaction durations (exemplarily shown for a sample treated for 5 minutes in Figure 4.29) up to 3 h, no oxide formation on the sample was observed, in fact, no difference was found compared to a polished sample, neither in an SEM investigation, nor to the naked eye.

In summary, oxide films can be obtained with the method published by Stefanovich *et al.*, when a sufficiently long reaction time is allowed. The randomly distributed holes are probably due to the benzoic acid, which can act as a weak etching agent. Compared to Stefanovich *et al.* the reaction duration necessary for film formation is rather long, this may be attributed to the setup used. Commonly, vertically arranged assemblies are used (such as the "Glass-Setup"), leading to an unhindered diffusion compared to the spatially confined "Copper-setup". The long reaction duration can also be an explanation for the appearance of holes, which may be formed via *chemical*, not *electrochemical*, etching involving benzoic acid, thus requiring longer times.

As the second step the "Anodization solution 2" was tested with the "Copper-setup" as the reaction vessel. The solution is the same as used in the anodization of titanium metal. In priciple, this mixture can also be used for other metals, since the mechanism for the pore formation is expected to be the same. Stefanovich *et al.* stated that the oxygen which was later found in the oxidic films on vanadium substrates originates from the borax in the solution, not from water or other sources, which would mean that oxide formation is obstructed or prevented in absence of borax or similar reactants. The experiments were conducted under the same conditiones as used for the anodization of titanium, i.e. a voltage of 30 V was used. The effect of a variation of the reaction duration was investigated.

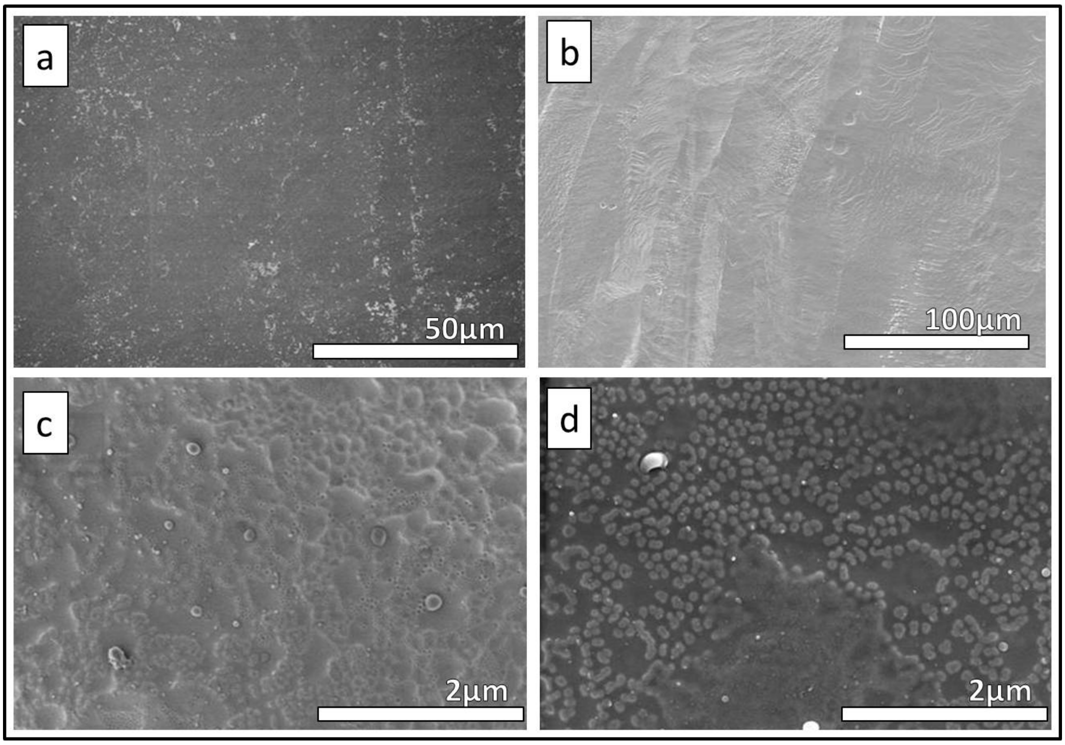

Figure 4.30: SEM images of vanadium oxide films obtained with "Anodiazation solution 2" at 30 V for different reaction durations: a) 3 h b) 72 h c) and d) 16 h.

After a 3 h anodization the surface is optically unchanged, as opposed to anodization of titanium in which a visible oxidic film is formed after the same time. In the case of vanadium only some small particles are found on the surface, there is no sign of a continuous film (see Figure 4.30 a). When the anodization is carried out for 16 h, a non-uniform sample is obtained (compare Figure 4.30). Few randomly distributed pores can be found on the sample, as well as areas with indentations and spongy structures. Other parts of the sample seem empty, with only a few small particles on the surface. The vanadium foil exhibits whitish areas, next to optically unchanged parts. After performing an anodization for as long as 72 h, the sample does not show any changes to the naked eye. When investigated by means of SEM, the surface seems empty, meither oxidic structures nor particles were found. Apparently the oxides formed on the sample after 3 h are dissolved again due to the prolonged anodization.

While oxidic films can, in principle, be obtained utilizing the "Anodization solution 1", it was found that the oxide formation is indeed obstructed, which is probably due to the absence of boric acid as oxygen donor. Furthermore, dissolution of the as-formed oxide occurs after prolonged anodization durations. A solution tailor made for the anodization of vanadium is required to obtain arrays of vanadium oxide nanotubes or pores.

Anodization of Vanadium Part II: Aqueous Solutions

The experiments described in this section were performed using aqueous, saturated boric acid solutions. Despite the solubility of vanadium oxides in water, there are several advantages to aqueous solutions. The high conductivity of water leads to a high current and thus a potentially more rapid reaction. Besides, the solubility of boric acid in water is higher than in other common solvents, leading to the presence of a comparably high amount of oxygen donor, which may facilitate the formation of a vanadium oxide. All reactions were performed in the "Copper-setup" at 40 or 75 V for a reaction duration of 5 or 30 minutes. The results are shown in Figure 4.31.

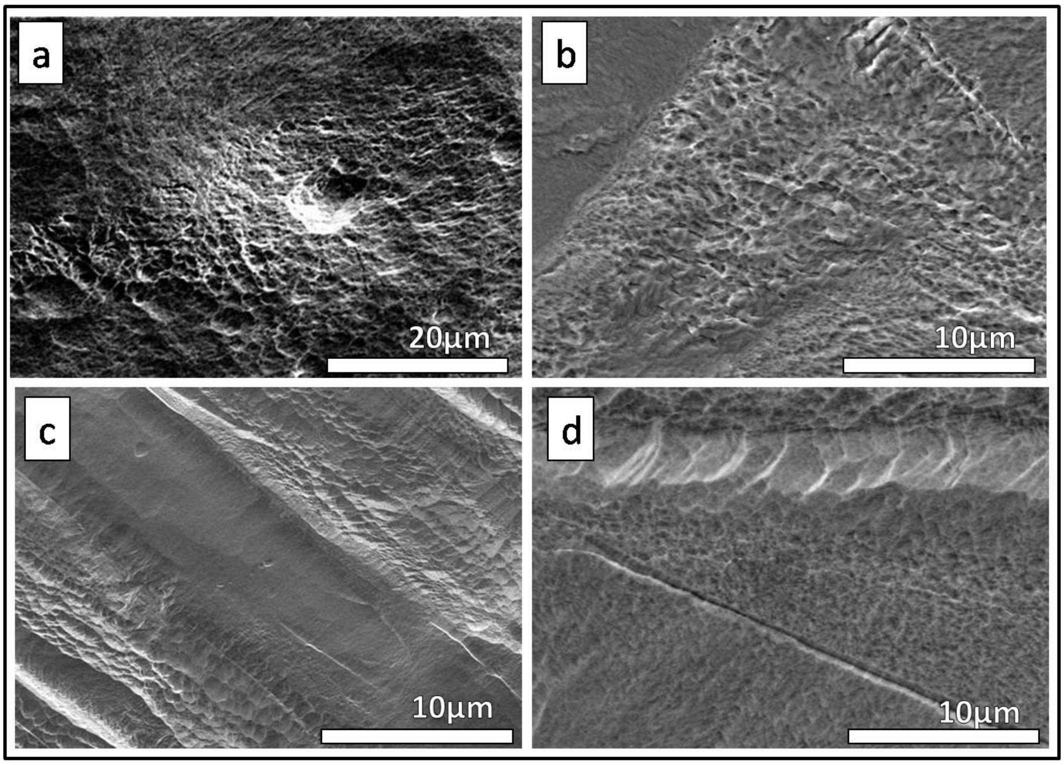

Figure 4.31: SEM images of the surface of vanadium foils after a treatment with a saturated boric acid solution in the "Copper-setup": a) 75 V, 30 min, c) 40 V, 30 min, b) and d) 40 V, 5 min.

The image in Figure 4.31 a was taken from a sample that was treated for 30 minutes at 75 V. The surface of the sample looks etched after the treatment, there is no sign of the formation of an oxide, neither in a SEM investigation, nor to the naked eye. There irregular indentations ranging up to one μm in size. The samples treated at 40

V for 30 and 5 minutes (see Figure 4.31 b, c and d) look rather similar, only the etched patterns are smaller; the indentations are well below 500 nm.

While the formation of an oxide layer on the vanadium foil using aqueous solutions was not succesful, etching of the samples occured. For the formation of vanadium oxide nano-tubes or -pores it would be interesting to be able to etch the vanadium foil in an organized fashion. Possibly a well arranged array of nanoindentations can serve as a substrate for the subsequent growth of nanotube on the same. A similar mechanism was described for the anodization of titanium (see section 4.3), in which case the addition of small amounts of fluoride leads to the desired growth of nanotubes, with an ordered array of nanoindentation below the oxide layer.

0.5 wt% of either ammonium fluoride or oxalic acid were added to the saturated boric acid solution, thereby dramatically increasing the conductivity of the respective solutions. As a consequence the current for the anodization was rather high (above 750 mA), which lead to the development of heat in the solutions. Thus, the reactions were only carried out for 10 minutes at 40 V or for 3 h at a voltage of only 10 V.

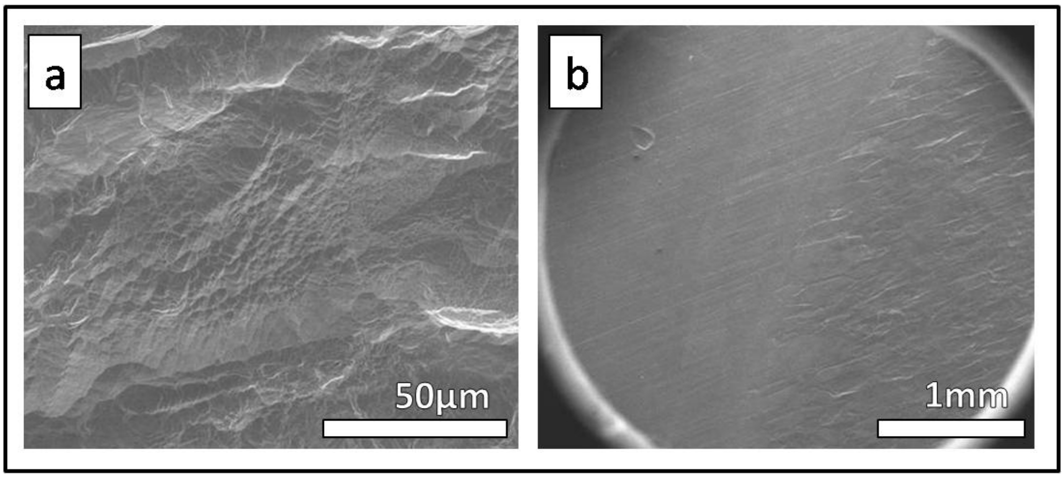

Figure 4.32: SEM images of the surface of a vanadium foil after treatment with a saturated boric acid solution containing 0.5 wt% oxalic acid in the "Copper-setup" for 3 h at 10 V.

Figure 4.32 exemplarily shows the outcome of the described experiments; SEM images of a sample treated for 3 h at 10 V with a saturated boric acid solution containing 0.5 wt% oxalic acid are shown. However, the observed results for the other experiments were indistinguishable from the ones shown in Figure 4.32. Additionally no significant difference compared to the samples obtained without oxalic acid or ammonium fluoride was observed. The samples were etched and no pores were found. In Figure 4.32 b the difference between the untreated and the etched part of the sample is shown, verifying the change in the sample upon the electrochemical treatment.

Aqueous solutions of boric acid with or without additives are not suitable for the anodization of vanadium foil. No oxide layer could be obtained, the samples were instead etched during the anodization. It was neither possible to alter the etching process to obtain ordered indentations, rather than irregular ones. The reaction solution was too "aggresive", owing to aforementioned high conductivity, caused by the high amount of dissolved boric acid and the rather rapid diffusion in the low viscosity solvent water, as well as the high solubility of vanadium oxides in water.

Anodization of Vanadium Part III: Organic Solvents

Ethylene glycol: "Standard conditions"

To address the issues mentioned in section 4.4.3 organic solvents were used in this part of the study. The increased viscosity of non-aqueous solvents was already utilized for the formation of TiO_2 nanotube arrays,[88] leading to a more controlled and ordered growth of the nanotubes. Additionally, both boric acid and vanadium oxides are less soluble in organic solvents, as compared to water, possibly favoring the formation of an oxide layer over an etching process.

First, ethylene glycol was studied as a solvent; owing to several advantages, such as sufficient solubility of reactants, miscibility with water in any ratio and a reasonably high viscosity and conductivity, EG is the most prominent solvent for the anodization of titanium. Additionally the "Anodization solution 2", which was also based on EG did exhibit some porous structures, making ethylene glycol a promising candidate as a solvent. The solution was made as described in the experimental section (2 wt% of water and 0.5 wt% of ammonium fluoride or oxalic acid dissolved in EG saturated with boric acid). The experiments were carried out for 3 h at a voltage of 40 V using the "Copper-setup". The conditions described here will be referred to as "Standard-conditions" from now on. Deviations from these conditions will be noted later in the text. The results are shown on Figure 4.33.

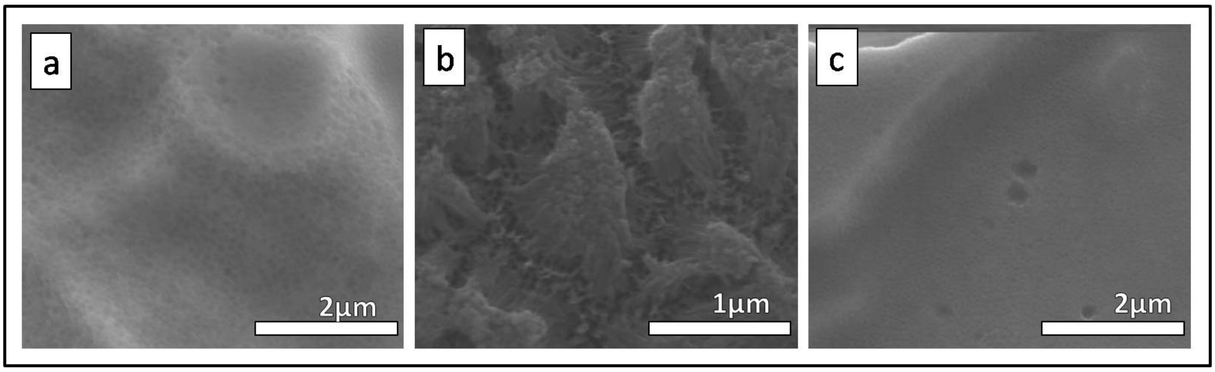

Figure 4.33: SEM images of the surface of vanadium foils after treatment under "Standard-conditions" (2 wt% of water and 0.5 wt% of ammonium fluoride or oxalic acid dissolved in ethylene glycol saturated with boric acid, 3 h reaction duration, 40 V, "Copper setup": a) Ammonium fluoride b) and c) Oxalic acid.

The surface of the sample obtained using NH_4F was corrugated, yet porous. The pores are polydisperse and no order is observable. As opposed to the samples shown before, the vanadium foil was not etched, but an oxide film was formed on top of it. The highest areas of the oxide layer seem rather flat, only shallow pores can be seen, which points towards the formation of a mesoporous oxide, rather than an array of nanotubes (see Figure 4.33 a). Another sample was produced using oxalic acid as an etching agent. While most parts of the film look similar to the "NH_4F" sample (see Figure 4.33 c), other areas show the formation of wire-like structures, that form bundles (see Figure 4.33 b), which can be affiliated to the more aggressive nature of $H_2C_2O_4$ as an etching agent and thus an etching process in the oxide layer.

However, in these experiments large areas exhibiting a porous structure were found for the first time. The presence of boric acid is necessary to form a continous oxide layer (compare section 4.4.3) and both NH_4F and $H_2C_2O_4$ can induce the formation of porous structures.

Ethylene glycol: Different setups

The samples shown in this section were made under the same condition as described above, only the "Teflon-Setup" was used instead of the "Copper-setup". The results are shown in Figure 4.34.

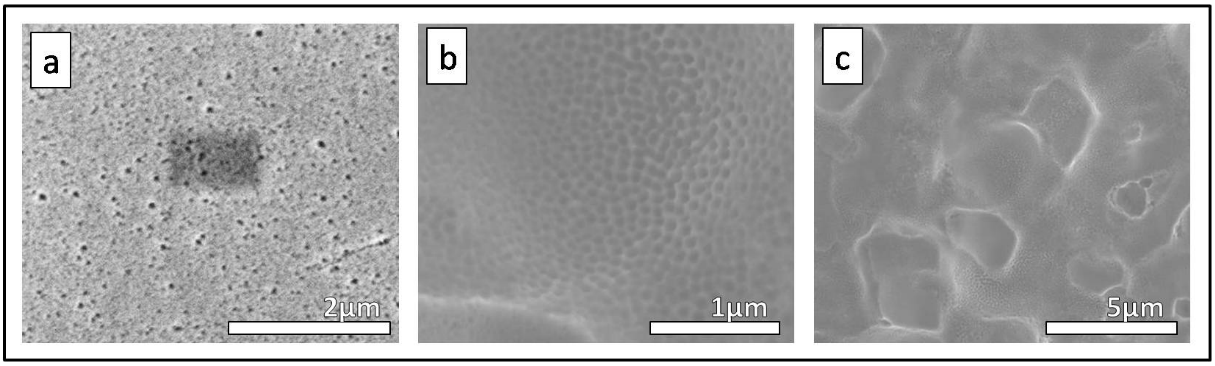

Figure 4.34: SEM images of the surface of vanadium foils after treatment under "Standard-conditions" (2 wt% of water and 0.5 wt% of ammonium fluoride or oxalic acid dissolved in ethylene glycol saturated with boric acid, 3 h reaction duration, 40 V, "Teflon-setup": a) ammonium fluoride b) and c) oxalic acid.

In this case, the differences between the "NH_4F and $H_2C_2O_4$ samples" were more pronounced compared to the previous section. The NH_4F sample, on one hand, was flat, no elevations or indentations were found. Pores were visible on the samples' surface, however, the pore-density was rather low, their distribution random and the shape irregular (see Figure 4.34 a). In case of the $H_2C_2O_4$ sample, on the other hand, the surface was completely covered with a dense, unordered array of nanopores (see Figure 4.34 b). Figure 4.34 c shows that the highest areas of the oxide layer on the vanadium foil were again rather flat (also compare 4.33 a). The difference between the two samples is clearly evident, which was a rather unexpected result. One possible explanation is a slower reaction progress due to the hindered diffusion in the "Teflon-setup" (the "tube" that connects the sample to the rest of the reaction vessel is longer, compared to "Copper-setup"). The slower reaction progress explains both the low pore density for the "NH_4F sample", as well as the missing wire-like structures in the "$H_2C_2O_4$ sample", i.e. no etching of the sample occurred. Based on these observations it is also reasonable to conclude that the reaction proceeds faster when oxalic acid is used instead of ammonium fluoride. Other than reaction velocity, the results obtained using the "Teflon-setup" were rather similar to the ones in the "Copper-setup". Due to the more rapid reaction progress, the "Copper-setup" is preferable.

Ethylene glycol: Temperature control

The samples described previously in this section were fabricated without an active temperature control, i.e. the experiments were conducted at room temperature. In order to aid the uniform growth of a vanadium oxide layer, all samples were from now on prepared at a controlled temperature of 25°C.

Figure 4.35 and c shows the surface of the "NH_4F samples", which are similar to the samples obtained without temperature control. The surface is corrugated and porous, neither order nor size control was achieved. The highest areas of the sample do not exhibit pores. The "$H_2C_2O_4$ sample", on the other hand, looks completely different (see Figure 4.35 b and c). It is completely non-uniform and uneven. Bubble-like structures are observed, additionally there is no complete pore-coverage and the size and shape of the pores is irregular.

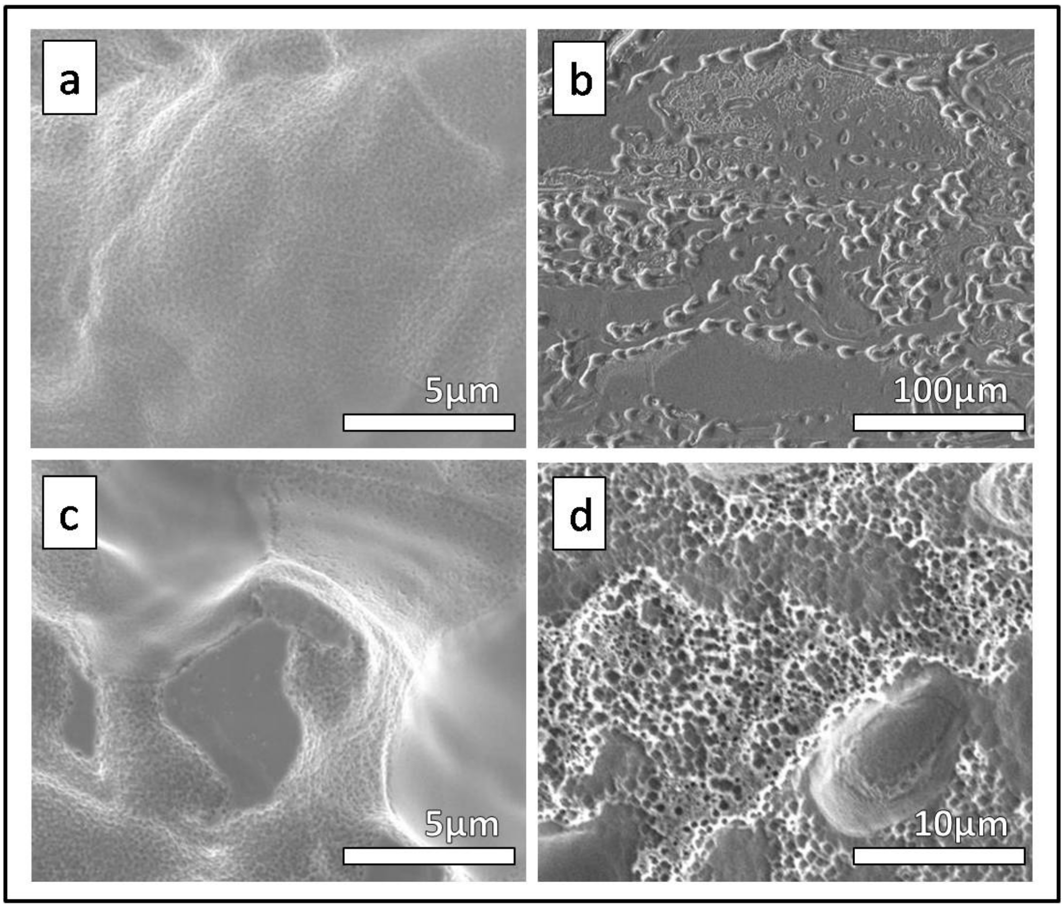

Figure 4.35: SEM images of the surface of vanadium foils after treatment under "Standard-conditions" (2 wt% of water and 0.5 wt% of ammonium fluoride or oxalic acid dissolved in ethylene glycol saturated with boric acid, 3 h reaction duration, 40 V, 25°C, "Teflon-setup": a) and c) Ammonium fluoride b) and d) Oxalic acid.

The results display a major drawback of the reactions discussed so far: A lack of reproducibility. There are multiple possible reasons for this behavior:

- The concave substrate leading to variations in the electric field on the vanadium foil.
- The solubility of boric acid in ethylene glycol depends on the ambient temperature.
- An aging effect of the anodization solution is possible, as shown for the electropolishing solution.
- The formation of an insoluble gel on top of vanadium foil.

However, pores were found in all samples, demonstrating the principal feasibility of the applied method.

Ethylene glycol: Components of the anodization solution

The composition of the reaction solution was based on work reported in literature and experience gathered *via* the anodization of titanium. It was stated earlier that in this work and in the literature [79] that boric acid or borax, respectively, represents a necessary component for growth of an oxide layer. The presence of an etching agent, such as oxalic acid was found to be a necessary prerequisite for the formation of pores or tubes, rather than a solid oxide layer, in the literature concerning anodizations.[13] In this line of experiments, the actual influence of the aforementioned components was investigated for the reaction system investigated in this study.

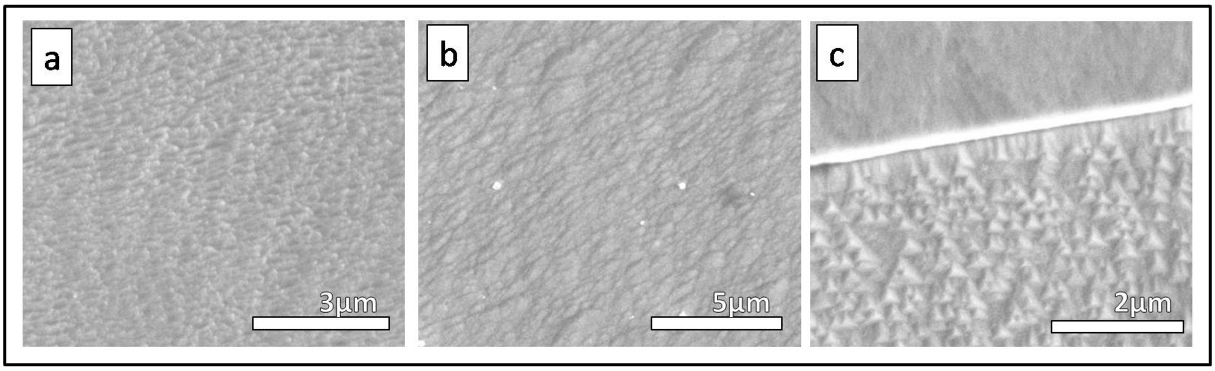

Figure 4.36: SEM images of the surface of vanadium foils after treatment under "Standard-conditions" (2 wt% of water and 0.5 wt% of ammonium fluoride or oxalic acid dissolved in ethylene glycol saturated with boric acid, 3 h reaction duration, 40 V, 25°C, "Teflon-setup"): a) No oxalic acid was used b) No boric acid was used c) Both oxalic and boric acid were left out.

Figure 4.36 a shows a SEM image of a vanadium foil anodized without oxalic acid. No trace of pores was observed, but a corrugated oxide layer was formed. When an anodization solution without boric acid was utilized, the sample exhibits etched structures, similar to those obtained in aqueous solutions. Again, no pore formation occurred (see Figure 4.36 b). If neither oxalic nor boric acid were used, most of the sample was completely flat (see upper part of 4.36 c), while tetrahedral structures were observed in some parts of the sample (see lower part of 4.36 c). Their origin is the subject of ongoing research.

In neither of the samples pore formation was observed; clearly demonstrating that all components are required to induce the growth of nanopores or tubes. The boric acid is most likely the oxygen source for the formation of the oxide layer, while the oxalic acid etches the pores into the same.

Ethylene glycol: Reaction duration

Judging from the contrast of the SEM images shown so far and the little optical changes of the vanadium foil before and after the anodization, the pores obtained are rather shallow. Thus, longer reaction durations were tested, in order to determine whether the pore length can be enhanced.

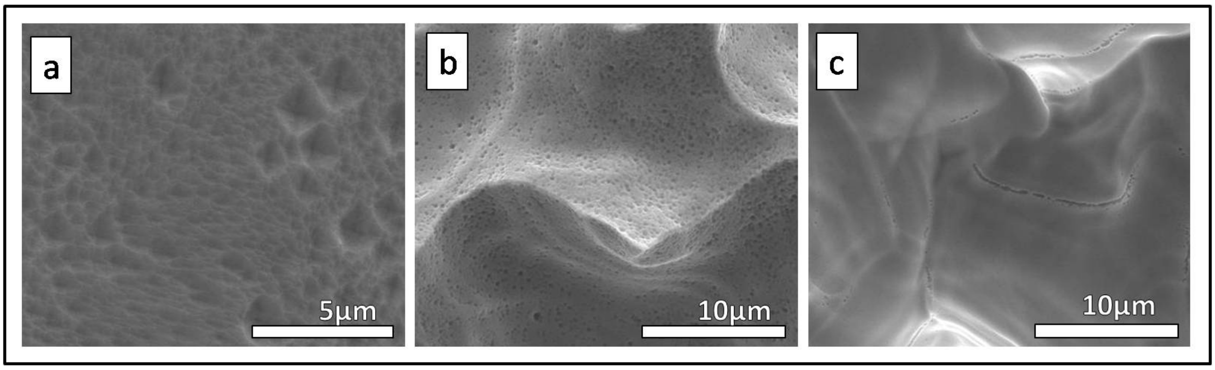

Figure 4.37: SEM images of the surface of vanadium foils after treatment under "Standard-conditions" but for a prolonged reaction duration of 16 h using: a) $H_2C_2O_4$ b) and c) NH_4F.

The results for the "$H_2C_2O_4$ sample" are shown in Figure 4.37 a. The sample is completely uniform, however, no pores were found on its' surface. It was observed that structures similar to the etched ones in the samples made with aqueous solutions were formed. Apparently no oxide film was formed, but the vanadium foil was etched during the reaction. For the anodization utilizing NH_4F, on the other hand, a corrugated oxide film was obtained. Parts of the sample were covered with unordered, polydisperse pores, while also non-porous areas were found. In general the pore-density was rather low.

In case of the oxalic acid it was concluded that the oxide film is corroded away by the oxalic acid. The current at the end of the long-term reaction is very low, leading to a dominance of chemical etching over the formation of an oxide layer, which is induced by the current. Based on this consideration it can be stated once again, that the NH_4F is a weaker etching agent than oxalic acid, which is most likely due to the chelate-effect of $H_2C_2O_4$, since the oxide film is still present after 16 h.

Ethylene glycol: Concentration of the etching agents

In order to elucidate the effect of the etching agents more clearly different amounts of NH_4F and $H_2C_2O_4$, respectively, were used in this line of experiments.

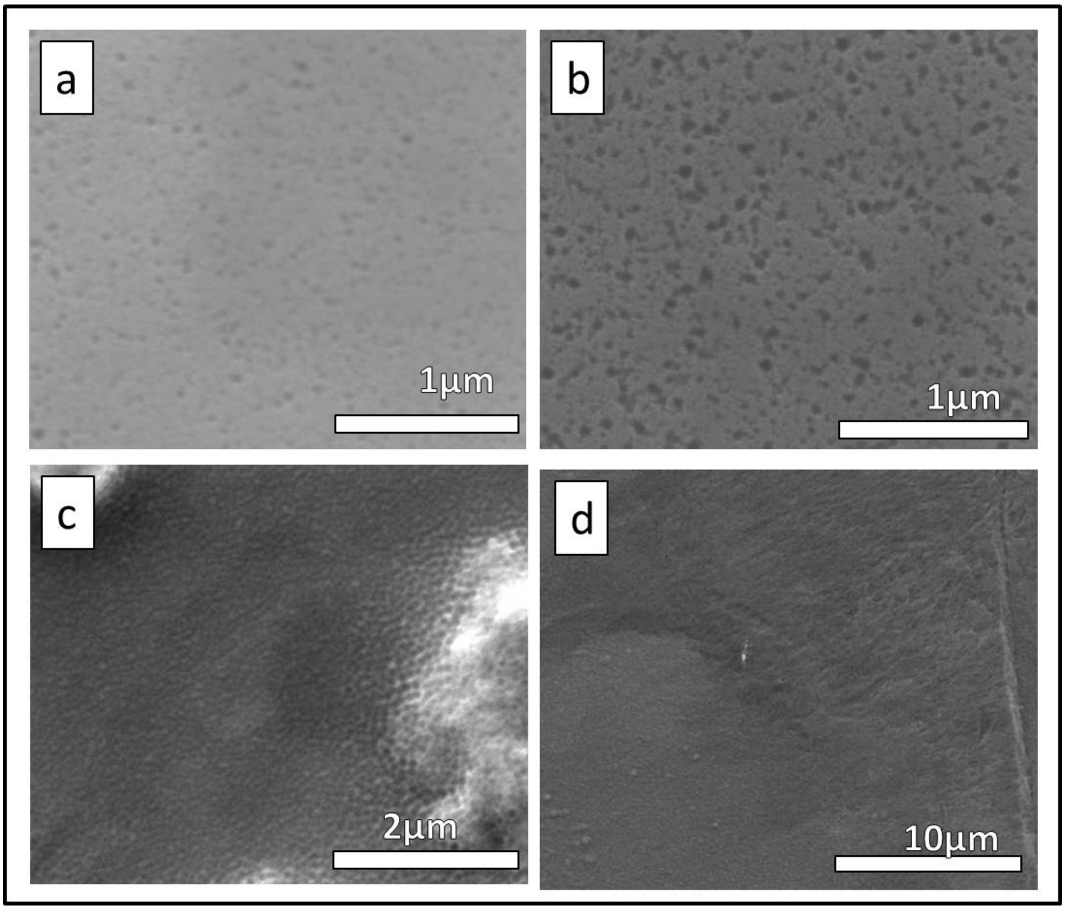

Figure 4.38: SEM images of the surface of vanadium foils after treatment under "Standard-conditions" but with a varying amount of NH_4F and $H_2C_2O_4$: a) 0.2 wt% NH_4F b) 0.2 wt% $H_2C_2O_4$ c) 0.7 wt% NH_4F and d) 0.7 wt% $H_2C_2O_4$.

The surface of the vanadium foils anodized with 0.2 wt% NH_4F (see Figure 4.38 a) was flat over large areas, as opposed to the corrugated surfaces observed in earlier experiments. However, the sample exhibits randomly distributed, polydsiperse, low density pores on the entire surface. Additionally the pores seem small, compared to a sample prepared with 0.5 wt% NH_4F. A quantification of the pore size is difficult due to the random size distribution. Very similar results were obtained for the sample anodized with 0.2 wt% $H_2C_2O_4$, the major difference being a larger pore size. The behavior is another indication for the stronger etching effect of oxalic acid. This phenomenon is even more evident for the samples anodized with 0.7 wt% $H_2C_2O_4$ and NH_4F (see Figure 4.38 c and d). In case of the NH_4F sample a corrugated surface was found again. While the lower parts of the sample are non-porous, there are several hills scatterd all over the sample, which are porous. For the $H_2C_2O_4$ sample, no pores were found at all. The surface seems strongly etched and relatively flat. The use of more etchant leads to a dominance of chemical etching compared to the electrochemical growth of the oxide layer. Essentially these experiments show that the amount AND nature of the etchant are both decisive. Too little leads to the formation of low density pores, too much leads to the dissolution of the oxide layer, which represents a random process and is thus not desirable for the formation of ordered arrays of nanopores. The evident difference of the etching effect of NH_4F and $H_2C_2O_4$ shows that the results obtained with the same amount of the respective agent are not comparable to each other. From now on, only oxalic acid was used, due to the more rapid nature of the etching process compared to NH_4F.

Ethylene glycol: Concentration of boric acid

It was already demonstrated that the complete omission of boric acid prevents the generation of an oxide layer and thus pore formation. While for the experiments described so far saturated boric acid solutions were used, herein the amount of boric acid was varied. Three different concentrations were used, i.e. 0.02 g/ml, 0.06 g/ml and 0.1 g/ml. For both of the lower concentrations the outcome was similar to the sample fabricated without boric acid (compare Figures 4.39 a and 4.36 b). No pores were found on the sample and the surface seemed etched. Apparently no oxide was formed in course of these reactions. On the surface of the sample made with a solution containing 0.1 g/ml boric acid pores were observed. The surface was corrugated and the pores, which were roundish and rather well ordered, were found on most parts of the sample. However, the pores were comparably shallow, judging from the weak contrast of the SEM images. Additionally, high amounts of unwanted particles were found on the sample. The last experiment nicely shows the different functions of the chemical species involved in the anodization. While the oxide formation is due to the boric acid, and is thus hindered if the amount of H_3BO_3 is reduced, the pores are formed due to the oxalic acid. If an oxide layer is formed (as in the sample containing 0.1 g/ml H_3BO_3), roundish pores are obtained when 0.5 wt% oxalic acid is used, as in the sample prepared with a saturated boric acid solution.

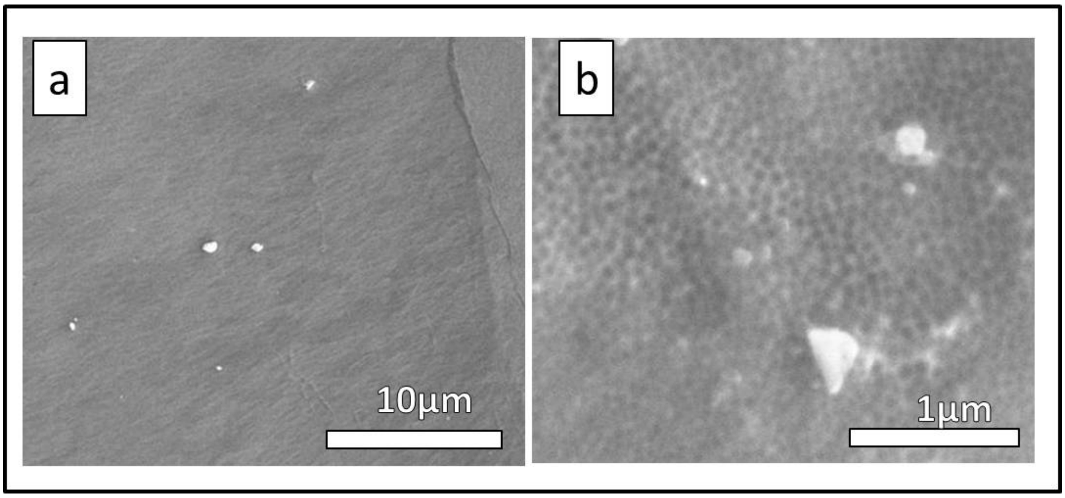

Figure 4.39: SEM images of the surface of vanadium foils after treatment under "Standard-conditions" but with a varying amount of boric acid: a) 0.02 g/ml b) 0.1 g/ml.

Tetra-ethylene glycol: "Standard conditions"

Porous oxide layers could be formed using ethylene glycol as a solvent for the anodization reactions; in some experiments even partially ordered ones were obtained. However, both reproducibility and uniformity of the samples was found to be problematic. The reproducibility issue can be addressed by carefully controlling the reaction parameters and other factors, such as the preparation of the reaction solutions and the vanadium foil. In principle, uniformity can be achieved by adjusting the ratio between oxide formation and etching of the pores into the vanadium oxide. This can be done *via* adjusting the amount or chemical nature of the etchant (see last section) or changing the solvent, which directly influences the solubility of the as-formed vanadium oxide and the rate at which the oxide will be etched.

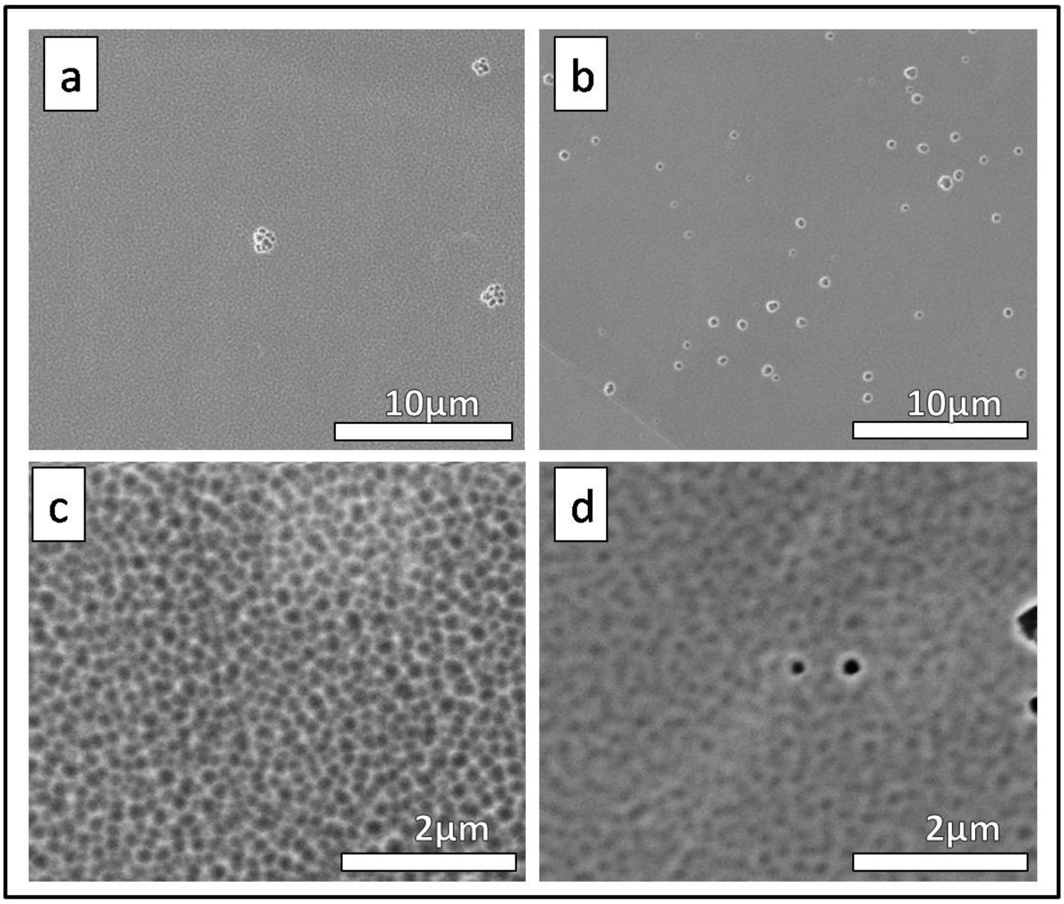

Figure 4.40: SEM images of the surface of vanadium foils after treatment under "Standard-conditions" with tetra-ethylene glycol as solvent using: a) and c) 0.5 wt% $H_2C_2O_4$ b) and d) 0.5 wt% NH_4F.

The viscosity of the solvent influences the diffusion of reactants in the solution; a solvent with a higher viscosity will thus lead to lowered diffusion and a decreased etching rate. Based on these considerations tetra-ethylene glycol was tested as a solvent for the anodization of vanadium foil.

The "Standard-conditions" are the same as described in the last section, only the solvent was changed (2 wt$\%$ of water and 0.5 wt$\%$ oxalic acid or ammonium fluoride dissolved in tetra-ethylene glycol (TEG) saturated with boric acid, 3 h reaction duration, 40 V, 25°C, "Copper-setup"). The results of the experiments are shown in Figure 4.40. It is noteworthy that both samples exhibit flat and uniform surfaces, additionally the reaction is completely reproducible. However, some defects are still found on top of the sample (see Figure 4.40 a and b). Both the samples prepared using $H_2C_2O_4$ (see Figure 4.40 a and c) as well as NH_4F (see Figure 4.40 b and d) are rather similar. The surfaces are completely covered with unordered, polydisperse pores with an average pore size of around 120 to 130 nm. In the case of ammounium fluoride as the etching agent, the pores seem rather shallow; similar observations were made before.

Tetra-ethylene glycol: Reaction duration

The solubility of vanadium oxides is lower in tetra-ethylene glycol, as compared to ethylene glycol. Additionally the effect of the etchant should be lowered, due to a decreased diffusion in TEG caused by its' higher viscosity. Thus, longer reaction durations in TEG may lead to a thicker, yet still uniform oxide layer, while avoiding the formation of corrugated oxide films.

The results for samples anodized for 1, 6, 16 and 65 h, respectively, are shown in Figures 4.41 and 4.42. The only significant difference compared to the sample made using the "Standard-conditions" is the amount of defects that were observed on the surface. While virtually none were found on the "1 h sample" (see Figure 4.41 a), significantly more were found on the vanadium foil after a treatment of 6 h (compare Figure 4.41 b). After 16 h the amount and size of the defects has further increased. Their shape is roundish and they are porous themselves (as shown in Figure 4.42 a). When the treatment was carried out for as long as 65 h the "defects" cover most of the surface of the metal foil. They exhibit an irregular shape and parts are porous, while others seem solid (see Figure 4.42 b). Beneath these defects and on the other parts of the samples, a uniform pore coverage similar to the sample made using "Standard-conditions" is found (compare Figure 4.41 b and d, as well as 4.42 b and d).

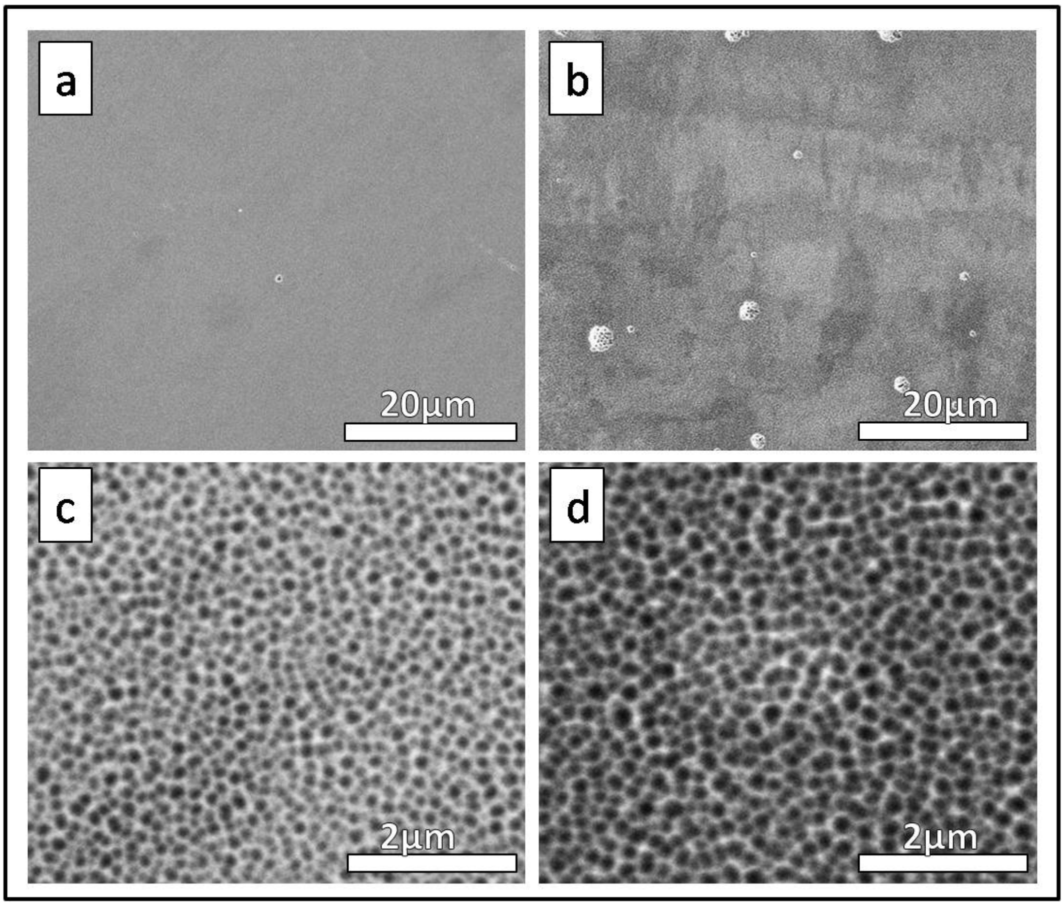

Figure 4.41: SEM images of the surface of vanadium foils after treatment under "Standard-conditions" with TEG as solvent and varying reaction conditions: a) and c) 1 h b) and d) 6 h. Only $H_2C_2O_4$ was used as etching agent.

The pore size for all four samples was found to be the same as the sample anodized for 3 h, i.e. 120 to 130 nm. As for the anodization of titanium, [89] the pore size does not depend on the reaction duration, but on the anodization voltage under otherwise similar conditions at sufficiently long reaction durations. Interestingly, it was observed that the size of pores varies in the vicinity of the defects for the 16 h sample (see Figure 4.42 b); the pores exhibit diameters of around 240 nm in this case. The origin of the defects and the varying pore size near them cannot be easily explained and is the subject of ongoing research. However, the original intention to form a thicker, yet uniform oxide layer could not be implemented due to the appearance of large defects.

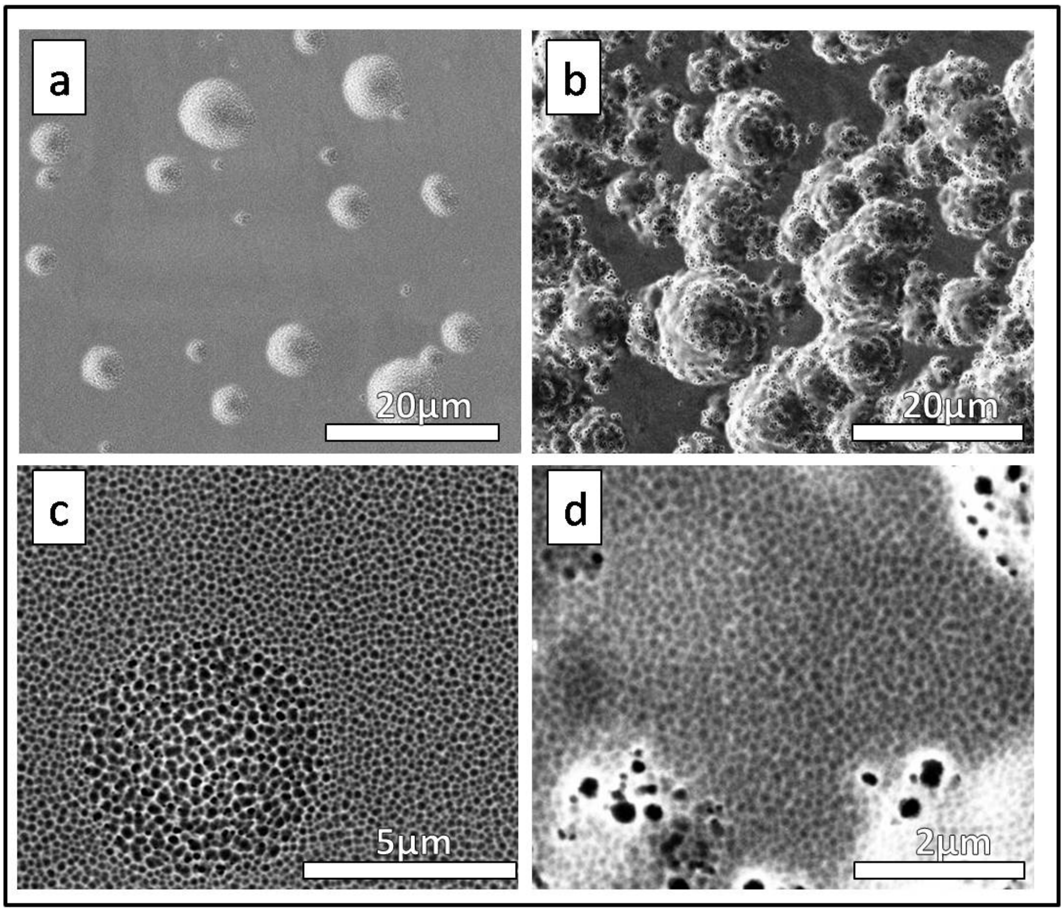

Figure 4.42: SEM images of the surface of vanadium foils after treatment under "Standard-conditions" with TEG as solvent and varying reaction conditions: a) and c) 16 h b) and d) 65 h. Only $H_2C_2O_4$ was used as etching agent.

Poly-ethylene glycol

The use of TEG as solvent under otherwise unchanged conditions (2 wt% of water and 0.5 wt% oxalic acid dissolved in tetra-ethylene glycol (TEG) saturated with boric acid, 3 h reaction duration, 40 V, 25°C, "Copper-setup") yielded to the formation of uniform samples with little defects. It is thus interesting to utilize a solvent with an even higher viscosity and lower solubility of vanadium oxides such as poly-ethylene glycol, under otherwise similar conditions. It should be noted that also less boric acid could be dissolved in PEG, compared to all other solvents used.

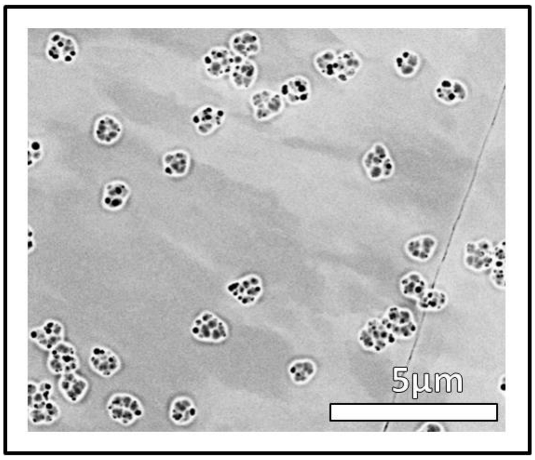

Figure 4.43: SEM image of the surface of a vanadium foil after treatment under "Standard-conditions" with poly-ethylene glycol as solvent. Only $H_2C_2O_4$ was used as etching agent.

No pores could be found on the sample anodized with PEG as solvent. Interestingly, defects similar to those observed in "TEG-samples" were found on this sample, too (see Figure 4.43). They consist of bundled holes of a roundish shape. Additionally cracks were observed (see right part of Figure 4.43), which points towards the formation of a flat oxide layer, since these cracks are not found on pristine samples. No etching of the oxide layer occured, most likely due to the limited diffusion owing to the high viscosity of PEG, as compared to the other solvents used.

Mixture of ethylene- and tetra ethylene glycol: "Standard conditions"

When ethylene glycol was used as solvent under "Standard conditions" (2 wt% of water and 0.5 wt% oxalic acid dissolved in the respective solvent saturated with boric acid, 3 h reaction duration, 40 V, 25°C, "Copper-setup") roundish pores on a corrugated surface were obtained as a result. If the solvent EG was exchanged with TEG, on the other hand, a uniform and even pore coverage with little defects was obtained. However, in this case the pores were irregularly shaped. A combination of the properties of both solvent (Viscosity, solubility of the reactants and vanadium oxide) may present a solution to this issue. In principle there are two possibilities to achieve this combination:

1. A mixture of TEG and EG can be used
2. Another solvent, such as di-etyhlene glycol, can be utilized

The first attempt was made with a 1:1 volumetric mixture of TEG and EG, which was saturated with boric acid after blending the two solvents. All other conditions remain as usual.

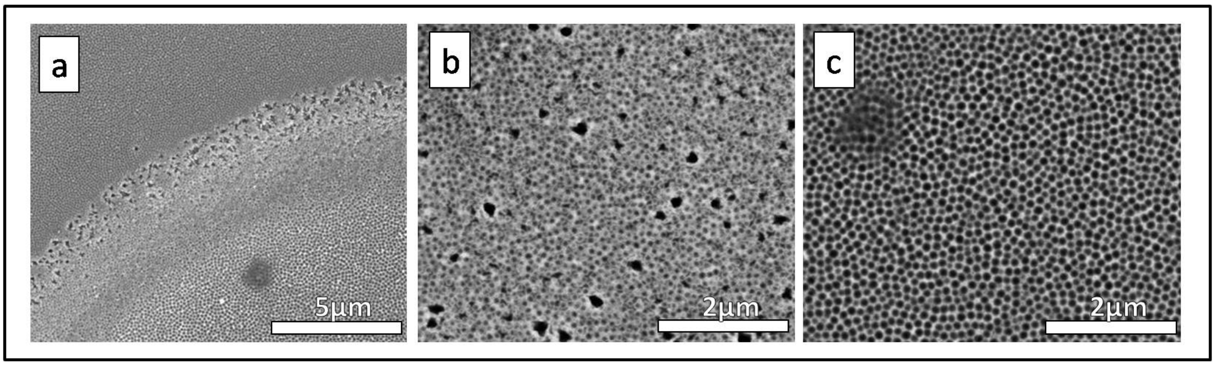

Figure 4.44: SEM images of the surface of vanadium foils after treatment under "Standard-conditions" with a volumetric (1:1) mixture of TEG and EG as solvent. Only $H_2C_2O_4$ was used as etching agent.

The samples obtained are rather uniform, yet a significant amount of defects can be observed (see Figure 4.44 a). Furthermore, the reaction is highly reproducible and the resulting porous oxide layers are not corrugated. The majority of the sample consists of roundish, partially ordered, polydisperse nanopores with a diameter of around 100 nm, as shown in Figure 4.44 c. Most of the observed defects are irregularly shaped holes/pores, while others are tube-like (compare Figure 4.44 b). It can be stated that the idea to combine two solvents to achieve a uniform pore coverage and a flat oxide film worked in principle. However, the pores are neither perfectly ordered nor monodisperse and the amount of defects was higher than originally desired. Interestingly, the diameter of the pores is about 30 nm smaller for the solvent mixture as compared to TEG. While the diameter of the pores is indeed determined by the voltage under otherwise similar conditions, a change of the solvent accompanied by a change of the conductivity of the anodization solution does have an effect on the pore size. The "effective voltage" on the sample is higher, if the conductivity of the solvent used is increased. [12]

Mixture of ethylene- and tetra ethylene glycol: "Anodization voltage"

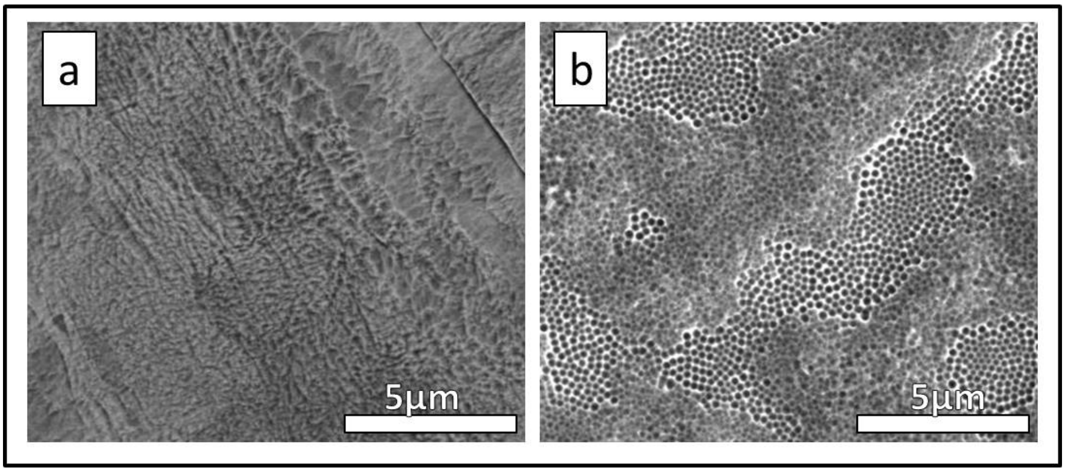

Figure 4.45: SEM images of the surface of vanadium foils after treatment under "Standard-conditions" with a volumetric 1:1 mixture of TEG and EG as solvent at different voltages: a) 20 V; b) 60 V. Only $H_2C_2O_4$ was used as etching agent.

After rather roundish and ordered pores were obtained under "Standard-conditions", the anodization voltage was varied in order to alter the size of the nanopores. Figure 4.45 a shows a SEM image of a sample anodized at 20 V. No pore formation was observed on the surface of the vanadium foil in this case, only etching of the sample occurred. Due to the resistivity of the anodization solution the " effective voltage" on the sample is lowered, preventing the formation of an oxide layer. This leads to the aforementioned dominance of chemical etching over the electrochemical reaction. If the voltage was raised to 60 V the surface of the sample became corrugated; only on the highest areas of the sample roundish pores were observed, while the other parts exhibited irregularly shaped pores (see Figure 4.45 b). This behavior may be attributed to the so called "breakdown voltage". [90]p At a certain voltage an oxide is detached from the surface of a metal. The exact value of this voltage depends on multiple parameters, such as conductivity of the solvent or reactivity of reactants in the solution. However, the exact reason for the beahvior is not understood, yet, and the influence of the anodization voltage is more compley than a simple size-tuning of the nanopores.

Di-ethylene glycol

In the previous section it was stated that the second option to obtain a solvent with properties of both EG and TEG is the use of di-ethylene glycol, which will be described in the following section. All other parameters were the same as in the "Standard-conditions" (2 wt% of water and 0.5 wt% oxalic acid dissolved in the respective solvent saturated with boric acid, 3 h reaction duration, 40 V, 25°C, "Copper-setup").

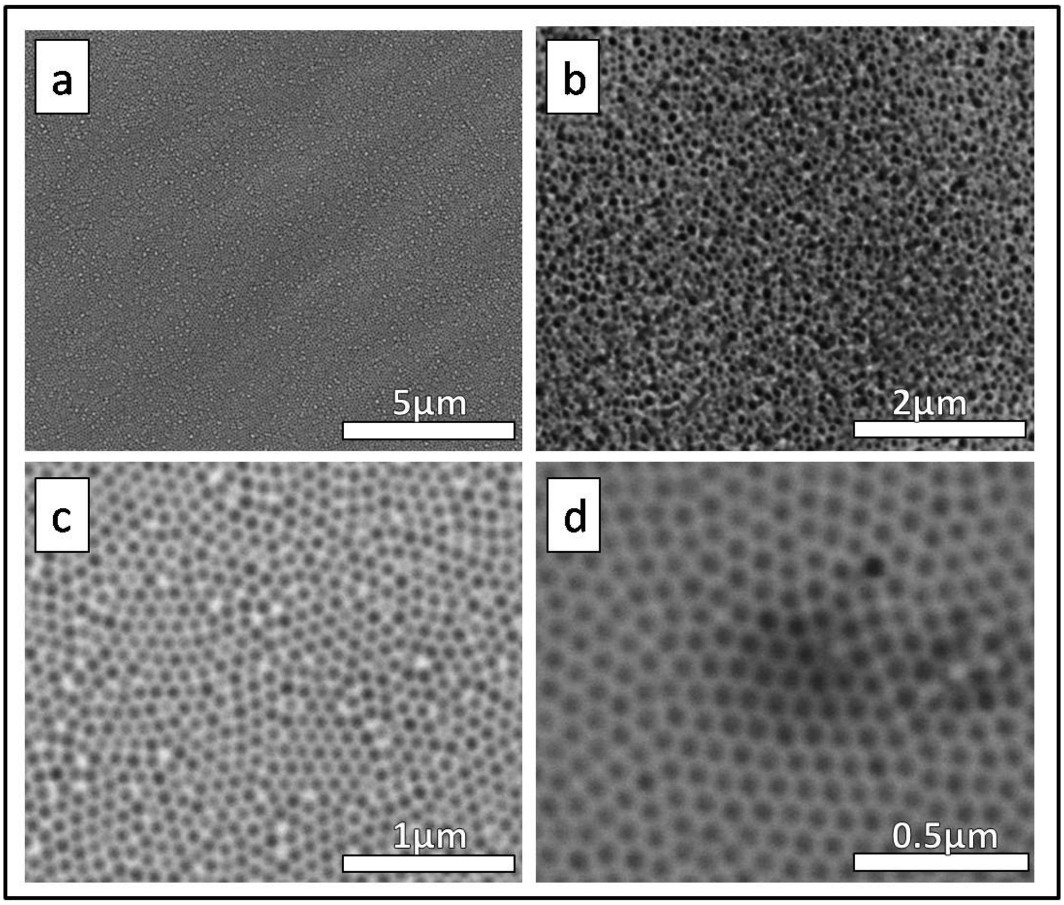

Figure 4.46: SEM images of the surface of vanadium foils after treatment under "Standard-conditions" with DEG as solvent: a) and c) "Sample 1"; b) and d) "Sample 2". Only $H_2C_2O_4$ was used as etching agent.

For the first experiment conducted using DEG as a solvent (see Figure 4.46 a and c) a perfectly uniform sample was obtained. Only a few unwanted particles are found on the surface. The pores are well ordered, nearly monodisperse and have a diameter of roughly 70 nm. The majority of another sample anodized with DEG as solvent also consisted of nicely ordered and monodisperse pores (see Figure 4.46 d), while parts of surface of the vanadium foil were covered with irregularly shaped, polydisperse pores and tubes (see Figure 4.46 b). It is also noteworthy that the well ordered pores on this sample have a diameter of around 90 nm, i.e. they are 20 nm larger than the pores of the first sample. This odd behavior cannot be explained so far. One approach towards an explanation is an altered conductivity of the solvent, which may be caused by water in the solvent or the other reactants. However, the explanation remains speculative, until this phenomenon is fully investigated. Regardless, it can be stated that the use of DEG resulted in samples that at least partially consist of the desired well ordered, monodisperse nanopores. These experiments were repeated several times, yet, the resutls of the first experiment could not be reproduced. While nicely ordered pores were always found, defects also occurred in every sample. The diameter of the pores was found to be between 70 and 90 nm for all samples. Despite these variations, apparently the pore size decreases with increasing conductivity, i.e. higher effective voltage on the sample, of the solvent in the anodization of vanadium.

Di-ethylene glycol: Reaction duration and anodization voltage

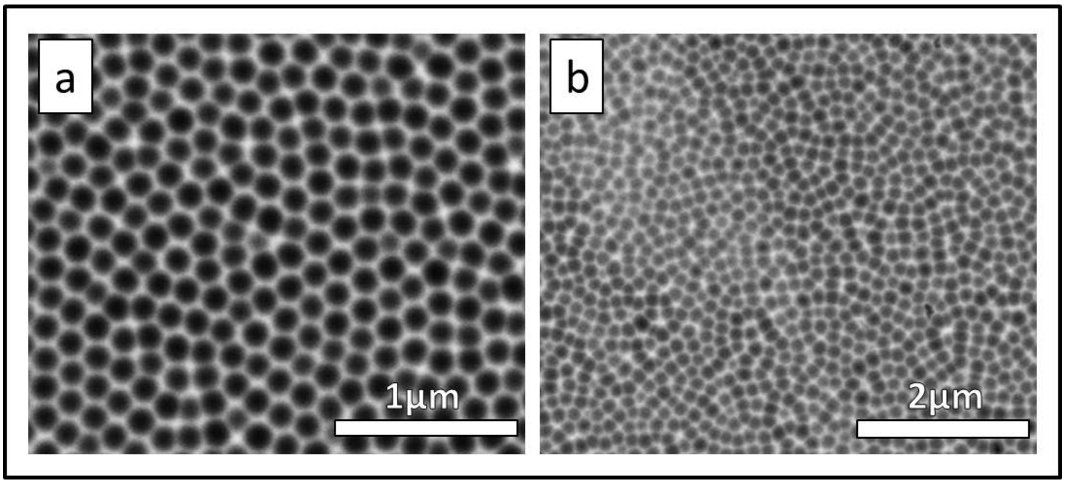

Figure 4.47: SEM images of the surface of vanadium foils after treatment under "Standard-conditions" with DEG as solvent and: a) a reaction duration of 16 h, as well as b) an anodization voltage of 60 V. Only $H_2C_2O_4$ was used as etching agent.

The reaction duration and anodization voltage were altered in order to determine the influence on uniformity of the sample and pore size, respectively. The other parameters were the same as in the "Standard conditions". The SEM image in Figure 4.47 a shows the surface of the vanadium foil anodized for 16 h. The only significant difference compared to samples anodized for 3 h is the pore size, which was increased to around 140 nm. As previously mentioned the pore size predominantly depends on the anodization voltage, however, the reaction duration needs to be long enough to ensure the maximum pore size was already reached. In other words, at the "beginning" of the anodizations the pores grow until the maximum diameter possible at the applied voltage is reached. Afterwards no additional pore growth is observed. [13] In the case describe here, this maximum diameter has not been reached after 3 h, causing the pore growth in the 16 h sample. It should not be neglected that on the surface of this sample irregularly shaped pores and other defects are found.

When the voltage is increased to 60 V and the reaction duration remains at 3 h, an increased pore diameter as compared to the sample prepared at 40 V is expected. Indeed, an increased diameter of 120 nm was found (see Figure 4.47 b). The pores obtained in this experiments are rather well ordered but not as monodisperse as before. Furthermore, large parts of the sample consist of irregularly shaped pores and other defects.

Di-ethylene glycol: The "Glass-setup"

If all parameters in the whole reaction cascade from the unpolished vanadium to the anodized foil are controlled carefully, a uniform sample is expected. However, nearly all samples exhibit parts with defects. It is thus likely that the defects arise from parameters that cannot be controlled very well, such as the ambient conditions (e.g. fluctuations of the humidity), the processing of the as-purchased vanadium foil, which is always concave, or the precipitation of a vanadium oxide on the surface of the foil, which represents a random process. Among these parameters, the precipitate on the surface of the vanadium foil can be prevented, while the influence on the other parameters is limited. The final set of experiments was thus conducted in the "Glass-setup" under otherwise similar conditions as described above (2 wt% of water and 0.5 wt% oxalic acid dissolved in the respective solvent saturated with boric acid, 3 h reaction duration, 40 V, 25°C). Due to the vertical arrangement of the vanadium foil and the counter electrode, the oxide does not precipitate on the vanadium foil.

Multiple samples were prepared under the experimental conditions described above (see SEM images in Figure 4.48 a, c and d). All samples were almost completely uni-

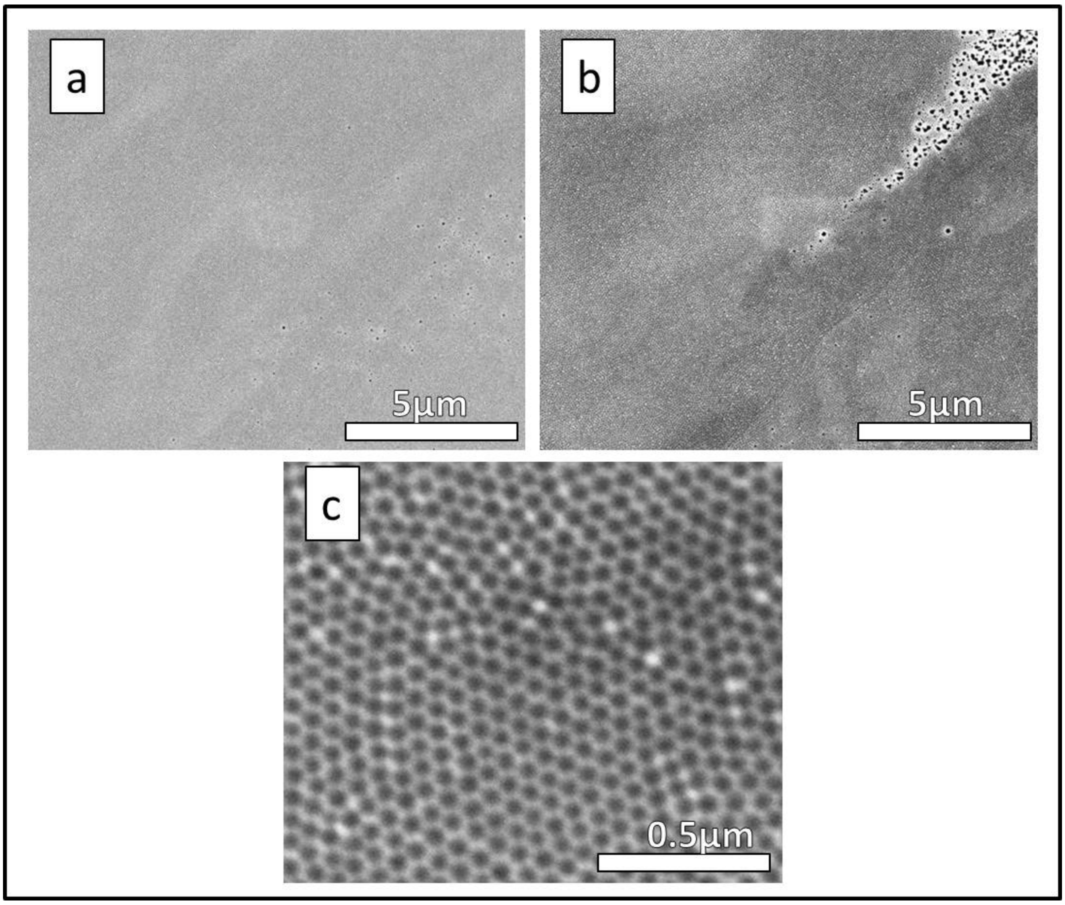

Figure 4.48: SEM images of the surface of vanadium foils after treatment under "Standard-conditions" with DEG as solvent in the "Glass-setup". Only $H_2C_2O_4$ was used as etching agent.

form, defects in form of irregularly shaped pores (compare Figure 4.48 b) were rarely found. The pores were monodisperse and well ordered, with a pore of 40 nm in all samples (see Figure 4.48 c). it should again be emphasized that the pore diameter depends on the anodization voltage, if all other parameters are the same. A change of the setup naturally leads to altered parameters. The diffusion in the "Glass-setup" is unhindered due to a lack of spatial confinement of the electrodes, which leads to a higher current (compare next section) and thus smaller pore diameters. The outcome is in line with the results presented earlier, where a higher conductivity of the solvent also led to a higher current and thus smaller pores. If the solution is stirred the current is further increased, however, the pore diameter remains at 40 nm. It is thus likely that the maximum pore density (i.e. minimum pore diameter) possible under these conditions was reached.

Anodization of Vanadium: Current-Time-Curves of Selected Samples

Typical current time-curves for the anodization of vanadium are shown in Figures 4.49 and 4.50. These curves exhibit a characteristic shape, which is mostly determined by the setup used for the anodization. Figure 4.49 shows the typical shape of the current-time curve in the "Copper-setup", which is exemplarily shown for a vanadium foil anodized under "Standard-conditions" (2 wt% of water and 0.5 wt% oxalic acid dissolved in the respective solvent saturated with boric acid, 3 h reaction duration, 40 V, 25°C, "Copper-setup") using DEG as a solvent.

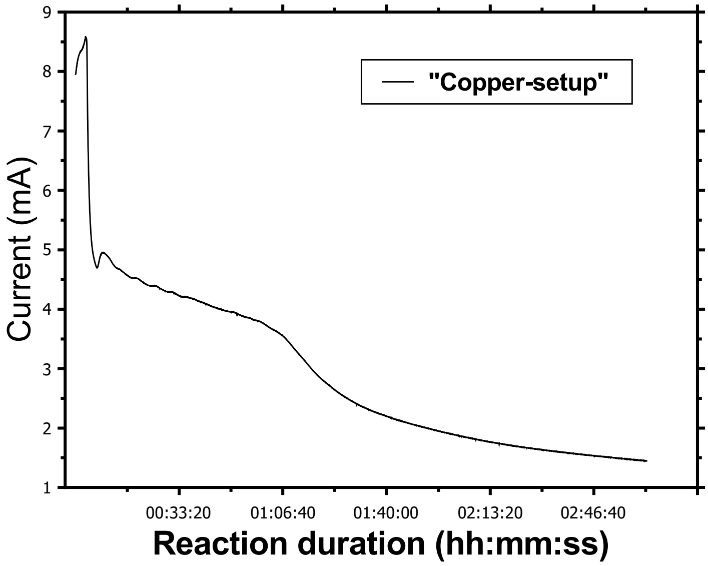

Figure 4.49: Current-time curves of an anodization carried out under "Standard-conditions" using DEG as solvent in the "Copper-setup".

The current quickly rises to its' maximum value, which is around 8.5 mA in this case, followed by a rapid decay to the first minimum. Afterwards there is a short rise of the current, subsequently followed by a steady decline. In this sample, the fall of the current is accelerated between rouhgly 1 h and 90 min reaction duration, which is followed by another steady decline. The current-time curves shows similarities to the corresponsing data obtained while anodizing titanium [2] and can thus be interpreted in a similar fashion. In a first step, the electric field is build up leading to the rise of the current to a maximum value. The subsequently following decrease is due to the formation of a barrier oxide, which starts dissolving due to the etching agent ($H_2C_2O_4$ or NH_4F). The dissolution, which is enhanced and controlled *via* the electric field, causes the barrier oxide to thin down leading to the small rise of the current. In the case of the anodization of titanium this is followed by a steady state, in which dissolution and formation of the oxide layer are in equilibrium leading to a constant current. There are three likely explanations for the described decay of the current observed for the anodization of vanadium:

1. The vanadium oxide formation is dominant over the dissolution, caused by either a slow etching process or rather rapid formation of vanadium oxide.
2. The precipitation of a vanadium oxide on top of the nanopores hinders the current flow.

Figure 4.50 shows the current-time curves for the anodization of vanadium conducted under "Standard-conditions" using DEG as solvent in the "Glass-setup" with and without stirring of the anodization solution in course of the reaction.

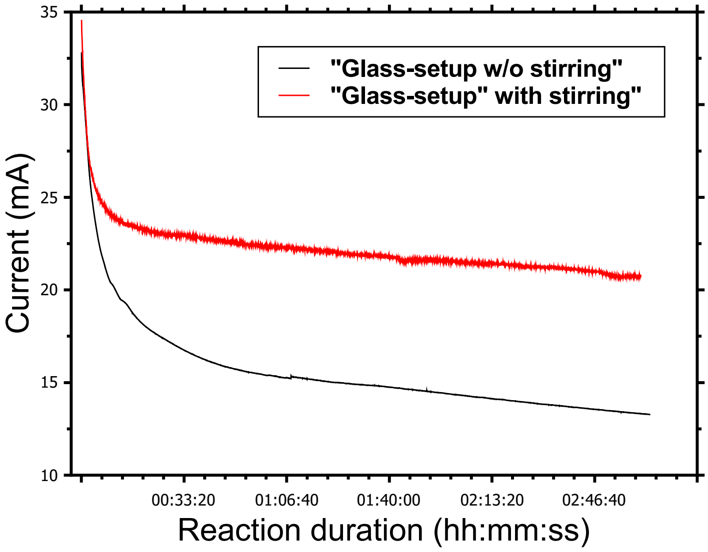

Figure 4.50: Current-time curves of anodizations carried out under "Standard-conditions" using DEG as solvent in the "Glass-setup".

As mentioned earlier, stirring of the reaction solution in the "Glass-setup" led to an increases current, but did not have an influence on the pore size. It did neither influence the shape of the current time curve, which exhibits an exponential decay when the "Glass-setup" is used. The argumentation is similar to the sample described in Figure 4.49. Owing to a lack of obstacles, the electric field builds up rapidly, i.e. the rise cannot be detected. The first current value is recorded after two seconds, which is a technical limitation of the recording device. Most likely the electric field is already completely built-up at that time. Afterwads the current decreases exponentially due to the formation of the barrier oxide. The onset of the dissolution of the oxide layer can neither be detected, most likely due to the high overall current. The final part of the current-time curve is a steady decay, as described above. Since the precipitation of vanadium oxide is prevented due to the vertical arrangement of the electrodes, this is most likely caused by a dominance of the formation of the vanadium oxide over the dissolution of the same.

Based on these considerations the determination of the thickness of the vanadium oxide nanoporous layer on the vanadium foil at the end of the reaction is necessary. It would furthermore be interesting to measure the thickness of the oxide layer at different stages of the reaction.

Anodization of Vanadium: AFM Measurements on selected samples

In order to determine the thickness of the porous vanadium oxide layer AFM measurements were conducted on a sample anodized under "Standard-conditions" using DEG as solvent in the "Glass-setup" (see Figure 4.51). From the depth profile the pore depth and thus the thickness of the porous vanadium oxide layer was determined to be 10 nm. This value is surprisingly low; a thicker vanadium oxide film was expected after 3 h of anodization. In order to elucidate whether the method AFM is suitble for the determination of film thicknesses of porous vanadium oxide films For comparison, a titanium foil anodized under the conditions described by Lee *et al.* [2] in the "Teflon-setup" was also measured (compare Figure 4.52). The thickness of nanotube array on this sample was determined to be around 1 μm *via* cross-sectional SEM measurements beforehand (compare 4.3). A pore depth of 10 nm was measured for the titanium sample, too, i.e. AFM is not suitable for the determination of pore depth in these samples. This is caused by a combination of the small pore diameter and the low angle at which the cantilever is oriented towards the sample. The cantilever cannot penetrate the pores completely.

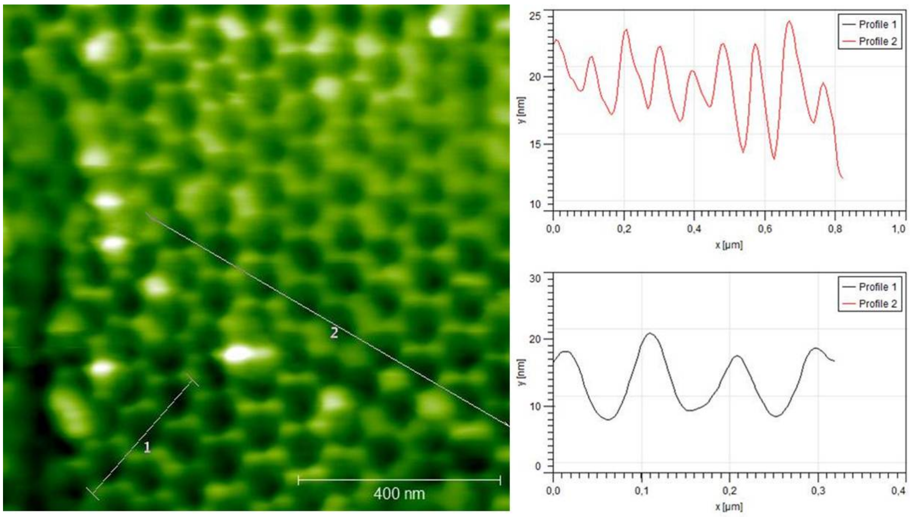

Figure 4.51: AFM image and corresponding depth profiles of a vanadium foil anodized under "Standard conditions" using DEG as solvent.

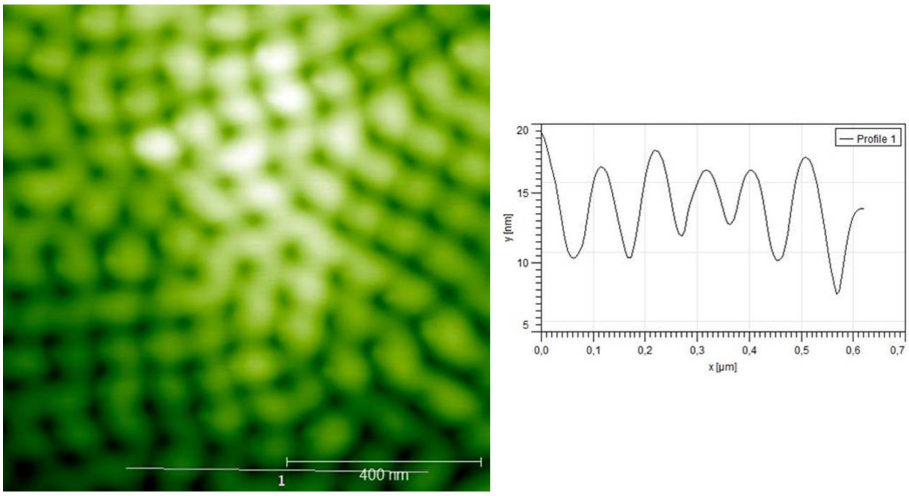

Figure 4.52: AFM image and corresponding depth profile of a titanium foil anodized for 5 minutes using the conditions described by Lee *et al.* [2] in the "Teflon-setup".

Anodization of Vanadium: Cross Section SEM

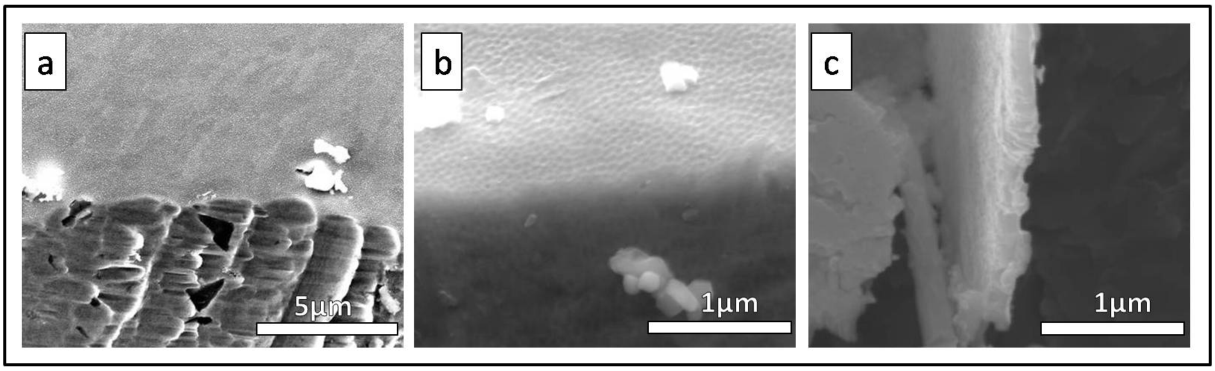

Figure 4.53: Cross-sectional SEM images of vanadium foils anodized under "Standard conditions" using DEG as solvent. The SEM images were obtained *via* different methods: a) The sample was scratched with a diamond cutter, b) the sample was cut with scissors and c) The sample was "shocked" at 400°C.

In case of the anodiaztion of titanium two methods were utilized to obtain cross-sectional SEM images (compare section 4.3):

1. For samples anodized for longer durations the comparably thick oxidic film detached itseld from the sample and could directly be measured.
2. For samples anodized for short durations the film was scratched with a diamond cutter. Parts of the oxide film were detached in the process and could subsequently be measured.

Figure 4.53 shows attempts to obtain cross-sectional SEM images of the anodized vanadium foil, neither of which was succesful.

Since the oxidic layer did not detach itself, it was scratched with a diamond cutter. As shown on Figure 4.53 a, no parts of the film were detached from the surface of the vanadium foil. Only a scratch originating from the diamond cutter was observed. The oxidic layer is either strongly attached to the vanadium foil or it is too soft. A second attempt to cut the sample with scissors (see Figure 4.53 b yielded similar results. The oxidic layer was too soft, which led the porous layer to bend over the cutting edge. Another possibility to detach an oxidic film from the underlying metal is temperature induced stress. For that purpose the as-anodized foils were transferred to a furnace preheated to 400°C. The results of this experiment can be seen in Figure 4.53 c. The thickness of the detached layer was determined to be around 200 nm, however, the porous structure was destroyed upon heating the sample. Thus, it cannot safely be stated that 200 nm is the actual thickness of the vanadium oxide layer. The determination of the film thickness is the subject of ongoing research.

Anodization of Vanadium: XPS Analysis of selected samples

Phase analysis of the as-anodized samples *via* X-ray diffraction was impossible, either due to the amorphous nature of the as-grown oxide or its insufficient thickness. Consequently, XPS analysis was used for a determination of the oxidation states of vanadium in the oxidic film.

In a first step it was attempted to determine the oxidation states of the vanadium oxide on the metal substrate by comparison to purchased vanadium standards (V_2O_3 (98%, Sigma-Aldrich), VO_2 (99%, Sigma-Aldrich), V_2O_5 (>98%, Sigma-Aldrich)). The data evalutaion was based on the XPS study published by Mendialdua *et al.* [91] All samples were kept in ultra-high vacuum over night prior to the measurement, in order to remove gaseous substances, such as oxygen, from their surface. A problem may arise due to the fact that the standards are powders. The non-uniform surface of the powders may lead to non-uniform charging of the sample, which is difficult to detect and leads to random shifts in the binding energies. Polycrystalline standards were used, i.e. different crystal faces may be exposed to the X-rays, leading to shoulders in the peaks and shifts in the binding energies. The same may happen due to the most likely amorphous nature of as-grown vanadium oxide [2]. All samples measured here were not treated in any way prior to measurement.

According to Mendialdua *et al.*, the O 1*s* peak of the vanadium is best suited as energy reference and the elemental ratio of vanadium to oxygen cannot be used to determine the oxidation state. Instead three values were used to determine differences in the oxidation state:

1. The energy difference between O 1*s* and V $2p_{3/2}$ ("δ"), which depends on the treatment of the sample and the oxidation state. In general it was found that δ decreases with increasing oxidations state.

2. The full width at half maximum (FWHM) of V $2p_{3/2}$ ("λ") decreases with increasing phase purity (on the surface) AND oxidation state. This value shows predominantly the surface oxidation, which contributes to the signal broadening while it does not the shift the peak maximum. The systematic change of λ is more visible for the V $2p_{3/2}$- than for O 1*s*-peak, where λ varies randomly with changing oxidation state of vanadium. It is noteworthy that λ strongly depends on the background correction performed and thus the data evaluation software.

3. The shape of the peaks indicates phase purity via shoulders or broadening.

The phase purity of the standards was confirmed *via* X-ray diffraction, however, it should be noted that the surface of the samples (only the first 3-10 nm can be detected *via* XPS) may differ from the bulk. According to Mendialdua *et al.* V_2O_3 is reoxidized on its' surface upon exposure to the ambient atmossphere. The surface of VO_2 is also readily over-oxidized when exposed to oxygen. V_2O_5, on the other hand, is partially reduced under ambient conditions. For these reasons Mendialdua *et al.* applied different treatments to oxides of vanadium in order to obtain a "phase pure" surface.

The results of the XPS measurements are summarized and compared to the corresponding literature values in table 4.1. The respective values for δ and λ are given in eV. Absolute energy values are not shown, since the position of the peaks was normalized with respect to the oxygen O 1*s* peak, which was set to 529.8 eV. The corresponsing XPS spectra are shown on Figure 4.54.

Table 4.1: Summary of the values for δ and λ (both in eV) for the vanadium standards and the anodized sample compared to the literature.

Sample	**λ O 1*s* (eV)**	**λ V 2$p_{3/2}$ (eV)**	**δ (O 1*s*-V 2$p_{3/2}$) (eV)**
V_2O_5 standard	1.54	1.28	12.9
V_2O_5 literature	1.60	1.40	12.8
VO_2 standard	1.71	2.61	12.7
VO_2 literature	2.80	4.0	14.35
V_2O_3 standard	1.88	2.54	13.2
V_2O_3 literature	2.0	4.8	14.84
Anodized foil	1.63	2.27	13.4

In the case of V_2O_5 the δ- and λ-values measured for the purchased standards and the literature values are comparable. The shapes of the O 1*s* and V 2$p_{3/2}$ peaks are rather symmetrical, small deviations from the symmetry indicate a slightly reduced V_2O_5. The measured FWHM for the VO_2 standard is also lower than the literature value for both V 2$p_{3/2}$ and O 1*s*, however, an increase was measured compared to

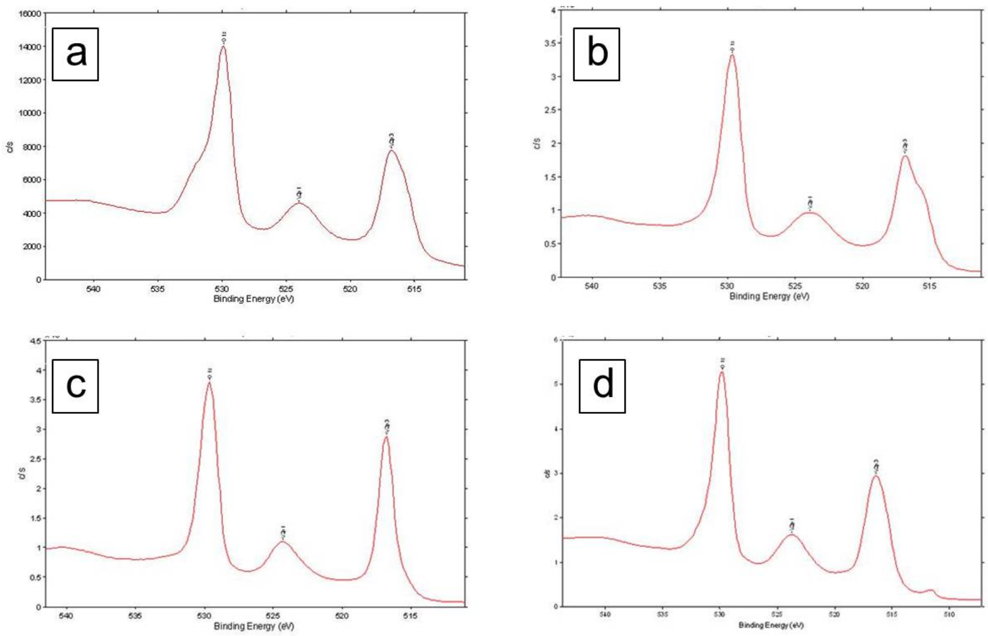

Figure 4.54: XPS spectra of different samples: a) V_2O_3 standard b) VO_2 standard c) V_2O_5 standard d) Vanadium foil anodized under standard conditions.

V_2O_5, as expected. Especially the V $2p_{3/2}$ peak is very unsymmetrical for the VO_2 standard, which may be related to over-oxidation of the surface. The value for δ is very similar to the value measured for V_2O_5, which was not expected. As opposed to the findings of Mendialdua *et al.*, a decreased value of δ for the V $2p_{3/2}$ in the V_2O_3 standard compared to the VO_2 standard peak was measured- statements by different trend for the FWHM is observed here. For the V_2O_3 standard sample, on the other hand, the δ-value increases, as compared to VO_2 which is in line with the findings in literature. A pronounced shoulder in the oxygen peak was found for the V_2O_3 standard, indicating multiple phases on the surface of the sample. The δ- and λ-values for the anodized foil are in the same roughly similar to the ones measured and the values found in literature.

As pointed out in the previous paragraph, the measured δ- and λ-values for the different vanadium oxide standards are not completely in line with the values from the work of Mendialdua *et al.* This observation will be discussed below. However, the mismatch between measured and literature values aggravates the data evaluation. The λ-value of the V $2p_{3/2}$ peak is in between the values for V_2O_5 and V_2O_3/VO_2, while the energy difference between these peaks (δ-value) would point towards V_2O_3

as the oxidation state of the anodized sample. When compared to the literature values, on the other hand, both the δ- and λ-value indicate a phase mixture of VO_2 and V_2O_5. Based on the data available an exact determination of the oxidation state of the oxide film on the anodized vanadium foil is not possible. However, it seems likely that the obtained composition is a phase mixture of VO_2 and V_2O_5.

The aforementioned inconsistencies of the in the XPS data may be due to multiple phenomena that all affect the XPS signal:

- The measured energy values change upon the setup, i.e. the instrument used has an influence on the results. The exact settings are rarely mentioned in publications. Additionally, the alignment of the instrument influences the outcome.
- The sample preparation influences the results strongly (as shown by Mendialdua *et al.*). Multiple procedures, such as sinterting, oxidation or reduction as well as exposure to the ambient atmosphere influence the results. For these reasons not even the standards can be compared easily to each other, let alone the anodized sample to the standards.
- The crystallinity and the nature of the sample influence the outcome, too. The anodized sample has a rather flat surface, compared to the standards and the literature samples, which were measured in form of powders. Additionally, the standards and the samples from literature are crystalline materials, while the anodized sample is amorphous in nature.
- Different studies of vanadium oxides are normally consistent within themselves (compare [91] and references therein) and the general trends mentioned before can normally be observed, but the obtained values are not comparable to each other.

In summary, the comparison of anodized vanadium foil to the standards or the literature does not lead to the desired result; the oxidation state cannot be determined clearly. The δ-value of a polished foil that was measured in XPS is 14.1 eV. Since this sample is the best comparison to the anodized foil it can be stated, that the oxidation state of the is increased upon anodization, but the starting and the final value cannot clearly be determined.

4.4.4 Conclusion and Outlook

Conclusion

In course of this study vanadium foils were successfully electropolished, i.e. they were electrochemically cleaned and the surface roughness was decreased. The best results were obtained using a solution that consists of a mixture of sulfuric acid, methanol and trace amounts of water at low voltages for short durations. It was found that the results could be significantly improved when the solution was left standing in the laboratory for roughly four days. Also fresh solutions that were already used for an anodization experiment led to better results, as compared to frehsly prepared solutions. The samples obtained were extremely flat and no debris was found on their surface. They were thus suitable for the subsequently following anodization.

A variety of different solvents and other experimental conditions were tested for the anodization of vanadium foil. Finally, an ordered array of vanadium oxide nanopores was succesfully prepared using a solution consisting of 0.5 wt$\%$ oxalic acid and 2 wt$\%$ of water dissolved in DEG saturated with boric acid. The anodization was carried out for 3 h at 40 V in the "Glass-setup". The fabricated samples were completely uniform and the procedure was reproducible.

However, interesting conclusions were also drawn from the other experiments performed. Anodizations utilizing the same solution as used for the anodization of titanium showed that it is possible to obtain porous structures on vanadium foils using EG as solvent and fluoride ions as etchant. Yet, the uniformity was low and large parts of the sample were not coated with an oxide. Saturated boric acid in water led to etched structures, neither pores nor an oxide layer were formed, which is most likely due to the solubility of vanadium oxides in water.

When EG saturated with boric acid was used as solvent porous structure were obtained upon addition of either oxalic acid or ammonium fluoride. The surface of the samples was corrugated and the sample were non-uniform, though. Additionally, reproducibility was an issue. However, it was found that both boric acid AND oxalic acid were necessary for the pore formation. Stefanovich *et al.* stated that the oxygen incorporated into the anodic film does not originate from the water in the solution,[79] but from borax dissolved in the solvent. Water, on the other hand, is a necessary ingredient that aids the dissolution of oxalic acid. In additional experiments oxalic acid was found to be the more potent etchant, compared to ammonium fluoride, as it enhances the reaction velocity. If the boric acid content in the solution was reduced, the reaction was first slowed down, before no pore formation was observed anymore.

TEG glycol was also used as solvent under otherwise similar conditions as described above. The samples anodized utilizing TEG were uniform and completely covered with polydisperse, unordered pores with a diameter of around 130 nm. At increased reaction durations the diameter did not change, however, the amount of defects increased. A mixture of TEG and EG as solvent led to the formation of roundish, nearly ordered pores with a size of 100 nm, accompanied with irregularly shaped pores. Nicely ordered, monodisperse pores with a diameter of around 80 nm were found using DEG as solvent. However, the samples were non-uniform and defects were found on each sample. When a vanadium foil was anodized in the a vertical arrangement ("Glass-setup") the samples consisted of nearly perfectly ordered, monodisperse nanopores with a diameter of 40 nm. It was found that a higher current (either caused by a higher anodization voltage or an increased conductivity of the solvent) lead to the formation of smaller pores.

Attempts were made to determine the pore depth or the thickness of the oxide layer using AFM and cross-section SEM, respectively. However, the desired results could not be obtained, yet. XPS was used to determine the oxidation state of the anodized samples, however, an exact determination was not possible due to several reasons. It can only be stated that surface of the vanadium foils exhibits a higher oxidation state after the anodization, as compared to a polished sample.

Outlook

The most important issue that needs to be adressed is the film thickness. First of all, a reliable method for the determination of the film thickness needs to be found. A possibility would be the use of Fabri-Perot interference. Another option is the evaluation of a mild sintering process to obtain a stable oxidic layer, which can subsequently be investigated using cross-section SEM. There are also indications that the oxide layer on the vanadium foil is rather thin, limiting the applications for the material. There are numerous options that may lead to an increased film thickness, such as:

- A variation of the water content in the anodization solution to alter the solubility of vanadium oxide.
- The growth of a solid oxide layer prior to anodization using a mixture of acetone, borax and benzoic acid subsequently followed by etching the oxide layer with the described anodization solution.
- This method can also be tested the other way round, i.e. the oxide would be grown on a patterned substrate.
- A second anodization step could be performed as in the anodization of titanium

Revealing the reaction progress or mechansim, which can elucidated by *via* "Snapshots" of the anodization, i.e. interrupting the anodization at different points during the reaction, would help to better understand the formation of the nanopores.

Even though the phase of the as-formed oxide film cannot be determined via X-ray diffraction or XPS it should be possible to determine the phase of a thicker oxide film after annealing. Finally even phase tuning may be performed that way. The possibility to tune and determine the crystallographic phase is required for the material to be used, e.g. in dye-sensitized solar cells.

CHAPTER 5

Synthesis of Copper- and Indium Chalcogenide Nanorods *via* Template-Assisted Precipitation

5.1 Introduction

Due to their size and shape dependent properties, semiconductor nanoparticles have attracted considerable scientific attention.[92] The most prominent examples in the case of p-type semiconductors are cadmiun and lead chalcogenides that have been studied intensively.[93][94] However, despite their interesting properties, the toxicity of lead and cadmium aggravates the application of these materials.[95] Thus, a promising alternative is the direct band gap semiconductor $CuInS_2$, with a tunable band gap of 1.5 eV, which leads to absorption in the visible regions of the suns' spectrum.[96][97] Additionally, the material is highly stable, less toxic as compared to its cadmium and lead counterparts and it exhibits a high extinction coefficient.[96][97] $CuInS_2$ is already widely used in thin film photovoltaic devices, [98] thus a nanostructured device based on $CuInS_2$ is very promising. Comparably few studies concerning a shape controlled synthesis of $CuInS_2$ nanoparticles have been conducted so far. The most promising way seems to be a synthesis based on copper and indium salts combined with a sulfur source in solution.[99] Another possibility is the thermal decomposition of single molecule precursors.[100] Herein, a precipitation reaction between the respective metal salts and a sulfur source inside the pores of a polycarbonate membrane is presented. Owing to the the templated synthesis, nanostructures such as long wires and tubes are accessible.

The utilization of a porous polycarbonate track-etched membrane as a template for the precipitation of different kinds of materials is well established. To just name some examples, it is possible to electrochemically deposit polypyrrole via a simple redox reaction between pyrrole and Fe^{3+};[101] additionally inorganic salts, like earth-alkaline fluorides,[102] earth-alkaline tungstates,[103] metal sulfides [19] or $CaCO_3$ [104] can be precipitated inside the pores of such a membrane.

In this work the polycarbonate membrane served as a template for the synthesis of different chalcogenide nanostructures. First the binary compounds CuS and In_2S_3 were synthesized. It was found that CuS can be obtained both in form of nanotubes and nanowires, depending on the experimental conditions, while indium sulfide was only obtained as nanowires. In order to elucidate the formation mechanism, other inorganic salts were precipitated as well. It was found that the reaction rate of the precipitation of the binary compounds CuS and In_2S_3 is rather different, aggravating their co-precipitation to form $CuInS_2$. By subsequently depositing CuS and In_2S_3, respectively, mixed copper-indium sulfides were synthesized. However, a control of the stoichiometry was not achieved so far.

The copper-indium sulfide nanostructures can be utilized in different ways:

- *Via* a removal of the membrane after the synthesis, e.g. by pyrolysis,[19] arrays of $CuInS_2$ nanowires can be obtained in principle. These arrays can, for example, be coated with an n-type polymer and subsequently be processed to form a nanostructured photolvoltaic device.
- The precipitation reaction can in theory be performed in TiO_2 nanotubular arrays, leading to a nanostructured solid-state solar cell directly.

5.2 Experimental Information

5.2.1 The Setup for the Template Assisted Precipitation

The setup for the synthesis of chalcogenide nanowires is shown in Figure 5.1. A polycarbonate track-etched membrane was mounted between two half's of a U-shaped cell. An aqueous solution of copper and/or indium salts as well as a solution of thioectamide or another sulfur source was filled into the respective half cells. The precipitation of the chalcogenide nanostructures occured inside the pores of the membrane during an incubation period of up to 4 days.

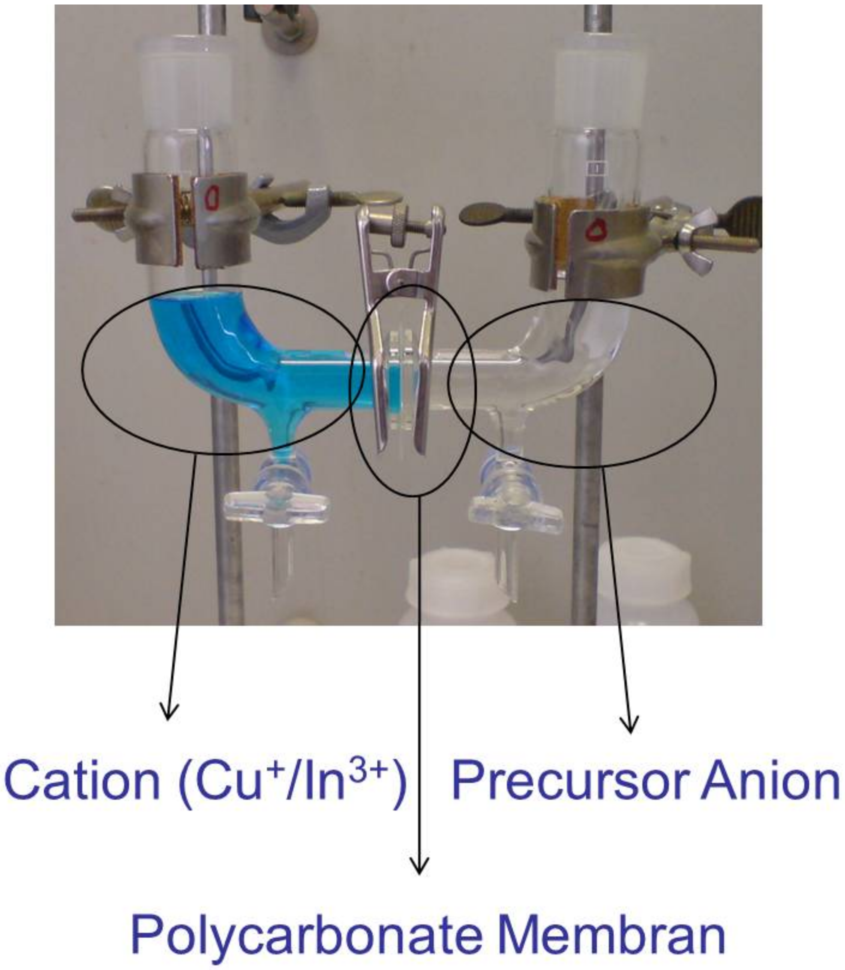

Figure 5.1: Photograph of the setup used for the template assisted precipitation of chalcogenide nanostructures.

5.2.2 Experimental: Procedure

Prior to the synthesis the surface of the polycarbonate track-etched membrane (Cyclopore PC, 0.1 μm pore diameter, 25 mm diameter, neoLab) was passivated in order to minimize particle formation on top of the membrane. A microcontact printed layer of OTS (Octadecyltrichlorsilane, 95 %, Sigma-Aldrich) was applied for the passivation. Based on the method established by Wong *et al.*[19], a 10 mM solution of OTS in hexane was administred to the surface of a PDMS (Polydimethylsiloxane)-Stamp. The hexane was allowed to evaporate and the membrane was pressed onto the stamp for 30 seconds. The procedure was performed on both sides of the membrane leading to a self-assembled monolayer of OTS on top of the membrane, i.e. the surface of the template became hydrophobic.

For the synthesis of CuS nanostructures 50 ml of a 0.05 M- 0.1 M solution of $Cu(NO_3)_2$ trihydrate (p.A., Merck) was filled in one half of the cell, while a solution of thioacetamide (p.A., for precipitation of heavy metals, Sigma-Aldrich) that served as the sulfide source in the same concentration was filled in the other half. When In_2S_3 nanostructures were synthesized, a 0.05 M $In_2(SO_4)_3$ (>98%, Sigma-Aldrich) solution was used, while concentration of the thioacetamide solution was 0.3 M. For the synthesis of indium chalcogenides 1 ml of nitric acid (65 wt% in water, Sigma-Aldrich) was added to both the $In_2(SO_4)_3$ and the thioacetamide solution. The experiments were conducted for 6 h when CuS was synthesized and for 96 h in the case of In_2S_3 synthesis. Acetic acid (p.A., Fluka), Na_2S monohydrate (technical, Sigma-Aldrich) and tri-sodium citrate (p.A., Merck) were also used for the indium sulfide synthesis, details will be noted in section 5.3.3.

Precipitation of $BaWO_4$ (from $Na_2WO_4 \cdot 2H_2O$ (p.A., Sigma-Aldrich) and $BaCl_2$ (99.9%, Sigma-Aldrich)) and AgCl (from $AgNO_3$ (99%, Sigma Aldrich) and NaCl (>98%, Sigma-Aldrich)) were conducted for 24 h at a concentration of 0.1 M for both solutions.

Upon completion of the reaction, undesired particles that precipitated on the surface of the membrane were removed by ultrasonication for roughly one minute. Afterwards the membrane was rinsed with water and ethanol (p.A., VWR). For TEM investigations of the as-synthesized nanomaterials the membrane was dissolved in roughly 5 ml of dichloromethane (p.A., Acros Organics).

5.2.3 Experimental: Techniques

TEM, HRTEM and EDX: The chalcogenide nanostructures were characterized by *transmission electron microscopy* (TEM) and *high resolution transmission electron microscopy* (HRTEM). For both TEM and HRTEM investigations the membranes were dissolved in dichloromethane and the suspension was sonicated for a few seconds. The mixture was subsequently applied on a carbon-coated copper grid.

TEM measurements were carried out with either a Philips 420 instrument with an acceleration voltage of 120 kV or a FEI TECNAI F30 S-TWIN transmission electron microscope working at 300 kV. TEM images and diffraction patterns were acquired with a CCD camera (14-bit GATAN 794MSC). Elemental analysis was performed by *energy dispersive X-ray* (EDX) spectroscopy and quantified within Emispec ESVision software.

SEM: *Scanning electron microcopy* was used to characterize the polycarbonate track-etched membrane. The surface topography of the template was investigated using high vacuum mode scanning electron microscopy on a FEI NovaNano FEG-SEM 630. The membrane was glued to an aluminum stub using conductive carbon tape.

5.3 Results and Discussion

5.3.1 The Template

Prior to the surface passivation and the synthesis, the membrane was investigated using SEM. The corresponding images of the surface of the polycarbonate track-etched membrane are shown in Figure 5.2. The top of the template is rather corrugated and irregular. Larger scratches and hills can be found. The pores with a diameter of roughly 100 nm are randomly distributed throughout the entire membrane. While the majority of the pores are isolated, some of them overlap and thus form irregularly shaped, larger pores.

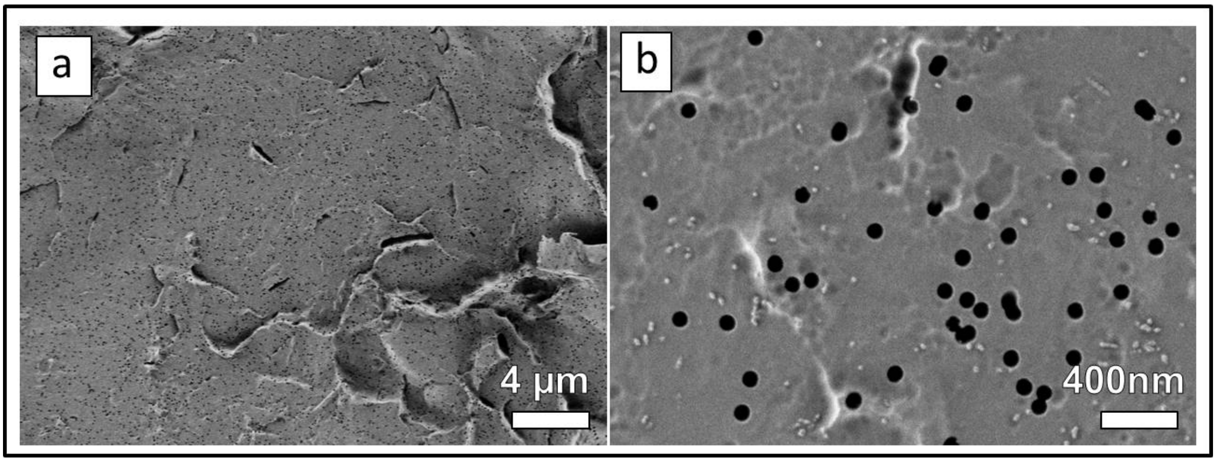

Figure 5.2: SEM images of the surface of the polycarbonate track etched membrane used as the template for the precipitation reactions.

5.3.2 Synthesis of CuS Nanostructures and other Inorganic Salts

In order to evaluate whether the precipitation of a ternary compound, such as $CuInS_2$ can be achieved, the binary compound CuS and In_2S_3 were synthesized before attempting to prepare $CuInS_2$. A binary system is easier to control and it is sufficient as a "proof of principle".

The first precipitations were performed with 1 M solutions of $Cu(NO_3)_2$ and thioacetamide, respectively, and a reaction duration of 24 h. Thioacetamide decomposes into hydrogen sulfide, acetic acid and ammonia when dissolved in water. This decomposition is accelerated significantly in the presence of heavy metal ions, such as copper or indium. The metal ions are subsequently precipitated by the S^{2-} from the hydrogen sulfide. However, due to the formation of large amounts of debris on the surface of the template it was difficult to characterize these samples. The precipitates could not be removed from the membranes' surface easily, likely owing to the prolonged reaction time. Extended ultrasonic treatment led to a damage of the template, which renders it impossible to separate the surface precipitate from the inside of the membrane. By decreasing the concentration of the both $Cu(NO_3)_2$ and thioacetamide to 0.1 M in combination with a reduced reaction duration of 6 h the formation of precipitates on the membranes' surface could be minimized. Figure 5.3 shows TEM images of a sample synthesized with 0.1 M solutions of $Cu(NO_3)_2$ and thioacetamide for 6 h.

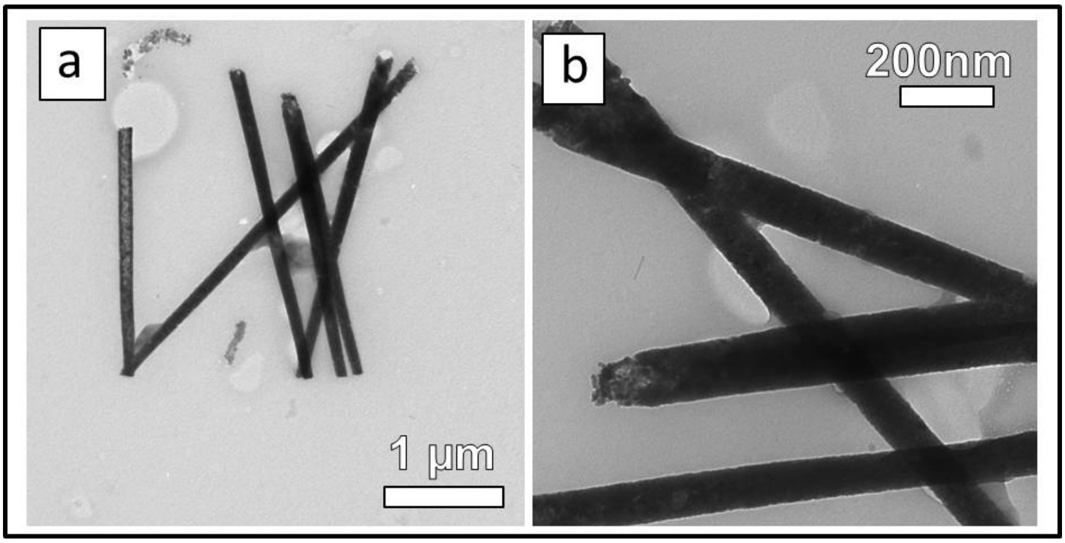

Figure 5.3: TEM images of CuS nanowires synthesized *via* template assisted precipitation.

The TEM image clearly shows that CuS nanowires were obtained *via* this method. The diameter of the wires was slightly above 100 nm and thus matches well with the size of the pores in the template. The length of the nanowires can reach up to 1 μm. In order to verify that the obtained nanostructures arise from the precipitated CuS inside the membrane, different tests were performed. First, the surface passivated membrane was dissolved in dichloromethane in order to evaluate whether wire-like structures can be found in or due to the template. Hydrogen sulfide may be oxidized owing to the atmospheric conditions and the prolonged reaction time. In order to exclude a precipitation of sulfur inside the membrane a reaction using water on one side of the U-shaped half cell and a 1 M thioacetamide solution on the other was performed for a reaction duration of 24 h. Additionally, the same reaction was conducted using a 1 M solution of $NaNO_3$ instead of pure water in order to exclude a redox reaction of the NO_3^- ions in the reaction solution with hydrogen sulfide, which could potentially lead to the formation of sulfur as well. The result of all these tests was negative, i.e. no particles were observed in the TEM. Furthermore, the membrane remained optically unchanged.

However, although solid nanowires were obtained as the main product, the formation of side products was observed (see Figure 5.4).

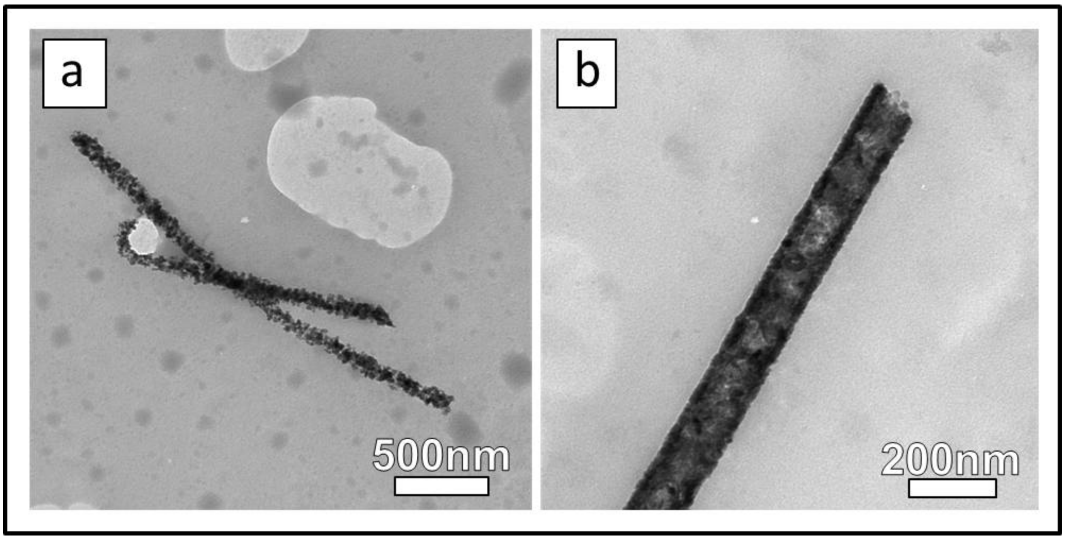

Figure 5.4: TEM images of the side products occuring during the synthesis of CuS nanowires.

As shown in figure 5.4 CuS nanotubes could also be found, as well as single particles aligned to wires. This phenomenon is believed to be concentration dependent.

Due to diffusion based on the laminar flow model, the ions consumed for the precipitaion will be replaced more rapidly in the center of the U-shaped half cell and thus in the center of the membrane. In other words, the growth is accelerated in the areas with a higher "effective" ion concentration. Since the formation of the nanowires is likely to start at the walls of the membranes [101] a lower concentration may lead to the formation of tubes. This assumption was verified by performing precipitations at lower concentrations, as discussed below. Due to the carbonate groups in the membrane, oxidic species are present on the interior of the pores, which can act as an anchor for approaching Cu^{2+} ions. These anchoring groups are not a necessity for the precipitation of CuS, however, they most likely have a directing effect on Cu^{2+}. Due to the surface passivation oxidic groups on the exterior of the template should be blocked. Regardless, a precipitation of CuS on the outside of the membrane is going to occur if sufficient concentrations of the respective ions are present. A diffusion of ions through the channels of the membrane cannot be excluded, especially for prolonged reactions. The alignment of particles to wires maybe due to two effects: First the membrane may simply act as a trap for small particles in suspension, secondly the ammonia set free by the decomposition of thioacetamide is potentially able to induce an alignment of CuS particles, compare O'Sullivan *et al.* [105]

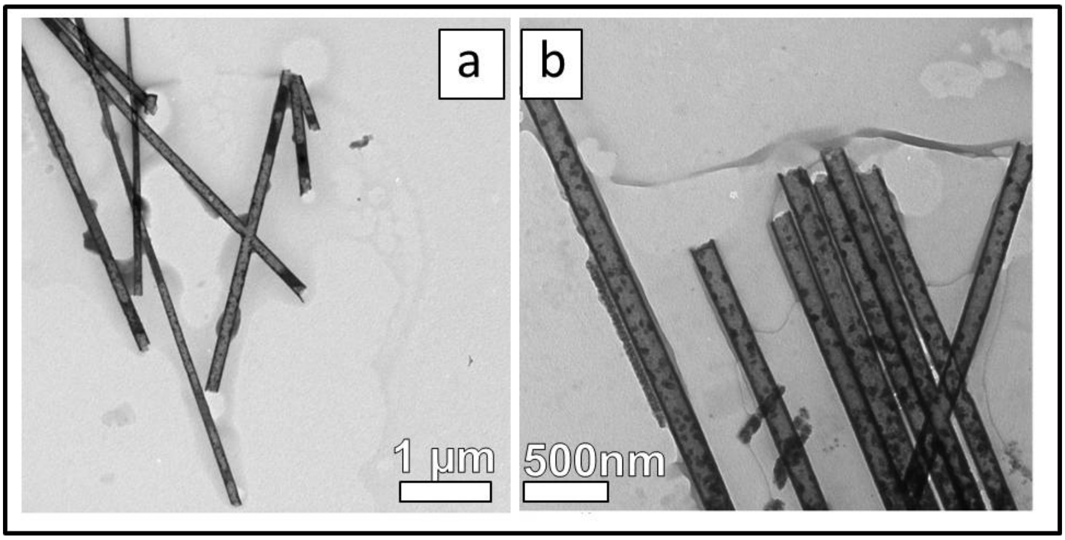

Figure 5.5: TEM images of CuS nanotubes synthesized *via* template assisted precipitation.

By decreasing the concentration of the reactants involved in the precipitation, nanotubes were formed almost exclusively. Figure 5.5 shows TEM images of as-synthesized nanostructures using 0.05 M solutions of $Cu(NO_3)_2$ and thioacetamide, respectively. The diameter of the nanotubes is similar to the one of the nanowires (compare Figure 5.3), however, their lengths can reach up to several micrometers. This result can be seen as the verification of the reaction mechanism proposed above. By reducing the concentration of the reactants involved, the reaction was slowed down and thus it was possible to obtain nanotubes as the only product. The formation of side product could not be completely suppressed, i.e. small particles aligned to wires were observed for these reactions as well (compare Figure 5.4).

The precipitation was performed for $BaWO_4$ and AgCl as well. These experiments were conducted in order to further the elucidate the precipitation process. In figure 5.6 $BaWO_4$ and AgCl nanowires are shown. These salts were precipitaed from 0.1 M solutions of $BaCl_2$ and Na_2WO_4 or $AgNO_3$ and NaCl, respectively. It is noteworthy that neither nanotubes nor other side products were found in either cases.

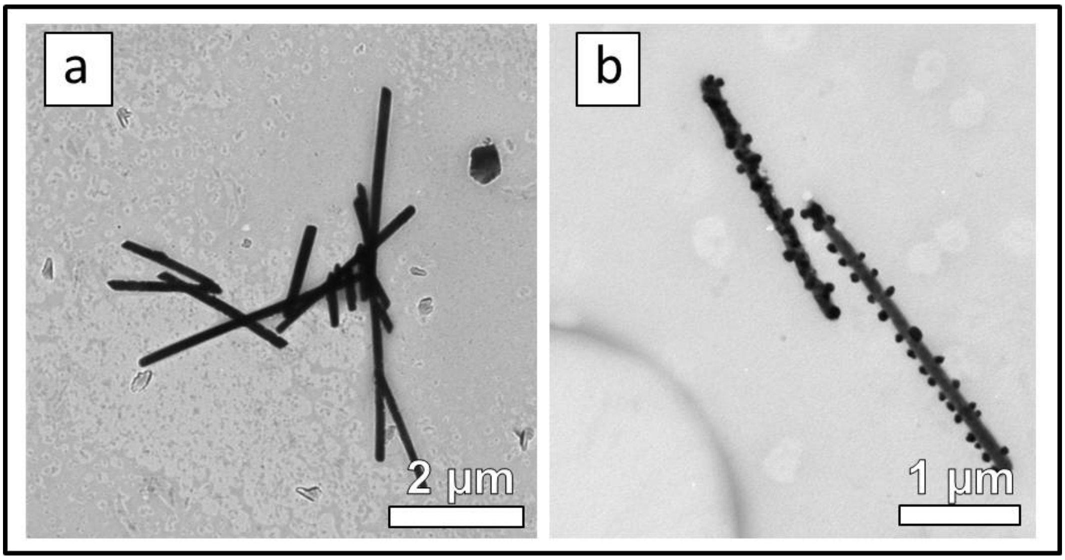

Figure 5.6: TEM images of other inorganic salts synthesized *via* template assisted precipitation: a) $BaWO_4$ b) AgCl

As for the $BaWO_4$ sample, almost no impurities were observed (see Figure 5.6 a), which is also evident from the fact that almost no precipitation occurred on the surface of the membrane. During the passivation process the surface of the template becomes hydrophobic due to the self-assembly of a monolayer of OTS, which binds to the carbonate groups of the membrane *via* Si-O-C bonds, thus the octadecyl-group is on the surface. The hydrophobic nature of the octadecyl-group renders the precipitation of an ionic species like $BaWO_4$ unlikely. In case of the more covalent species AgCl, significantly more precipitates on the template were observed. On the other hand, less debris was found in comparison with a CuS precipitation conducted under the same conditions. This was to be expected since CuS is not only a covalent species, but it also has the lowest solubility of the investigated compounds. Nevertheless, surface passivation helps to prevent the precipitation of CuS on the membrane. This is probably due to the blocking of oxidic species on the membranes' surface, which could otherwise act as an anchoring group for Cu^{2+} ions. It is noteworthy that the precipitated AgCl turned grey immediately after exposure to light. This can be explained by the photochemical reduction of Ag^{+}, which is a well known phenomenon. Every AgCl nanowire found was decorated with Ag particles. As expected, the diameter of the AgCl nanowires was well below 100 nm due to the formation of silver particles.

5.3.3 Synthesis of In_2S_3 Nanowires

NExt, the precipitation of In_2S_3 was studied. The most significant difference compared to the precipitation of CuS was an enhanced reaction duration (6 h for both CuS nanowires and tubes compared to 96 h for the precipitation of In_2S_3). Additionally, a precipitation of In_2S_3 was not possible from solutions containing solely $In_2(SO_4)_3$) (0.1 M) and thioacetamide (0.3 M), respectively. No precipitation occurred within 120 h, which was the longest reaction duration investigated. For all reactions an excess of thioacetamide was used in order to ensure the generation of a sufficient amount of hydrogen sulfide. Acids as well as bases accelerate the decomposition of thioacetamide into H_2S, NH_3 and acetic acid and can, thus, be utilized as additives. However, even the use of mild bases such as tri-sodium citrate lead to the precipitation of amorphous, white indium oxides/hydroxides. Despite the passivation of the membranes surface, most of the precipitates were formed on top of the template and nanowires could not be found. Another option to accelerate the precipitation of In_2S_3 is the use of Na_2S instead of thioacetamide, in which case no decomposition of the precursor is necessary and thus sulfide ions are directly available for the reaction. However, the sulfide ion is a strong base, thus again the formation of oxides/hydroxides was favored over the precipitation of In_2S_3. This behavior can be explained according to the "Pearson concept" of hard and soft acids and bases. In^{3+} is a Pearson hard ion and preferably forms bonds with the Pearson hard hydroxide ion, while Cu^{2+} is of medium hardness and Cu^{+} as well as S^{2-} are Pearson soft.[58] Cu^{2+} ions are used as the precursor for the precipitation of copper sulfide, however, in fact copper is incorporated in form of Cu^{+} into the compound CuS, which should better be written as ${Cu_3}^{1+}({S_2}^{2-}S^{1-})$. Upon addition of H_2S to solutions containing Cu^{2+} ions, they are reduced to Cu^{+} while S^{2-} is oxidized to "S^{-}". 2/3 of the sulfur atoms form diatomic ${S_2}^{2-}$ units, while one defect electron is located in the 3p-band built by the sulfur atoms.[58] The higher affinity of both Cu^{2+} and Cu^{+} towards S^{2-} explains the accelarated reaction.

Lowering the pH-value by using acidic additives decreases the amount of "free" S^{2-} in the solution due to its' basic nature, however, the formation of hydroxides can be suppressed under these conditions and thus acidic additives were tested for the precipitation of In_2S_3. It was found that mild acids, such as acetic acid, indeed suppressed the hydroxide formation, which was tested by adding 1 ml of glacial acetic acid to the respective reaction solutions (0.1 M $In_2(SO_4)_3$, 0.3 M thioacetamide). No

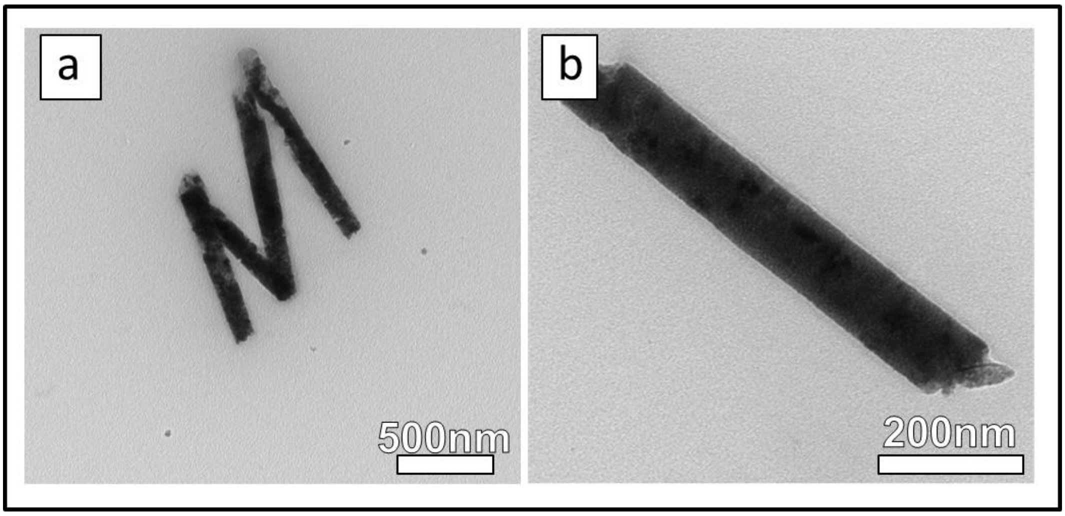

Figure 5.7: TEM images of In_2S_3 nanowires synthesized *via* template assisted precipitation.

precipitation occurred at all, neither whitish oxide was observed, norIn_2S_3 nanowires were formed even after 120 h reaction duration. The concentration of hydroxide ions was further decreased by using 1 ml of 65 wt% nitric acid as an additive for the precipitation in both solutions. After a reaction duration of 96 h, the precipitation was stopped and In_2S_3 nanowires were observed for the first time (compare Figure 5.7). Their diameter matches the pore thickness of the template. It is noteworthy that the length of the nanowires only reaches up to 1 µm, which is rather low compared to reactions investigated so far, especially taking into account the prolonged reaction duration. This phenomenon is likely due to the extremely slow reaction. The In_2S_3 nanowires were further characterized by means of HRTEM and EDX. The results are shown in section 5.3.5.

5.3.4 Synthesis of Copper-Indium Sulfide Nanowires

The precipitation of a ternary compound is rather difficult, as compared to binary compounds. In the case of $CuInS_2$ this is mostly due to the large difference in reaction velocity. While the precipitation of CuS is finished after 6 h and can be performed without using any additives in the reaction solution, the precipitation of In_2S_3 requires low pH-values and long reaction durations. For this reason a two-step reaction was performed. First CuS nanotubes were precipitated, as decribed above, followed by the precipitation of In_2S_3 inside the tubes. The reaction conditions for both precipitations were the same as for the synthesis of the respective binary compounds. Compact nanowires could succesfully be synthesized after the two subsequent precipitations (see Figure 5.8). No sign of core-shell structure was observed, i.e. the Cu^+ ions did not remain at the membrane walls. An investigation of the composition and the copper to indium ratio in these nanowires was conducted *via* HRTEM and EDX, as shown in section 5.3.5.

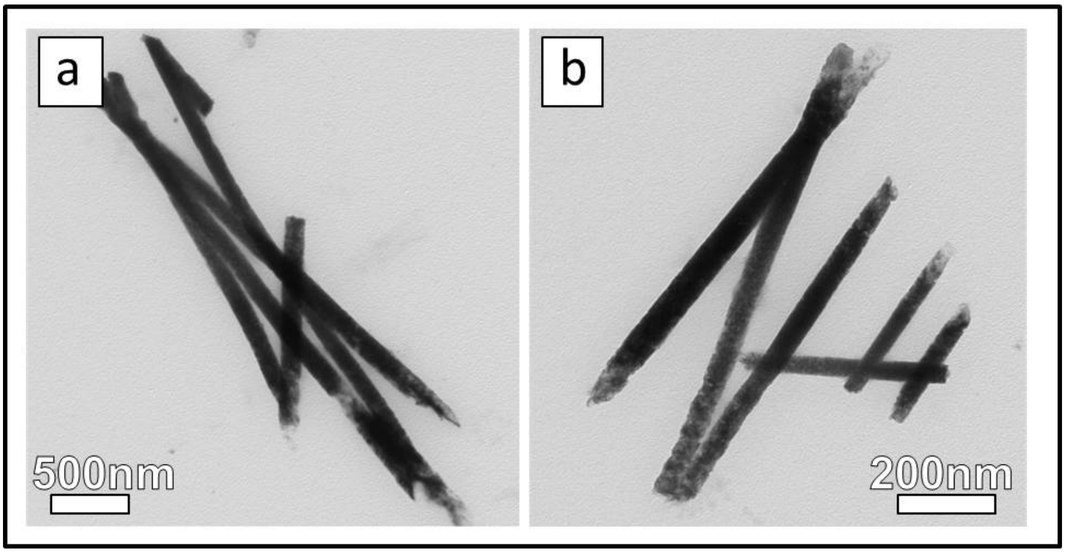

Figure 5.8: TEM images of copper-indium sulfide nanowires synthesized *via* template assisted precipitation.

5.3.5 HRTEM and EDX studies of In_2S_3 and Copper-Indium Sulfide Nanowires

The determination of the the exact composition of the obtained nanowires remains an issue. The amount of sample obtained in one synthesis is rather low (around 3-5 mg), as a consequence, multiple syntheses have to be carried out for a X-ray diffraction experiment. In addition, the composition could not be determined using X-ray diffraction due to the amorphous nature of the synthesized nanostructures. HRTEM was thus chosen for the determination of the crystal structure and composition of the synthesized materials.

Figure 5.9a shows the HRTEM image of an indium sulfide nanorod whereas Figure 5.9b shows the corresponding Fourier transform. The d-values obtained from the Fourier transform correspond well with the literature values of In_2S_3. [106] Additionally EDX was performed on the indium sulfide nanorods. After quantification of the results an indium to sulfur ratio of 2:3 was found. No significant amounts of other elements could be detected, with the exception of copper, which arises from the TEM grid. The combination of both HRTEM and EDX conclusively shows the formation of In_2S_3 nanowires.

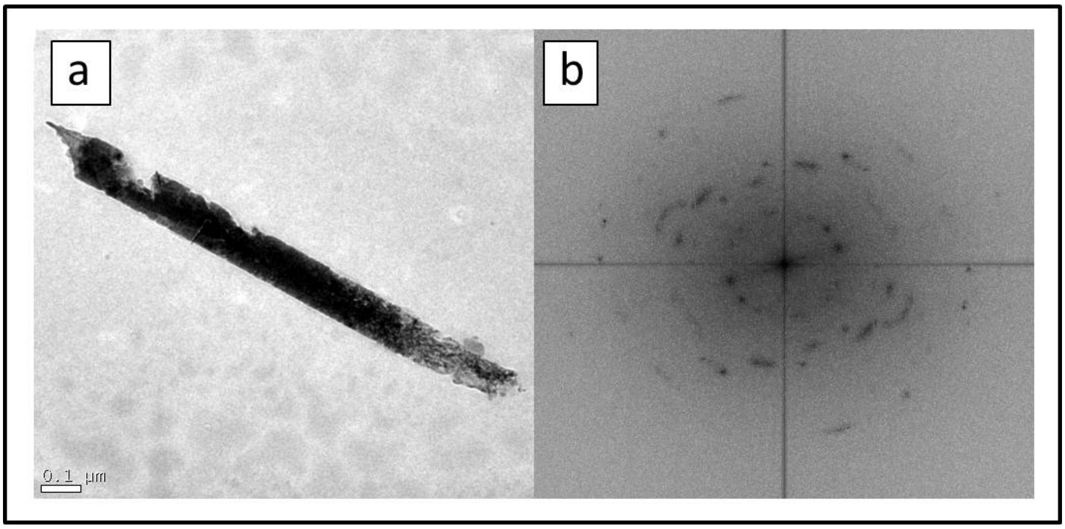

Figure 5.9: a) HRTEM images of an In_2S_3 nanowire synthesized *via* template assisted precipitation b)The corresponding Fourier transform showing d-distances that match the crystal structure of In_2S_3.

Copper indium sulfide nanorods were also characterized by means of HRTEM and EDX. Owing to the comparably low crystallinity of the as-obtained nanowires, all results discussed in this section are preliminary at best. In Figure 5.10a a high resolution TEM image of a copper indium sulfide nanowire is shown. It can be seen that the crystallinity of the nanowire was rather low, however, nanocrystalline areas can be observed. Figure 5.10b shows the Fourier transform corresponding to the crystalline domain encircled by a red square in Figure 5.10a. The obtained d-values correspond well with the values for $CuIn_5S_8$,[107] however, large parts of the nanowires were too amorphous for an investigation via electron diffraction. Thus, the composition $CuIn_5S_8$ cannot be assumed for the entire sample. EDX analysis did not lead to a conclusive picture. While copper and indium could be detected in every nanowire, the copper-content varies strongly within one wire and in the whole sample. It was found that copper and indium are not distributed evenly throughout the nanowires. Further investigations are necessary in order to elucidate the composition of the as-obtained nanowires.

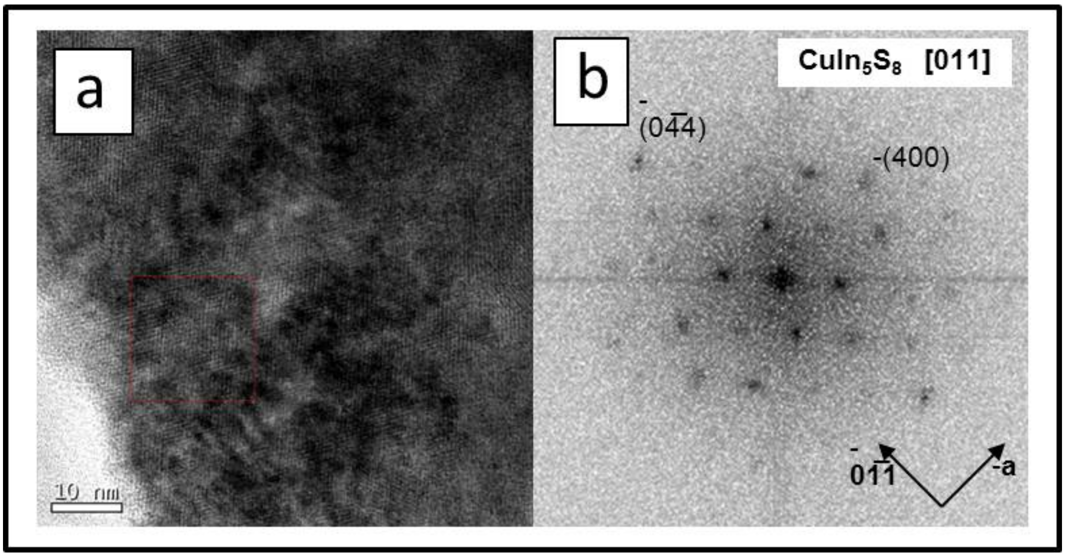

Figure 5.10: a) HRTEM images of a copper-indium sulfide nanowire synthesized *via* template assisted precipitation b)The Fourier transform corresponding to the red square in in a) showing d-distances that match the crystal structure of $CuIn_5S_8$.

5.4 Conclusion and Outlook

5.4.1 Conclusion

In course of this study it was shown that chalcogenide nanostructures can be obtained *via* a relatively simple precipitation reaction inside the pores of a polycarbonate track-etched membrane. For this purpose metal salts and thioacetamide were utilized as the reactants. Both, CuS nanowires and nanotubes were synthesized by adjusting the experimental conditions accordingly. It was found that the precipitation of CuS starts at the inner walls of the membrane, i.e. the reaction product could be controlled *via* an adjustment of the respective concentrations of the reactants leading to an altered reaction rate. In_2S_3 nanowires could also be synthesized by an acidification of both the solution containing In^{3+} and thioacetamide, respectively. It is noteworthy that the precipitation of indium sulfide required longer reaction durations as compared to the precipitation of CuS. Furthermore, the use of basic precursors or additives led to the formation of indium oxides/hydroxides instead of indium sulfide, which was attributed to the Pearson hardness of the chemical species involved. The composition of the indium sulfide nanowires was verified to be In_2S_3 *via* HRTEM and EDX studies. Owing to the different reactions rates of the formation of CuS and In_2S_3, an attempt to synthesize a ternary copper indium sulfide was carried out as a two-step reaction, utilizing the same experimental conditions as for the respective binary compounds. Compact nanowires were obtained, however, indium and copper were not distributed evenly in the nanorods and thus the determination of the nanowires' exact compositon was not possible so far.

5.4.2 Outlook

The main issue of the nanostructures synthesized in this study is their low crystallinity, which leads to problems in the determination of the composition of the as-synthesized nanostructures, as well as limitations in the application. While the composition of the indium sulfide nanorods could be determined *via* HRTEM and EDX, the same was not possible for the ternary compound synthesized. Besides the low crystallinity also an even distribution of copper and indium in the nanowires needs to be achieved in order to synthesize a pure compound rather than an inhomogeneous solid solution. A possible strategy to achieve both a higher crystallinity of the synthesized compounds and a better distribution of the metal cations in the ternary compound is a sintering step under inert conditions that need to be applied to prevent an oxidation of the sulfur. After the sintering it is most likely possible to investigate the nanostructures *via* X-ray diffraction, if a sufficient amount is synthesized.

In a next step the chalcogenide nanostructures can be utilized in two ways:

- The precipitation can in principal be transferred from the polycarbonate track-etched membranes to a template consisting of TiO_2 nanotubes (see chapter 4), which would represent the chemical synthesis of a nanostructured photovoltaic device.
- The membrane can be removed, for example *via* pyrolysis, which would leave an array of freestanding nanowires that can be utilized as the basis for the a nanostructured photovoltaic device, for example by coating with a semiconducting polymer.

Furthermore, it would be interesting to investigate the growth of nanostructures to learn more about their formation. This may enable one the synthesize of nanostructures other than the ones shown in this study, such as indium sulfide nanotubes. In the case of ternary compound it may not only reveal the growth process of the nanowires but also the evolution of their composition, which could be utilized for a control of the copper to indium ratio.

Bibliography

[1] Patrick Oberle, New Nanomaterials for Dye-Sensitized Solar Cells. Ph.D. thesis, Johannes Gutenberg Universität Mainz, 2006.

[2] Shin, Y.; Lee, S. *Nano Letters* **2008**, *8*, 3171–3173.

[3] O'Regan, B.; Grätzel, M. *Nature* **1991**, *353*, 737–740.

[4] Grätzel, M. *Nature* **2001**, *414*, 338–344.

[5] Barnes, P. R. F.; Anderson, A. Y.; Durrant, J. R.; O'Regan, B. C. *Physical Chemistry Chemical Physics* **2011**, *13*, 5798.

[6] van de Lagemaat, J.; Frank, A. J. *The Journal of Physical Chemistry B* **2001**, *105*, 11194–11205.

[7] Ihara, M.; Kanno, M.; Inoue, S. *Physica E: Low-dimensional Systems and Nanostructures* **2010**, *42*, 2867–2871.

[8] Pan, X.; Chen, C.; Zhu, K.; Fan, Z. *Nanotechnology* **2011**, *22*, 235402.

[9] Chen, C.-C.; Chung, H.-W.; Chen, C.-H.; Lu, H.-P.; Lan, C.-M.; Chen, S.-F.; Luo, L.; Hung, C.-S.; Diau, E. W.-G. *Journal of Physical Chemistry C* **2008**, *0*, 0.

[10] Yang, M.; Ding, B.; Lee, S.; Lee, J.-K. *The Journal of Physical Chemistry C* **2011**, *115*, 14534–14541.

[11] Qiu, J.; Zhuge, F.; Lou, K.; Li, X.; Gao, X.; Gan, X.; Yu, W.; Kim, H.-K.; Hwang, Y.-H. *Journal of Materials Chemistry* **2011**, *21*, 5062.

[12] Rani, S.; Roy, S. C.; Paulose, M.; Varghese, O. K.; Mor, G. K.; Kim, S.; Yoriya, S.; LaTempa, T. J.; Grimes, C. A. *Physical Chemistry Chemical Physics* **2010**, *12*, 2780.

[13] Ghicov, A.; Schmuki, P. *Chemical Communications* **2009**, 2791.

[14] Wang, J.; Lin, Z. *Chemistry of Materials* **2010**, *22*, 579–584.

[15] Shin, K.; Seok, S. i.; Im, S. H.; Park, J. H. *Chemical Communications* **2010**, *46*, 2385.

[16] Wang, Q.; Zhu, K.; Neale, N. R.; Frank, A. J. *Nano Letters* **2009**, *9*, 806–813.

[17] Zhang, X.-T.; Taguchi, T.; Wang, H.-B.; Meng, Q.-B.; Sato, O.; Fujishima, A. *Research on Chemical Intermediates* **2007**, *33*, 5–11.

[18] Li, B.; Wang, L.; Kang, B.; Wang, P.; Qiu, Y. *Solar Energy Materials and Solar Cells* **2006**, *90*, 549–573.

[19] Zhang, F.; Wong, S. S. *Chemistry of Materials* **2009**, *21*, 4541–4554.

[20] Adachi, M.; Murata, Y.; Harada, M.; Yoshikawa, S. *Chemistry Letters* **2000**, 942–943.

[21] Hsu, C.-Y.; Chiu, T.-C.; Shih, M.-H.; Tsai, W.-J.; Chen, W.-Y.; Lin, C.-H. *The Journal of Physical Chemistry C* **2010**, *114*, 4502–4510.

[22] Huang, J.; Cao, Y.; Deng, Z.; Tong, H. *Journal of Solid State Chemistry* **2011**, *184*, 712–719.

[23] Lundström, I. *Sensors and Actuators B: Chemical* **1996**, *35*, 11–19.

[24] Kavan, L.; Kalbac, M.; Zukalova, M.; Exnar, I.; Lorenzen, V.; Nesper, R.; Graetzel, M. *Chemistry of Materials* **2004**, *16*, 477–485.

[25] NGAMSINLAPASATHIAN, S. *Journal of Photochemistry and Photobiology A: Chemistry* **2004**, *164*, 145–151.

[26] Izawa, H.; Kikkawa, S.; Koizumi, M. *The Journal of Physical Chemistry* **1982**, *86*, 5023–5026.

[27] Kasuga, T.; Hiramatsu, M.; Hoson, A.; Sekino, T.; Niihara, K. *Langmuir* **1998**, *14*, 3160–3163.

[28] Chen, Q.; Du, G.; Zhang, S.; Peng, L.-M. *Acta Crystallographica Section B Structural Science* **2002**, *58*, 587–593.

[29] Bavykin, D. V.; Walsh, F. C. *European Journal of Inorganic Chemistry* **2009**, *2009*, 977–997.

[30] Huang, J.; Cao, Y.; Huang, Q.; He, H.; Liu, Y.; Guo, W.; Hong, M. *Crystal Growth & Design* **2009**, *9*, 3632–3637.

[31] Andrusenko, I.; Mugnaioli, E.; Gorelik, T. E.; Koll, D.; Panthöfer, M.; Tremel, W.; Kolb, U. *Acta Crystallographica Section B Structural Science* **2011**, *67*, 218–225.

[32] Birkel, C. S.; Mugnaioli, E.; Gorelik, T.; Kolb, U.; Panthöfer, M.; Tremel, W. *Journal of the American Chemical Society* **2010**, *132*, 9881–9889.

[33] Birkel, A.; Reuter, F.; Koll, D.; Frank, S.; Branscheid, R.; Panthöfer, M.; Rentschler, E.; Tremel, W. *CrystEngComm* **2011**, *13*, 2487.

[34] Zhao, B.; Chen, F.; Jiao, Y.; Zhang, J. *Journal of Materials Chemistry* **2010**, *20*, 7990.

[35] Peng, C.-W.; Richard-Plouet, M.; Ke, T.-Y.; Lee, C.-Y.; Chiu, H.-T.; Marhic, C.; Puzenat, E.; Lemoigno, F.; Brohan, L. *Chemistry of Materials* **2008**, *20*, 7228–7236.

[36] Horvath, E.; Kukovecz, a.; Konya, Z.; Kiricsi, I. *Chemistry of Materials* **2007**, *19*, 927–931.

[37] Ellingboe, J. L.; Runnels, J. H. *Journal of Chemical & Engineering Data* **1966**, *11*, 323–324.

[38] Nagase, T.; Ebina, T.; Iwasaki, T.; Hayashi, H.; Onodera, Y.; Chatterjee, M. *Chemistry Letters* **1999**, 911–912.

[39] MENG, X.; WANG, D.; LIU, J.; Zhang, S. *Materials Research Bulletin* **2004**, *39*, 2163–2170.

[40] YUAN, Z. *Colloids and Surfaces A: Physicochemical and Engineering Aspects* **2004**, *241*, 173–183.

[41] Dominik Koll, New Electrode Materials for Dye Sensitized Solar Cells: Synthesis and Structural Investigation of Sodium Titanate Nanowires. Ph.D. thesis, Johannes Gutenberg Universität Mainz, 2008.

[42] Nazeeruddin, M. K.; Angelis, F. d.; Fantacci, S.; Selloni, A.; Viscardi, G.; Liska, P.; Ito, S.; Takeru, B.; Grätzel, M. *Journal of the American Chemical Society* **2005**, *127*, 16835–16847.

[43] Kay, A.; Grätzel, M. *Solar Energy Materials and Solar Cells* **1996**, *44*, 99–117.

[44] Sheng, J.; Hu, L.; Xu, S.; Liu, W.; Mo, L.; Tian, H.; Dai, S. *Journal of Materials Chemistry* **2011**, *21*, 5457.

[45] Ohsaki, Y.; Masaki, N.; Kitamura, T.; Wada, Y.; Okamoto, T.; Sekino, T.; Niihara, K.; Yanagida, S. *Physical Chemistry Chemical Physics* **2005**, *7*, 4157.

[46] Alivov, Y.; Fan, Z. Y. *Applied Physics Letters* **2009**, *95*, 063504.

[47] Wong, D. K.-P.; Ku, C.-H.; Chen, Y.-R.; Chen, G.-R.; Wu, J.-J. *ChemPhysChem* **2009**, *10*, 2698–2702.

[48] Schlichthörl, G.; Park, N. G.; Frank, A. J. *The Journal of Physical Chemistry B* **1999**, *103*, 782–791.

[49] Ding, Z.; Lu, G. Q.; Greenfield, P. F. *The Journal of Physical Chemistry B* **2000**, *104*, 4815–4820.

[50] Diaz-Guerra, C.; Umek, P.; Gloter, A.; Piqueras, J. *The Journal of Physical Chemistry C* **2010**, *114*, 8192–8198.

[51] Chang, X.; Huang, J.; Cheng, C.; Sui, Q.; Sha, W.; Ji, G.; Deng, S.; Yu, G. *Catalysis Communications* **2010**, *11*, 460–464.

[52] Masuda, H.; Fukuda, K. *Science* **1995**, *268*, 1466–1468.

[53] Mills, A.; Davies, R. H.; Worsley, D. *Chemical Society Reviews* **1993**, *22*, 417.

[54] Choi, Y. J.; Seeley, Z.; Bandyopadhyay, A.; Bose, S.; Akbar, S. A. *Sensors and Actuators B: Chemical* **2007**, *124*, 111–117.

[55] Antonelli, D. M.; Ying, J. Y. *Angewandte Chemie International Edition in English* **1995**, *34*, 2014–2017.

[56] Lakshmi, B. B.; Dorhout, P. K.; Martin, C. R. *Chemistry of Materials* **1997**, *9*, 857–862.

[57] Jan Macak, Growth of Anodic Self-Organized Titanium Dioxide Nanotube Layers. Ph.D. thesis, Universität Erlangen-Nürnberg, Erlangen, 2008.

[58] Riedel, E.; Janiak, C. *Anorganische Chemie*, 5th ed.; De Gruyter: Berlin [u.a.], 2002.

[59] Chudnovskii, F. *Journal of Solid State Chemistry* **1992**, *98*, 137–143.

[60] Chernova, N. A.; Roppolo, M.; Dillon, A. C.; Whittingham, M. S. *Journal of Materials Chemistry* **2009**, *19*, 2526.

[61] Jayalakshmi, M.; Rao, M. M.; Venugopal, N.; Kim, K.-B. *Journal of Power Sources* **2007**, *166*, 578–583.

[62] Li, B.; Xu, Y.; Rong, G.; Jing, M.; Xie, Y. *Nanotechnology* **2006**, *17*, 2560–2566.

[63] Wang, Y.; Cao, G. *Chemistry of Materials* **2006**, *18*, 2787–2804.

[64] Parida, M. R.; Vijayan, C.; Rout, C. S.; Sandeep, C. S. S.; Philip, R.; Deshmukh, P. C. *The Journal of Physical Chemistry C* **2011**, *115*, 112–117.

[65] Arico, A. S.; Bruce, P.; Scrosati, B.; Tarascon, J.-M.; van Schalkwijk, W. *Nature Materials* **2005**, *4*, 366–377.

[66] Muhr, H.-J.; Krumeich, F.; Schönholzer, U. P.; Bieri, F.; Niederberger, M.; Gauckler, L. J.; Nesper, R. *Advanced Materials* **2000**, 231–234.

[67] Luca, V.; Hook, J. M. *Chemistry of Materials* **1997**, *9*, 2731–2744.

[68] Manthiram, A.; Kim, J. *Chemistry of Materials* **1998**, *10*, 2895–2909.

[69] Takahashi, K.; Limmer, S. J.; Wang, Y.; Cao, G. *The Journal of Physical Chemistry B* **2004**, *108*, 9795–9800.

[70] Popa, A. I.; Vavilova, E.; Täschner, C.; Kataev, V.; Büchner, B.; Klingeler, R. *The Journal of Physical Chemistry C* **2011**, *115*, 5265–5270.

[71] Zwilling, V.; Darque-Ceretti, E.; Boutry-Forveille, A.; David, D.; Perrin, M. Y.; Aucouturier, M. *Surface and Interface Analysis* **1999**, *27*, 629–637.

[72] Shin, Y.; Lee, S. *Nanotechnology* **2009**, *20*, 105301.

[73] Qiu, X.; Howe, J. Y.; Meyer III, H. M.; Tuncer, E.; Paranthaman, M. P. *Applied Surface Science* **2011**, *257*, 4075–4081.

[74] Sieber, I.; Hildebrand, H.; Friedrich, A.; Schmuki, P. *Electrochemistry Communications* **2005**, *7*, 97–100.

[75] Banerjee, S.; Mohapatra, S. K.; Misra, M. *Chemical Communications* **2009**, 7137.

[76] Habazaki, H.; Konno, Y.; Aoki, Y.; Skeldon, P.; Thompson, G. E. *The Journal of Physical Chemistry C* **2010**, *114*, 18853–18859.

[77] Berger, S.; Tsuchiya, H.; Ghicov, A.; Schmuki, P. *Applied Physics Letters* **2006**, *88*, 203119.

[78] Jehng, J.-M.; Deo, G.; Weckhuysen, B. M.; Wachs, I. E. *Journal of Molecular Catalysis A: Chemical* **1996**, *110*, 41–54.

[79] Stefanovich, G. B.; Pergament, A. L.; Velichko, A. A.; Stefanovich, L. A. *Journal of Physics: Condensed Matter* **2004**, *16*, 4013–4024.

[80] Yang, Y.; Kim, D.; Yang, M.; Schmuki, P. *Chemical Communications* **2011**, *47*, 7746.

[81] Ellis, B. H.; Hopper, M. A.; Smet, D. J. d. *Journal of The Electrochemical Society* **1971**, *118*, 860.

[82] Lu, K.; Tian, Z.; Geldmeier, J. A. *Electrochimica Acta* **2011**, *56*, 6014–6020.

[83] Zhu, K.; Neale, N. R.; Miedaner, A.; Frank, A. J. *Nano Letters* **2007**, *7*, 69–74.

[84] Dvorak, O.; Diers, J.; Armond, M. K. d. *Chemistry of Materials* **1992**, *4*, 1074–1077.

[85] Larsen-Olsen, T. T.; Bundgaard, E.; Sylvester-Hvid, K. O.; Krebs, F. C. *Organic Electronics* **2011**, *12*, 364–371.

[86] Piotrowski, O.; Madore, C.; Landolt, D. *Plating and Surface Finishing* **1998**, 115–119.

[87] Sainio, C. A.; Duquette, D. J.; Steigerwald, J.; Murarka, S. P. *Journal of Electronic Materials* **1996**, *25*, 1593–1598.

[88] MACAK, J.; Schmuki, P. *Electrochimica Acta* **2006**, *52*, 1258–1264.

[89] Lockman, Z.; Sreekantan, S.; Ismail, S.; Schmidt-Mende, L.; MacManus-Driscoll, J. *Journal of Alloys and Compounds* **2010**, *503*, 359–364.

[90] Sul, Y.-T.; Johansson, C. B.; Petronis, S.; Krozer, A.; Jeong, Y.; Wennerberg, A.; Albrektsson, T. *Biomaterials* **2002**, *23*, 491–501.

[91] Mendialdua, J.; Casanova, R.; Barbaux Y., *Journal of Electron Spectroscopy and Related Phenomena* **1995**, 249–261.

[92] Alivisatos, A. P. *The Journal of Physical Chemistry* **1996**, *100*, 13226–13239.

[93] Rzigalinski, B. A.; Strobl, J. S. *Toxicology and Applied Pharmacology* **2009**, *238*, 280–288.

[94] Quan, Z.; Valentin-Bromberg, L.; Loc, W. S.; Fang, J. *Chemistry - An Asian Journal* **2011**, *6*, 1126–1136.

[95] Peng, X. *Nano Research* **2009**, *2*, 425–447.

[96] Krunks, M. *Thin Solid Films* **1999**, *338*, 125–130.

[97] Zhong, H.; Zhou, Y.; Ye, M.; He, Y.; Ye, J.; He, C.; Yang, C.; Li, Y. *Chemistry of Materials* **2008**, *20*, 6434–6443.

[98] Green, M. A. *Journal of Materials Science: Materials in Electronics* **2007**, *18*, 15–19.

[99] Kruszynska, M.; Borchert, H.; Parisi, J.; Kolny-Olesiak, J. *Journal of the American Chemical Society* **2010**, *132*, 15976–15986.

[100] Castro, S. L.; Bailey, S. G.; Raffaelle, R. P.; Banger, K. K.; Hepp, A. F. *The Journal of Physical Chemistry B* **2004**, *108*, 12429–12435.

[101] Martin, C. R.; van Dyke, L. S.; Cai, Z.; Liang, W. *Journal of the American Chemical Society* **1990**, *112*, 8976–8977.

[102] Mao, Y.; Zhang, F.; Wong, S. S. *Advanced Materials* **2006**, *18*, 1895–1899.

[103] Mao, Y.; Wong, S. S. *Journal of the American Chemical Society* **2004**, *126*, 15245–15252.

[104] Loste, E.; Meldrum, F. C. *Chemical Communications* **2001**, 901–902.

[105] O'Sullivan, C.; Gunning, R. D.; Sanyal, A.; Barrett, C. A.; Geaney, H.; Laffir, F. R.; Ahmed, S.; Ryan, K. M. *Journal of the American Chemical Society* **2009**, *131*, 12250–12257.

[106] Adenis, C.; Olivier-Fourcade, J.; Jumas, J.; Philippot, E. *Revue de Chimie Minerale* **1987**, 10–21.

[107] Orlova, N. S.; Bodnar, I. V.; Kudritskaya, E. A. *Crystal Research and Technology* **1998**, *33*, 37–42.